## UNCOUPLED DUAL-MECHANISM SYSTEM FOR SEISMIC RESILIENCE: PARAMETRIC ANALYSES AND PRELIMINARY DESIGN PROCEDURE

by

#### Farideh Rezagholizadehomran

B.Sc., Shahrood University of Technology, 2008 M.Sc., University of Khayyam, 2021

# THESIS SUBMITTED IN PARTIAL FULFILLMENT OF THE REQUIREMENTS FOR THE DEGREE OF MASTER OF APPLIED SCIENCE IN ENGINEERING

UNIVERSITY OF NORTHERN BRITISH COLUMBIA

September 2025

©Farideh Rezagholizadehomran, 2025

#### **Abstract**

Achieving enhanced seismic resilience in modern high-rise buildings requires advanced structural systems capable of controlling damage from both first-mode and higher-mode responses. This study develops a preliminary design procedure for a novel dual-mechanism system that allows the uncoupling of overturning and lateral responses at the base of high-rise buildings. The system combines both rocking and shear mechanisms to mitigate higher-mode effects. By developing the design procedure, the study aims to facilitate the broader adoption of the system to improve the seismic resilience of high-rise buildings.

To support the development of this procedure, a simplified numerical model was created to represent the seismic behaviour of the uncoupled dual-mechanism system. After establishing the ranges of key design parameters governing the system's strength and component dimensions, a series of parametric studies were conducted using nonlinear response history analyses for two seismic locations: Los Angeles in the United States and Vancouver in Canada. Seismic performance spectra were generated based on these analyses to guide the development of a preliminary design procedure for practical engineering applications.

The parametric study established that for buildings up to approximately 300 m in height, a practical range of geometric and strength parameters exists to successfully limit maximum inter-story drift ratios to 1.5%, while controlling base displacements to a feasible 800 mm. Beyond this height, it was found that the required dimensions of the rocking mechanism components become impractically large for constructability and cost-effectiveness, defining the system's effective application limit.

#### **Table of Contents**

Abstract	ii
Table of Contents	iii
List of Tables	vii
List of Figures	ix
Acknowledgement	xiii
1. Introduction	1
1.1. High-Rise Development and Higher-Mode Effects	1
1.2. The Need for Resilient Seismic Design	2
1.3. Uncoupled Dual-Mechanism System	3
1.4. Research Objectives	4
1.5. Scope and Limitations	5
1.6. Organization	5
2. Literature Review	7
2.1. High-Rise Buildings: Definition and Seismic Hazards	7
2.2. Seismic Design of High-Rise Buildings and Higher-Mode Effects	8
2.3. High-Performance Systems for High-Rise Buildings	10
2.3.1. RockinSystems	11
2.3.2. Base Isolation Systems	13
2.4. Dual-Mechanism Systems	15
2.5. The MechRV3D System	16
2.5.1. Configuration and Mechanics	16
2.5.2. Numerical Validation	20

2.5.3. Preliminary Design Procedure in the Initial Study	
2.6. Summary23	
3. Methodology25	
3.1. Technical Roadmap25	
3.2. Design Parameters	
3.2.1. Fundamental Period ( <i>T</i> <sub>1</sub> ) of Generic Buildings	
3.2.2. Aspect Ratio ( <i>H/B</i> ) of Generic Buildings28	
3.2.3. Moment ReductionFactor (R <sub>M</sub> )	
3.2.4. Rocker Depth ( $D$ ) and Mega-Column Spacing ( $d_{c2c}$ )	
3.2.5. Mega-Column Height (hc)	
3.2.6. Shear Reduction Factor ( $\mu$ v)	
3.2.7. Initial Stiffnes Factor for the Shear Mechanism $(r_K_{b1})$ 51	
3.2.8. Post-yield Shear Stiffness ( $\alpha_K$ )	
3.3. Initial Stiffness of the Base Mechanisms ( $K_{\text{base\_initial}}$ ) and Mega-Column's Negative	/e
Stiffness54	
3.4. Ultimate Strength of Shear Mechanism (V <sub>u</sub> )56	
3.5. Summary of Parameters and Rationale for Their Ranges57	
3.6. Numerical Model62	
3.6.1. Stick Model of the Superstructure63	
3.6.2. Rocking Mechanism Components64	
3.6.3. The Gap Size in the End Connections of Mega-Columns67	
3.6.4. Shear Mechanism Components70	
3.6.5. Leaning Columns72	
3.6.6. Damping in the Model73	
3.6.7. Loading	

3.7. Pushover Analysis74	
3.7.1. Activation of the Rocking Mechanism76	
3.7.2. Engagement of the Shear Mechanism	
3.8. Parametric Nonlinear Response History Analyses	
3.9. Ground Motion Selection and Scaling80	
3.9.1. Los Angeles Site80	
3.9.2. Vancouver Site84	
3.10. Parametric Analyses89	
3.11. Design Code Requirements for Seismic Responses90	
3.12. Summary of Methodology92	
4. Results and Discussion94	
4.1. Procedure for Constructing Seismic Performance Spectra94	
4.1.1.Performance-Based Design Framework and the Role of Performance Targets	
95	
4.2. Seismic Performance Spectra for Shear Reduction Factor ( $\mu$ v) as Constant96	
4.2. Seismic Performance Spectra for Shear Reduction Factor ( $\mu$ v) as Constant96 4.2.1. Seismic Performance Spectra for $\mu$ v = 0, Los Angeles97	
4.2.1. Seismic Performance Spectra for $\mu_V = 0$ , Los Angeles	
4.2.1. Seismic Performance Spectra for $\mu_V = 0$ , Los Angeles	
4.2.1. Seismic Performance Spectra for $\mu_V = 0$ , Los Angeles	
4.2.1. Seismic Performance Spectra for $\mu_{V} = 0$ , Los Angeles	
4.2.1. Seismic Performance Spectra for $\mu_{V} = 0$ , Los Angeles	
4.2.1. Seismic Performance Spectra for $\mu_V = 0$ , Los Angeles	
4.2.1. Seismic Performance Spectra for $\mu_V = 0$ , Los Angeles	
4.2.1. Seismic Performance Spectra for $\mu_V = 0$ , Los Angeles	

4.3.3. Seismic Performance Spectra for $h_c = 12$ m, Los Angeles
4.3.4.Seismic Performance Spectra for hc=2.5 m (hc=4 m for 120-story), Vancouver
116
4.3.5. Seismic Performance Spectra for $h_c = 6$ m, Vancouver
4.3.6. Seismic Performance Spectra for $h_c=12$ m ( $h_c=15$ m for 120-story), Vancouver
120
4.4. Summary of Results from Seismic Performance Spectra
4.5. Preliminary Design Procedure Using Seismic Performance Spectra123
4.6. Maximum Base Displacement (∆b,max) and the Stability of Mega-Columns133
4.7. Effective Period Elongation of the MechRV3D System
5. Conclusions and Recommendations
5.1. Conclusions
5.2. Recommendation for Future Research
References141
Appendix A: Rocker Dimension Correlations
Appendix B: Selected and Scaled Ground Motions for All Generic Buildings at MCE Level

### **List of Tables**

Table 3-1: Fundamental periods of generic RC buildings using KBC 2009 formula 28
Table 3-2: Properties of the generic buildings
Table 3-3: $d_{c2c}$ and $D$ values of the rocker for different values of $R_M$ for Los Angeles site
Table 3-4: The ratio of weight of the rocker to the weight of the core stick for different $R_{\rm M}$
values at the Los Angeles site
Table 3-5: Design properties of mega-column for specified height of building
Table 3-6: Lower- and upper-bound of shear mechanism strength $(V_y)$
Table 3-7: Initial stiffness for shear mechanism based on $\Delta_{b,max}$ =800 mm at the base for all
generic buildings at the Los Angeles site
Table 3-8: Initial stiffness values of shear mechanism for all generic buildings at Los
Angeles site
Table 3-9: Buttressing force, $V_{u,c}$ provided by mega-columns at 800 mm displacement for
the Los Angeles site
Table 3-10: Range of parameters of MechRV3D system to conduct parametric analyses 62
Table 3-11: Gap distance values for different height of building with $\Delta_b = 40 \text{ mm} \dots 70$
Table 3-12: Parameters to select ground motion records for analyses
Table 3-13: Period range [18], for scaling ground motions for buildings of different heights
82
Table 3-14: Scale factors for buildings of different heights in Los Angeles site location 83
Table 3-15: Properties of earthquake events for different scenario-specified in Vancouver
85
Table 3-16: Properties of earthquake events for In-slab source in Vancouver
Table 3-17: Properties of earthquake events for Interface source in Vancouver

Table 3-18: Ground motion and scale factors for all buildings for	or $T_{RS1}$ , in-slab sources,
Vancouver site	88
Table 3-19: Ground motion and scale factors for all buildings for	$T_{RS2}$ , interface sources,
Vancouver site	89
Table 4-1: Differences between nominal period $(T_a)$ and system pe	riod $(T_{\rm sys})$ for all generic
buildings	136

## **List of Figures**

Figure 1-1: Configuration of the MechRV3D system [15]
Figure 2-1: Geographical distribution of high-rise buildings, seismic hazard zones and
densely populated cities [4]
Figure 2-2: Potential positioning of second-mode period comparing to first-mode period of
a high-rise building on the pseudo-acceleration response spectrum [21]9
Figure 2-3: Rocking action of a rigid block under seismic load
Figure 2-4: Conceptual illustration of the effect of base isolation under lateral load Left:
conventional fixed-base structure, right: base-isolated structure showing deformation
concentrated at the isolation level [39]14
Figure 2-5: MechRV3D system incorporated at the base of superstructure [15]
Figure 2-6: Shear mechanism components [15]
Figure 2-7: Rolling mega-columns between the rocker and foundation [15]20
Figure 2-8: Simplified model of the MechRV3D system with a stick-model superstructure
[15]21
Figure 3-1: Comparison of fundamental periods from KBC 2009 and ASCE 7-10 empirical
formulas with measured fundamental periods (T) with ambient vibration method [51]27
Figure 3-2: Typical floor plan of the generic buildings (left), height and width of a building
to calculate aspect ratio, <i>H/B</i> (right)
Figure 3-3: The variation of $d_{c2c}$ with rocker depth (D) for $R_{\rm M}=8$
Figure 3-4: The variation of $d_{c2c}$ with rocker depth (D) for 15-story building, $R_M=836$
Figure 3-5: The variation of $d_{c2c}$ with rocker depth (D) for 120-story building, $R_M=836$
Figure 3-6: Modelling the cross-sectional area of mega-columns, $d_c$ =1500 mm (left),
dimensions of mega-columns [15] (right)
Figure 3-7: Results of analyses to design mega-columns (diameters:1000-6400 mm) 42

Figure 3-8: Results of analyses to design mega-columns (lower diameters: 1000-2200 mm)
43
Figure 3-9: Maximum height of mega-column suggested for 15-story building, column
diameter =1000 mm
Figure 3-10: Maximum height of mega-column suggested for 30-story building, column
diameter =1500 mm
Figure 3-11: Maximum height of mega-column suggested for 50-story building, column
diameter =2200 mm
Figure 3-12: Maximum height of mega-column suggested for 70-story building, column
diameter =3500 mm
Figure 3-13: Maximum height of mega-column suggested for 100-story building, column
diameter =5000 mm
Figure 3-14: Maximum height of mega-column suggested for 120-story building, column
diameter =6400 mm
Figure 3-15: A modelled BRBF with deformation ( $\Delta_y$ ) in yielding point and $20\Delta_y$ in ultimate
strength [64]
Figure 3-16: Two-dimensional model of the MechRV3D system incorporated into the core-
stick superstructure
Figure 3-17: Modelling of the connection between mega-column and rocker at the top (left),
and the material model used for simulation, selected from the OpenSees library (right). 65
Figure 3-18: Modelling of the connection between mega-column and foundation at the
bottom (left), and the material model used for simulation, selected from the OpenSees
library (right)
Figure 3-19: The rotation in the rocker, $\theta_{\text{rocker}}$ (left), the rotation in the mega-column, $\theta_{\text{m}}$
(right) when the mega-columns sway in the opposite direction of the applied force 68

Figure 3-20: Rotation in the rocker ( $\theta_{\text{rocker}}$ ) that affect the gap distance when the mega-
columns sway in the same direction of the applied force
Figure 3-21: Modelling of shear mechanism as a translational spring (bottom), and the
material model used for simulation, selected from the OpenSees library (top)71
Figure 3-22: Loading profile for pushover analysis to activate rocking mechanism 76
Figure 3-23: Lateral capacity curve and base rocking rotation, using the 15-story building
as a representative example at Los Angeles site
Figure 3-24: Shear Mechanism behaviour during first-mode pushover
Figure 3-25: Shear mechanism engagement when lateral load is applied at 0.1 <i>H</i>
Figure 3-26: Principal faults at the vicinity of Los Angeles (LA) site [66]
Figure 3-27: MCE response spectra and ground motions scaled for 15-story building, $T_1$ =
1 sec
Figure 4-1: Combined plots for inter-story drift ratio and base displacement, $\mu_V = 0$ , Los
Angeles
Figure 4-2: Combined plots for inter-story drift ratio and base displacement, $\mu v=0.5$ , Los
Angeles
Figure 4-3: Combined plots for inter-story drift ratio and base displacement, $\mu_V = 1$ , Los
Angeles
Figure 4-4: Combined plots for inter-story drift ratio and base displacement, $\mu_V = 0$ ,
Vancouver
Figure 4-5: Combined plots for inter-story drift ratio and base displacement, $\mu_V = 0.5$ ,
Vancouver
Figure 4-6: Combined plots for inter-story drift ratio and base displacement, $\mu_V = 1$ ,
Vancouver

Figure 4-7: Combined plots for inter-story drift ratio and base displacement, $h_c$ =2.5 m, Los
Aneles
Figure 4-8: Combined plots for inter-story drift ratio and base displacement, h <sub>c</sub> =6 m, Los
Angeles
Figure 4-9: Combined plots for inter-story drift ratio and base displacement, h <sub>c</sub> =12 m, Los
Angeles
Figure 4-10: Combined plots for inter-story drift ratio and base displacement, $h_c$ =2.5 m,
Vancouver
Figure 4-11: Combined plots for inter-story drift ratio and base displacement, h <sub>c</sub> =6 m,
Vancouver
Figure 4-12: Combined plots for inter-story drift ratio and base displacement, $h_c$ =12 m,
Vancouver
Figure 4-13: Flowchart suggested to preliminary design of MechRV3D system 124
Figure 4-14: Finding the acceptable area for 70-story building when $R_M=8$ , $\mu_V=0$ 129
Figure 4-15: Finding the acceptable area for 70-story building when $R_M=8$ , $\mu v=0.5$ 130
Figure 4-16: Finding the acceptable area for 70-story building when $R_{\rm M}$ =8, $h_{\rm c}$ =6 m 131
Figure 4-17: Finding the acceptable area for 70-story building when $R_M=8$ , $h_c=12$ m 132

#### Acknowledgement

The preface opens with the name of the Pure World-Lord, the One who brings forth the verdant growth from the soil, who bestowed height upon the lofty heavens and opened the eyes of the wise and discerning. Wisdom springs from His teachings, and hearts yield in submission to His will. The world is suffused with His wisdom and command. His decrees are manifest, yet His wisdom remains veiled. (Sharafnameh by Nizami, 1203 CE)

I would like to express my deepest gratitude to all those who supported me during the course of my thesis. My sincerest thanks to my supervisor, Dr. Fei Tong, for his invaluable guidance, encouragement, and support throughout this research. His insights and constructive feedback were crucial in shaping this work.

I would also like to thank Drs. Jianhui Zhou and Thomas Tannert for their support and valuable suggestions as members of my supervisory committee. Their guidance and insights have greatly contributed to the development of this thesis.

Special thanks to my dear friend Maral Jafari, for her constant support, insightful discussions, and encouragement. I am also truly thankful to other research students, including Houman Ganjali, Abdul Basit, and Mohammad Hossein Asadi Jafari for sharing their experiences and advice during my study. Additionally, I am grateful to the University of Northern British Columbia (UNBC) for the support, facilities, and opportunities that greatly contributed to the progress of my thesis.

My heartfelt gratitude goes to my parents for their unwavering support, love, and understanding throughout this long journey. As my first teachers, they taught me timeless lessons about patience, diligence, and gratitude, which helped me stay on track during difficult times. I am also deeply grateful to my siblings, whose constant encouragement and comforting presence were a source of strength, especially at the most challenging moments.

Without the help and support of all the people mentioned above, this thesis would not have been possible. Finally, I dedicate my own contribution in this work to my homeland, Iran, whose rich literary heritage and the noble hearts of its people have instilled in me the true meaning of dignity and gratitude.

#### 1. Introduction

#### 1.1. High-Rise Development and Higher-Mode Effects

As more people are moving into urban areas, the demand for housing and commercial spaces continues to increase in big cities [1]. However, affordable land is not always available in urban areas to meet the growing demand. High-rise buildings offer a solution by providing vertical housing that uses less ground space per resident. They play an important role in addressing urbanization challenges and are expected to be a key part of future city planning and development [2].

A significant portion of this global high-rise development is concentrated in regions of high seismicity, such as the Pacific Ring of Fire [3]. This intersection of dense urban environments with significant seismic hazard creates a critical engineering challenge: ensuring the safety, and increasingly the resilience of high-rise structures under earthquake loading. Conventional seismic design has focused primarily on preventing collapse, but the potential for extensive damage and long-term loss of function in these vital structures has highlighted the need for more advanced design philosophies [4].

Designing high-rise buildings presents distinct challenges not typically found in low-rise construction. A primary concern is the significant contribution of higher-vibration modes to the overall seismic response [4]. While the fundamental (first) mode often governs the response of shorter buildings, higher modes in high-rise structures can be strongly excited by earthquake ground motions. This phenomenon leads to a dynamic amplification of shear forces and overturning moments [5].

Conventional design procedures, which are often based on a first-mode-dominated lateral force distribution, may fail to capture these amplified demands. Consequently, structural elements, particularly in upper stories, can experience shear forces that exceed their

capacity, leading to brittle failures that undermine the intended ductile behaviour of the structure [6], [7]. This discrepancy between design assumptions and actual seismic demands represents a critical vulnerability [8], [9].

#### 1.2. The Need for Resilient Seismic Design

In modern seismic design, the primary focus is on life safety and collapse prevention during major earthquakes. While these remain essential goals, the building codes that follow this approach implicitly permit significant structural and non-structural damage. The economic losses and extended loss of function resulting from such damages, as witnessed in recent earthquakes, have highlighted the need for a more advanced design philosophy: seismic resilience. Resilience is defined as the ability of a structure to maintain functionality during an earthquake and enable rapid recovery after the event [10].

Achieving seismic resilience in high-rise buildings necessitates systems that can effectively control the damage induced by both first-mode and higher-mode responses. This has led to the development of high-performance systems, which can be broadly categorized into: (1) rocking systems, (2) base isolation systems, and (3) combination of these two concepts.

A rocking system is a type of lateral-load-resisting system that is intentionally designed to step up at its base. The motion is driven by the seismic overturning moment and resisted by a restoring moment from the structure's self-weight. A rocking system rests on its base instead of being attached to it. Thus, tensile forces at the foundation are prevented. As a result, instead of developing plastic deformations near the base, a gap opens at the interface between the structure and its foundation [11].

Base isolation is considered one of the reliable strategies for safeguarding buildings against earthquakes. In base-isolated structures, flexible isolators and energy-dissipating devices are installed at the base, decreasing the effective stiffness of the structure and thereby increasing its fundamental period, which helps reducing the seismic demand on the superstructure [12].

While existing high-performance systems offer significant benefits, each of them comes with limitations. Rocking mechanisms effectively control overturning moments at the expense of providing limited control over higher-mode shear demands [13]. In contrast, base isolation systems can mitigate the higher-mode effects, but it may be subjected to tension due to significant overturning moments or may be overstressed in compression beyond their safe limits [14]. These limitations highlight the need for a novel solution that can independently and effectively control both overturning and shear responses in high-rise buildings.

#### 1.3. Uncoupled Dual-Mechanism System

Tong [15] proposed a solution that allows the uncoupling of the overturning and lateral responses at the base of high-rise buildings using a novel dual-mechanism system. This system is located at the base of superstructure, with a rocking mechanism at the centre and a shear mechanism at the periphery. It is referred to as the MechRV3D system, where "Mech" denotes the mechanism, "R" stands for rocking, "V" represents shear, and "3D" refers to the three-dimensional action.

As illustrated in Figure 1-1, the configuration of the MechRV3D system consists of a rocking mechanism (rocker and rolling mega-columns), and a shear mechanism (buckling-restrained braced frames (BRBFs) and a skirt diaphragm). The reinforced concrete (RC) core walls of the superstructure are monolithically integrated with the top of the rocker [15].

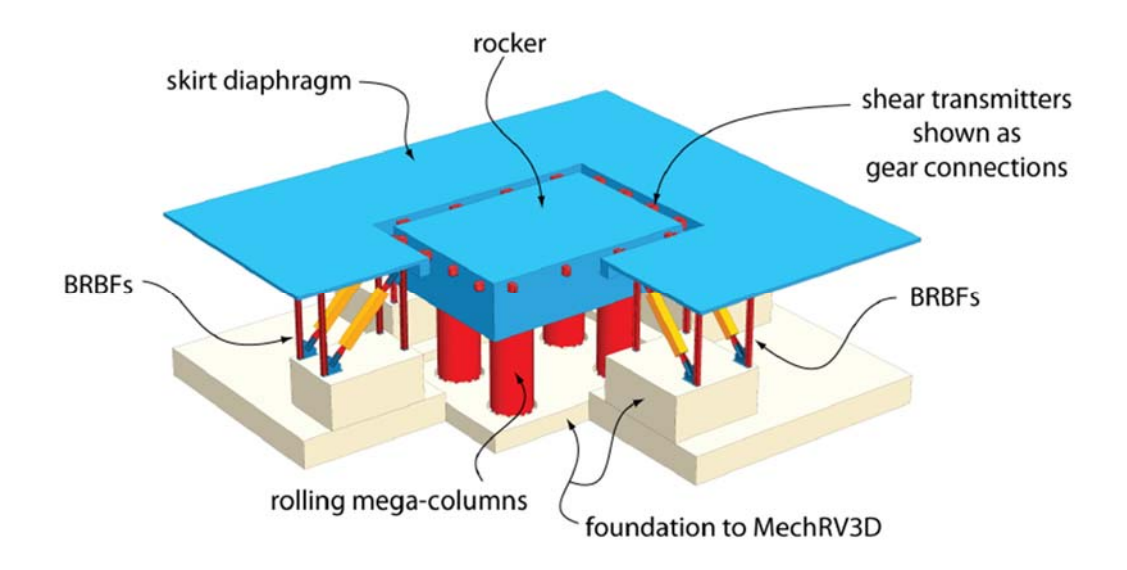


Figure 1-1: Configuration of the MechRV3D system [15]

In the previous study, the configuration of the new system was idealized and investigated numerically through nonlinear static and response history analyses. A physical embodiment of this concept was developed and then validated through numerical verification of a 42-story RC core-wall building [15].

By using MechRV3D system, the superstructure can benefit from the reduction of higher-mode effects through its uncoupled shear mechanism, which acts as a ductile fuse to cap the total base shear transmitted into the superstructure while the rocking mechanism acts as a flexural fuse to cap the first-mode overturning moment at the base. The superstructure can be designed to remain in the elastic range, potentially reducing construction and repair costs. This will make the MechRV3D system more effective and reliable for future urban construction, ultimately enhancing the safety and resilience of high-rise buildings.

#### 1.4. Research Objectives

The initial research by Tong [15] established the theoretical concept of the MechRV3D system and demonstrated its feasibility using a simplified numerical model where key components were represented as springs. This simplification, however, did not account for

the geometric properties of the structural components involved in the rocking mechanism or the associated  $P-\Delta$  effects from the mega-columns, leaving a critical gap in understanding the system's practical behaviour and limitations.

The primary objective of this research is to bridge this gap by developing a more refined preliminary design procedure for the MechRV3D system. This is achieved by explicitly incorporating the geometry of the rocking mechanism components as key design variables. The specific objectives are:

- Development of an enhanced design procedure by providing a systematic, step-by-step methodology for selecting key system parameters, including the newly introduced geometric variables. This procedure is specifically designed to address the limitations of the initial conceptual model by explicitly accounting for system stability and the P-Δ effects associated with the mega-columns.
- To Investigate the effects of key geometric properties—such as depth and height—
  of the rocking mechanism components through parametric analyses, treating these
  dimensions as essential design variables and evaluating the P-Δ effect induced by
  these parts.

#### 1.5. Scope and Limitations

The scope of this research is strictly focused on the seismic design and performance of the MechRV3D system, which leads to the development of a preliminary design procedure. Accordingly, important related topics such as wind load effects, the development of codified design standards, and detailed economic analysis are considered outside the boundaries of this study.

#### 1.6. Organization

Chapter 1 provides a brief introduction to the research topic, its background, and the objectives of this study. Chapter 2 presents a literature review that includes the main design challenge of high-rise buildings, specifically higher-mode effects. It also reviews previous solutions to address this challenge in terms of resistance systems, summarizes the previously developed MechRV3D system, and provides a brief overview of the design criteria of this system in relation to seismic responses in previous research.

In Chapter 3, the procedure for determining the acceptable range of parameters in the current study to conduct parametric analyses is explained, followed by a discussion of rebuilding the nonlinear numerical model. A plan and procedure for parametric nonlinear response history analysis are then presented.

Chapter 4 discusses the results of the analyses and presents the development of the design procedure. This procedure is based on the seismic performance spectra obtained for two different selected sites: Los Angeles in the United States, and Vancouver in Canada. Finally, Chapter 5 draws conclusions, outlines the developed design requirements for the MechRV3D system, and discusses future studies.

#### 2. Literature Review

#### 2.1. High-Rise Buildings: Definition and Seismic Hazards

A high-rise building is distinguished by its height which is generally taller than the surrounding structures [16]. While no single definition is universal, the Council on Tall Buildings and Urban Habitat (CTBUH), typically considers a building with 14 or more stories or a height exceeding 50 m to be a tall building [17].

The global increase in the construction of such structures is significant; over 2,200 buildings exceeding 200-m in height had been completed by 2023 [3]. As illustrated in Figure 2-1, a substantial portion of this high-rise development is concentrated in populous urban centres that are also located in regions of high seismic hazard [4]. This intersection of high population density, significant economic assets, and seismic risk highlights the critical need for advanced seismic design procedures that can ensure the resilience of these high-rise buildings.

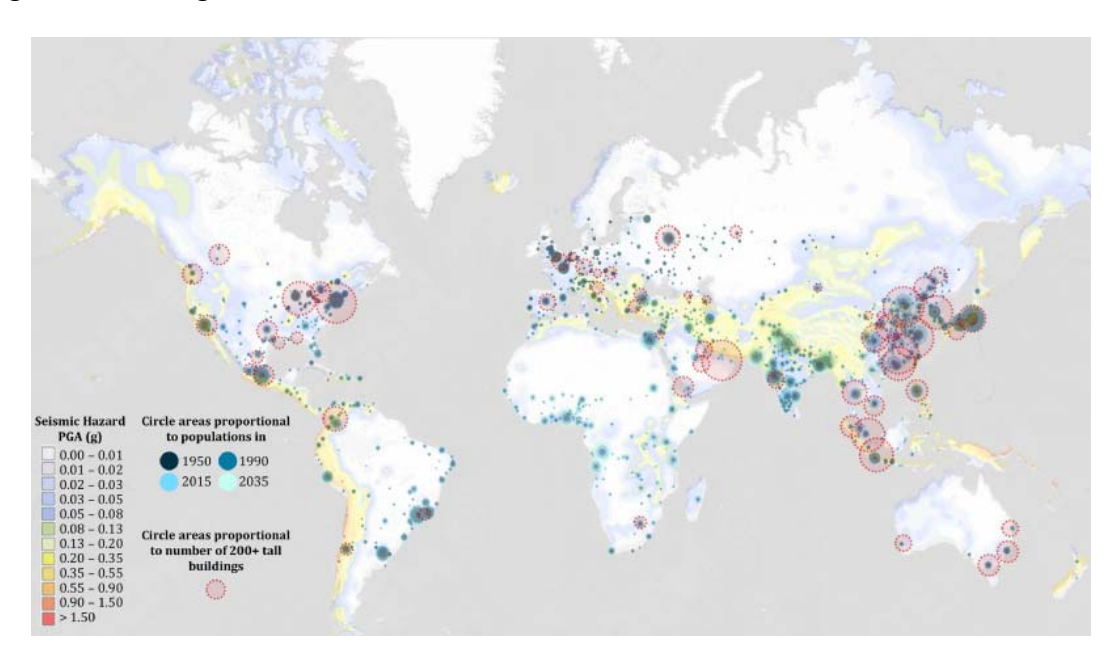


Figure 2-1: Geographical distribution of high-rise buildings, seismic hazard zones and densely populated cities [4]

#### 2.2. Seismic Design of High-Rise Buildings and Higher-Mode Effects

Modern seismic design codes worldwide primarily focus on ensuring life safety and preventing structural collapse during major earthquakes [18]. Structures designed to this philosophy are expected to undergo controlled inelastic deformation in designated elements to dissipate energy [4]. While effective for life safety, this permitted damage can lead to significant repair costs and extended loss of building function, which is often inconsistent with modern resilience objectives [19].

To achieve enhanced performance targets, Performance-Based Seismic Design (PBSD) is often employed. PBSD provides a framework for verifying that a structure will meet specific performance objectives (e.g., immediate occupancy, collapse prevention) under different seismic hazard levels [20].

The design of high-rise structures is particularly challenging due to the significant contribution of higher vibration modes. High-rise buildings behave as continuous dynamic systems, but are often idealized as flexible multi-degree-of-freedom (MDOF) systems with long fundamental periods. While the first-mode period ( $T_1$ ) may fall on the descending branch of the acceleration response spectrum, the higher modes periods—particularly the second ( $T_2$ ) and third ( $T_3$ ) modes —which are fractions of the fundamental period, may align with the spectrum's high-acceleration plateau region, as shown conceptually in Figure 2-2 [5].

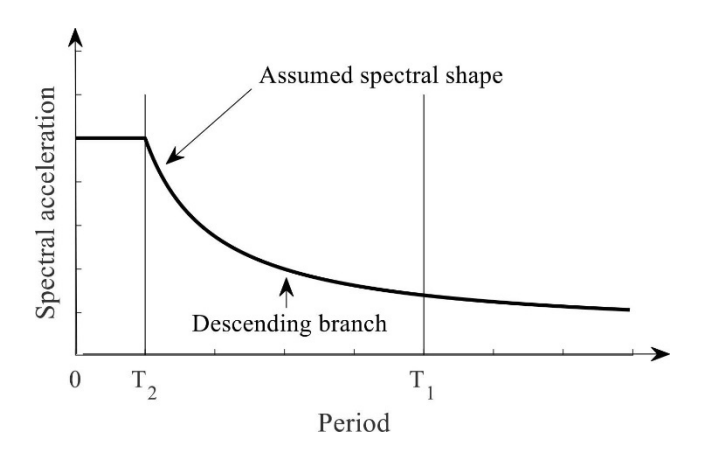


Figure 2-2: Potential positioning of second-mode period comparing to first-mode period of a highrise building on the pseudo-acceleration response spectrum [21]

This can lead to a dynamic amplification of shear forces and overturning moments that is not captured by design methods based on a first-mode force distribution. As a result, the contribution of higher modes to the total response would be significant and cannot be ignored in high-rise buildings [5].

Higher-mode effects on the amplification of seismic demands in tall or slender structures have been an ongoing research topic since the 1940s. However, research on higher-mode effects in the inelastic range began with the seminal numerical work of Blakeley et al. (1975) [22]. They identified the phenomenon of dynamic shear amplification, where shear demands in the upper stories significantly exceed those predicted by first-mode-based methods. This critical finding, further explored in subsequent numerical studies [23], [24] and [25], was later validated by large-scale shake table experiments [26], [7], which physically confirmed that amplified shear from higher modes is a crucial design consideration for tall, ductile structures.

In response to these consistent research findings, seismic design codes began to incorporate provisions to account for higher-mode effects. In the United States, acknowledgement of higher-mode effects gained prominence in the late 1990s when the Structural Engineers Association of California (SEAOC) published a commentary recommending the use of

shear amplification factors from the New Zealand codes [27]. This influential recommendation paved the way for the eventual inclusion of such provisions in national standards like ASCE 7 [18]. U.S. codes and PBSD procedures recommend using Nonlinear Time History Analysis (NLTHA) for the design of high-rise buildings, which inherently accounts for dynamic shear amplification due to higher-mode effects. The current National Building Code of Canada, NBCC 2020 [28] also includes shear amplification factors in the equivalent lateral force procedure to account for the increase in design shear force along the height of a structure due to higher-mode effects [4].

Although modern building codes have incorporated simplified provisions, such as dynamic shear amplification factors, to better estimate strength demands from higher modes [28], these methods are primarily calibrated to ensure life safety and prevent brittle failure [29]. Simply meeting these prescriptive strength requirements does not guarantee that a building will achieve modern resilience goals, such as limiting repair costs, minimizing downtime, or ensuring rapid re-occupancy [30], [10]. Consequently, the focus in state-of-the-art research and practice has expanded beyond prescriptive compliance. The design of resilient high-rise buildings now emphasizes comprehensive performance-based analyses that explicitly model and control damage to meet specific post-earthquake recovery objectives [31]. This shift in design philosophy from mere life safety to enhanced resilience has in turn driven the development of new structural technologies.

#### 2.3. High-Performance Systems for High-Rise Buildings

Achieving low-damage performance by simply increasing a conventional structure's strength is an inefficient strategy for mitigating higher-mode effects in high-rise buildings. This approach requires a significant increase in material use and stiffness along the entire height of the structure to address a shear-related issue that is primarily concentrated in the upper stories. Furthermore, increasing the stiffness of the structure may unintentionally

amplify its response to high-frequency seismic content, thereby aggravating the very issue it seeks to mitigate.

This highlights a fundamental limitation of conventional strength-based design, which has led to the development of advanced low-damage systems. Unlike traditional methods that resist increasing internal forces, these systems are designed to limit the seismic demands transmitted to the superstructure. By fundamentally reducing the energy input or capping the forces that excite the higher modes, these systems can prevent dynamic shear amplification much more efficiently and economically than a simple strength increase.

To overcome the inherent performance limitations of conventional structural systems in high-rise buildings, researchers have developed advanced high-seismic performance systems designed to explicitly control seismic damage. These systems are specifically developed to improve control of structural response and associated damage during strong ground motions. Low-damage response targets beyond life safety can be obtained by using these systems that help to provide more resilient high-rise buildings. Three main categories of these systems are discussed in this section.

#### 2.3.1. Rocking Systems

Figure 2-3 illustrates the fundamental principle of a rocking mechanism. When subjected to a lateral load, a freestanding block may uplift at one corner and pivot around the opposite corner, which acts as a temporary point of rotation. This motion is resisted by a restoring moment generated by the gravity load acting through the block's centre of mass. This inherent self-centring capacity, combined with energy dissipation that can be provided by supplemental devices or through controlled impact, allows a properly designed rocking mechanism to limit structural damage while maintaining stability [32]. A key characteristic

of rocking systems is their negative post-uplift stiffness, which effectively isolates the structure from seismic resonance and helps eliminate permanent displacements [15].

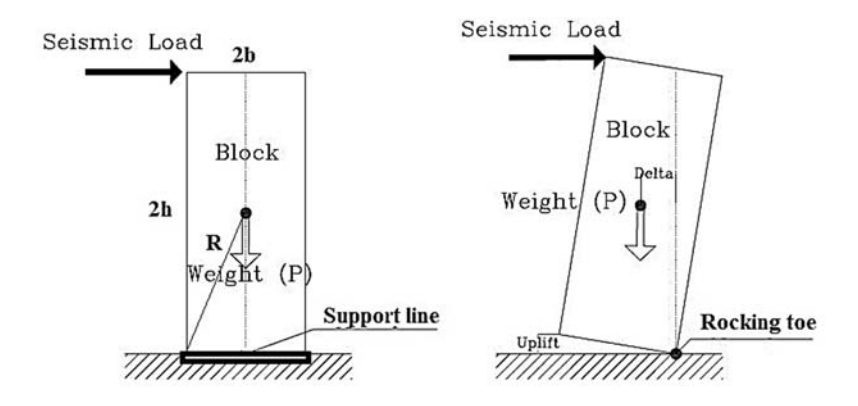


Figure 2-3: Rocking action of a rigid block under seismic load

The rocking behaviour of rigid blocks under seismic ground motion has been a subject of interest since the early  $20^{th}$  century, with renewed research attention in recent decades. Previous studies have found that the rocking behaviour is highly sensitive to parameters such as the size  $R = \sqrt{b^2 + h^2}$  (b and h are shown in Figure 2-3) and slenderness ratio ( $\alpha = atan(b/h)$ ) of the rocking block [33], [34]. As the rotation of a rocking block increases, the horizontal distance between the block's centre of mass and the pivot corner (the lever arm for the restoring gravity force) decreases. This reduction in the lever arm directly causes the restoring moment decreases, a key characteristic that defines the negative post-uplift stiffness of the system.

When the rotation angle, which measures the block's tilt from its at-rest position, exceeds the slenderness ratio ( $\alpha$ ), the structure becomes unstable. The structure needs to be slender enough to allow rocking motion (the aspect ratio (b/h) less than the coefficient of static friction ( $\mu$ ) at its base) [35]. However, it also needs to be wide enough to maintain stability (the slenderness ratio  $\alpha$  greater than the peak rotation angle induced by the ground motion) [33].

To assess the feasibility of applying rocking mechanism to high-rise buildings, Nielsen et al. [36] demonstrated that employing a rocking core wall system in a building as tall as 200 m could effectively limit the base overturning moment to a predefined capacity. This resulted in a moment demands up to 30% lower than that of a comparable fixed-base structure, without causing significant effects in other response quantities, such as peak inter-story drift.

While this reduction in moment demand demonstrates the system's effectiveness in controlling the first-mode-dominated overturning response, it is well-established that a base rocking mechanism provides limited mitigation of higher-mode effects. These effects primarily manifest as dynamic shear amplification in the upper stories of a high-rise building, a phenomenon that is largely uninfluenced by the rotational release at the base [37].

#### 2.3.2. Base Isolation Systems

An alternative high-performance strategy is base isolation, which aims to decouple the superstructure from the ground motion. As illustrated in Figure 2-4, this is achieved by introducing a flexible interface, or isolation layer at the base of the structure [14]. This added flexibility elongates the fundamental period of the system, shifting it away from the peak region of the typical earthquake acceleration spectrum and thereby reducing the inertial forces transmitted to the superstructure [38].

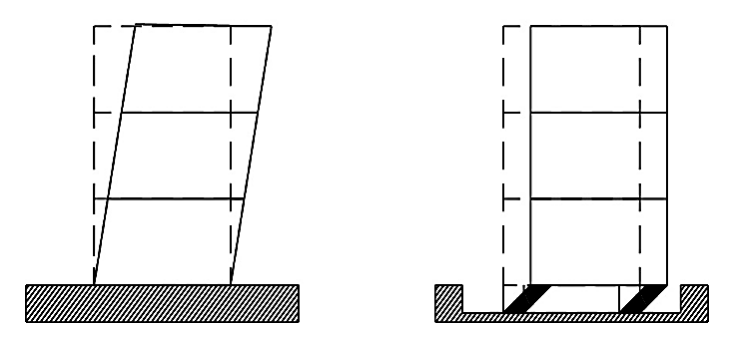


Figure 2-4: Conceptual illustration of the effect of base isolation under lateral load Left: conventional fixed-base structure, right: base-isolated structure showing deformation concentrated at the isolation level [39]

While highly effective for low- to medium-rise structures, the application of conventional base isolation to high-rise buildings presents significant challenges [40]. First, as the inherent flexibility of a high-rise building is already high, the period elongation provided by the isolation system is less pronounced, reducing its overall effectiveness. Second, and more critically, the large overturning moments generated in slender high-rise structures can induce net tensile forces or compressive overstress in the isolators. Tensile uplift can compromise the stability of elastomeric bearings, while compressive loads from the massive weight of the superstructure can exceed the isolators' capacity, especially when combined with large lateral deformations [41], [42].

To address these challenges, researchers have explored hybrid approaches that combine base isolation with other mechanisms. Calugaru [43] proposed a dual-mechanism seismic protection system for a 20-story RC core-wall building that combines base isolation with rocking core walls. However, in this system the two mechanisms were arranged in series, meaning the isolators had to resist significant axial tension and shear forces before the rocking mechanism could be activated. This in-series configuration makes it difficult to fully decouple the demands and prevent compressive overloading, highlighting a persistent challenge for such systems.

To evaluate the response reduction effect of the base isolation system on high-rise buildings, Ogura et al. [44] conducted a parametric analysis. The results revealed that the response reduction due to use of base isolation, tended to decrease as the natural period of the superstructure increased. However, even for natural periods between 3 and 4 seconds, the response displacement was reduced by approximately 30-40% compared to a non-isolated system [45].

It was also found that if the design of the yield shear force and the post-yielding stiffness of the base isolation system is appropriately selected, high-rise buildings can achieve high seismic performance using base isolation systems [45]. This suggests that with proper tuning of the system's yield and post-yielding properties, base isolation can be effective in reducing seismic response and improving stability even for high-rise buildings.

#### 2.4. Dual-Mechanism Systems

Other research has explored dual-mechanism systems, such as the controlled rocking steel braced frames (CRSBFs) that combined a base rocking frame with self-centring braces acting as a first-story shear fuse [19], [46]. In this configuration, the rocking and shear mechanisms act in series.

While this approach can provide excellent self-centring and limit damage to the main frame, the in-series arrangement presents a critical stability challenge. It concentrates all inelastic deformation into the first story, creating a soft-story mechanism. For high-rise buildings, the large inter-story drift in this single location, combined with the significant gravity load from the superstructure, leads to a highly amplified P- $\Delta$  effect that can cause system instability [15].

Consequently, the previously proposed dual systems, such as CRSBFs [10] and the base-isolated rocking core wall system by Calugaru [38], each have their own limitation. They

rely on two mechanisms -one for flexural response and another for shear response- but these mechanisms were configured in a way that prevent them from being engaged independently. Their in-series configuration can lead to unwanted damage to the mechanism during a seismic event. This limitation highlights the need for an alternative dual-mechanism topology—specifically one that avoids the soft-story mechanism and is therefore suitable for achieving low-damage performance in high-rise applications.

#### 2.5. The MechRV3D System

#### 2.5.1. Configuration and Mechanics

The MechRV3D system allows for the uncoupling of the flexural and lateral responses through a novel configuration that combines rocking and shear mechanisms [15]. Both rocking and shear mechanisms are positioned at the base of the superstructure as shown in Figure 2-5. While the rocking mechanism controls the overturning response, the parallel shear mechanism is specifically designed to mitigate the adverse effects of higher modes. A key advantage of this uncoupled arrangement is that the shear mechanism is isolated from the primary gravity load path, protecting it from the significant axial demands present in high-rise buildings.

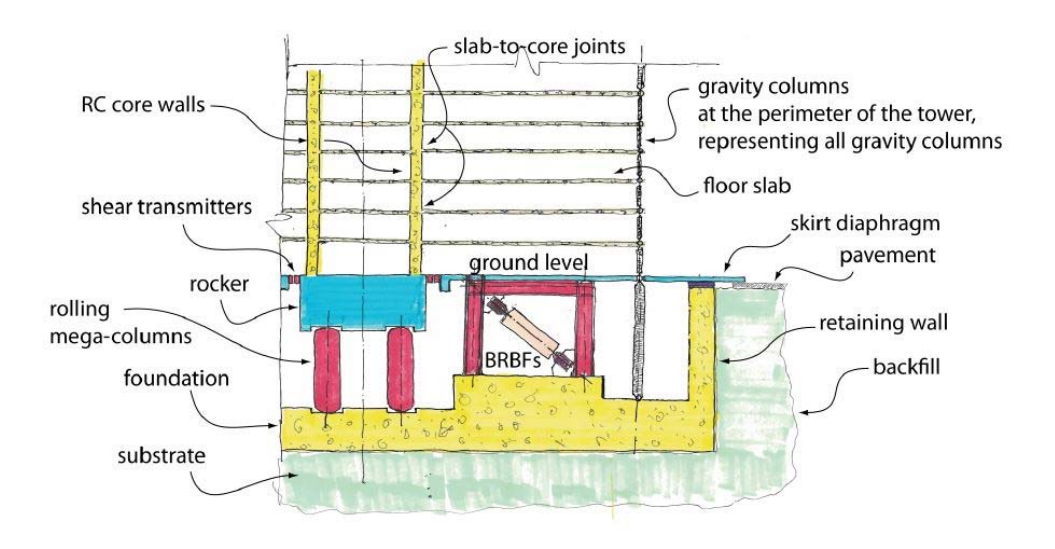


Figure 2-5: MechRV3D system incorporated at the base of superstructure [15]

The central near-rigid block, referred to as the rocker, is cast monolithically with the RC walls assumed as lateral-force-resisting system of superstructure in the initial study. The rocker rests atop four high-capacity columns (in a three-dimensional setup) and is intended to undergo rocking motion by lifting above two or three of these columns, corresponding to line-pivoting (rocking on an edge) and point-pivoting (rocking on a corner) states, respectively. The rocking action initiates at the top of the large columns when the base overturning moments,  $M_b$ , generated by applied lateral forces, calculated about the rocking toe overcome the restoring moment generated by the combined gravity loads of the core of the superstructure and the weight of the rocker about that same point.

The high-capacity columns, referred to as the rolling mega-columns, are positioned centrally to support the rocker directly beneath the superstructure's core. This centralized layout leaves the peripheral space between the rocker and the retaining walls available for the installation of the separate shear mechanism below ground level. Mega-columns with their special endpoints are employed to achieve a reliable and nearly shear-free rocking mechanism by avoiding unpredictable changes in the coefficient of friction from contamination or wear, and sliding uncertainties (potential for stick-slip motion or unintended sliding if friction is overcome) that can compromise performance under real conditions [15].

The term "rolling" refers to the smooth rotational behaviour of the mega-columns, which is enabled by the geometry of their end connections. This geometry creates an instantaneous centre of rotation at the point of contact, allowing the column to undergo large angular displacements with negligible moment resistance. This is fundamentally different from a conventional pinned joint, as it accommodates both rotation and the associated horizontal translation seamlessly [15].

The rocking mechanism functions as an integrated system. When lateral forces induce an overturning moment on the superstructure, the rigid rocker transmits this moment to the supports below. This causes the entire rocker-and-core assembly to tilt, creating compression in the leeward mega-columns while allowing uplift to occur at the windward mega-columns. The rolling connections at the ends of the mega-columns are critical, as they allow the columns to sway and accommodate the horizontal movement of the rocker with negligible shear and moment resistance [15]. Therefore, the combination of the tilting rocker and the accommodating rolling mega-columns constitutes the complete rocking mechanism of the MechRV3D system.

The shear mechanism is located on the periphery of the rocker, as shown in Figure 2-6. It includes a skirt diaphragm, or simply skirt, along with shear fuses that can be a series of buckling restrained braced frames (BRBFs) which connect the skirt to the foundation. The skirt is composed of the ground floor slab outside the central core area, which is designed to function as a rigid diaphragm. This high in-plane stiffness is a critical design requirement, as it ensures uniform engagement of all peripheral shear-resisting elements when lateral loads are transferred from the rocker [15].

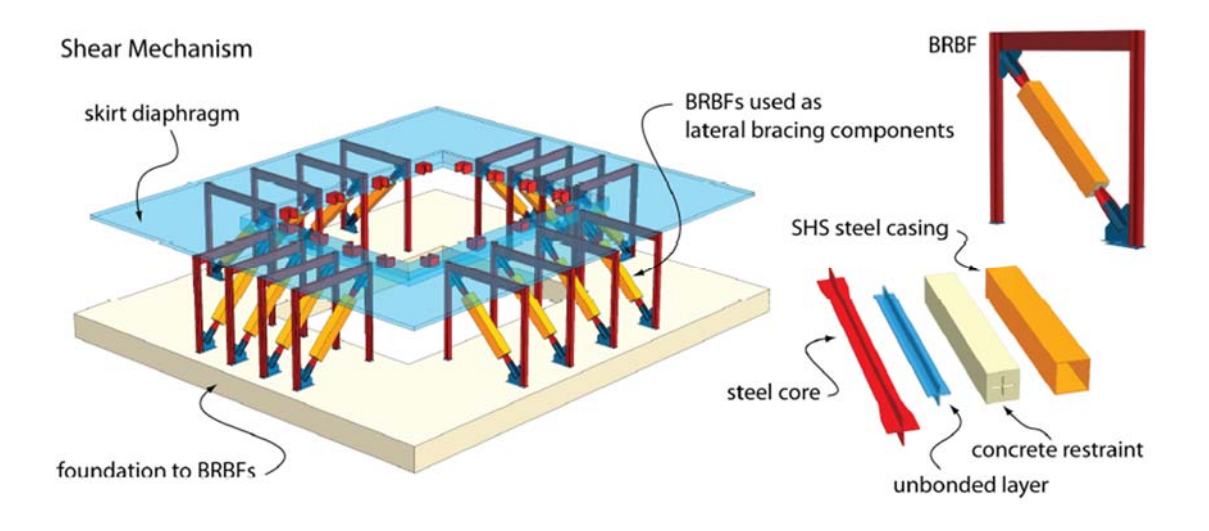


Figure 2-6: Shear mechanism components [15]

The BRBFs are arranged in parallel on each side of the rocker, as shown in Figure 2-6. The base shear of the RC core is transferred to the shear mechanism through a series of connectors between the rocker and the skirt diaphragm. The skirt diaphragm is not cast monolithically with the rocker; instead, there is a gap between them [15].

The rocker transfers shear forces to shear fuses through skirt diaphragm and vertical forces to the mega-columns. This decoupled behaviour is achieved through two types of specialized connections originating from the rocker. The connection between the rocker and skirt diaphragm—attached to the shear fuses—referred to as shear transmitters are designed to transfer shear forces and any torsional moments about the vertical axis. Conversely, to ensure the rocking mechanism is not restrained, the transmitters are detailed to provide negligible resistance to out-of-plane movements, specifically vertical displacement and rotations about the horizontal axes (rocking) [15].

Another key connection in the MechRV3D system is the pipe-pin rolling joint, located at both ends of the mega-columns allows the rocker to uplift freely at the top of the mega-columns. Each mega-column is designed to carry the entire gravity load of the superstructure's core and rocker's self-weight within the elastic range. This is the most critical loading condition for mega-columns that occurs during point-pivoting, where the structure temporarily pivots on a single corner [15].

The rolling mega-columns always remain under compression, preventing them from lifting off the foundation. Since moments are released at both ends due to their end connections' behaviour, these mega-columns do not carry any lateral forces [15]. In the envisioned physical embodiment of the system, the mega-columns would be prefabricated and installed using a dry connection method, where they would be seated into recessed sockets cast into the foundation and the rocker, as shown in Figure 2-7 [15].

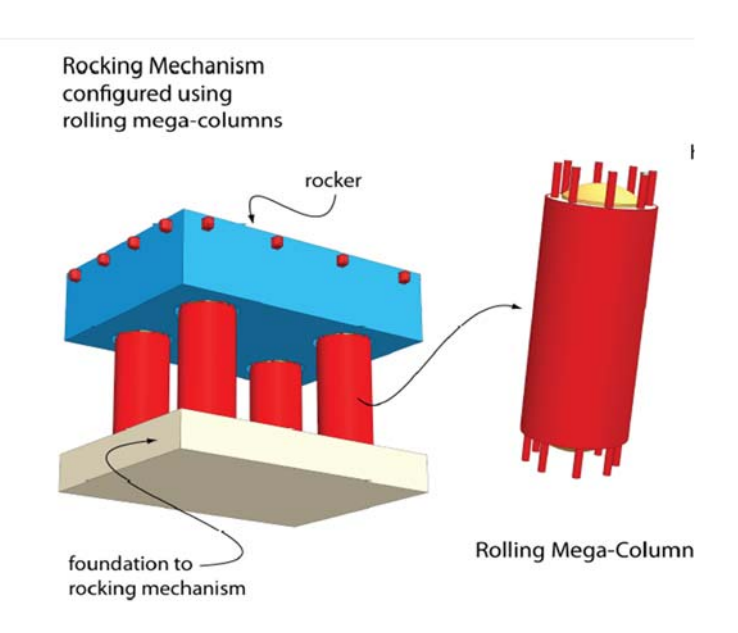


Figure 2-7: Rolling mega-columns between the rocker and foundation [15]

#### 2.5.2. Numerical Validation

The initial research thoroughly investigated the MechRV3D system integrated into a high-rise building, focusing on its structural behaviour and performance under seismic loading. Following the initial conceptual study, a detailed conceptual design for the physical components of the system was developed. The feasibility of the proposed implementation was numerically validated through a 42-story RC core wall building as a case study using pushover and nonlinear response history analyses (NLRHAs).

The case study building was assumed to be in Los Angeles, and design requirement were adopted from the American Society of Civil Engineers (ASCE/SEI 7, 41) codes, as well as related guidelines for designing high-rise buildings such as those from the Los Angeles Tall Buildings Structural Design Council (LATBSDC) and the Performance-based Seismic Design of Tall Buildings (TBI guideline) [18], [47], and [31].

By evaluating the MechRV3D system integrated into a superstructure in the case-study model, the research demonstrated that the MechRV3D system improves seismic performance by establishing a clear strength and deformation hierarchy. All inelastic action

is intentionally confined to the replaceable mechanisms at the base, which act as ductile fuses to limit the forces transmitted to the superstructure. This protective action enables the superstructure, including the primary RC walls, to be capacity-designed to remain essentially elastic even under the Maximum Considered Earthquake (MCE) [15].

#### 2.5.3. Preliminary Design Procedure in the Initial Study

To generalize the findings from the case-study, nonlinear parametric analyses were conducted to develop a preliminary design procedure. These analyses employed the simplified model shown in Figure 2-8, in which the superstructure is represented by an elastic stick model supported at its base by rotational and translational springs simulating the rocking and shear mechanisms, respectively [15].

Using this simplified model, parametric nonlinear analyses were performed on a set of generic RC core-wall buildings with fundamental periods ranging from 1 to 7 sec corresponding to the building height from 45 m to 375 m. The parametric analyses focused on two governing seismic responses: maximum inter-story drift ratio ( $\delta_s$ ), which controls damage in the superstructure, and maximum base displacement ( $\Delta_b$ ) which dictates the demand on the base mechanism and its stability [15].

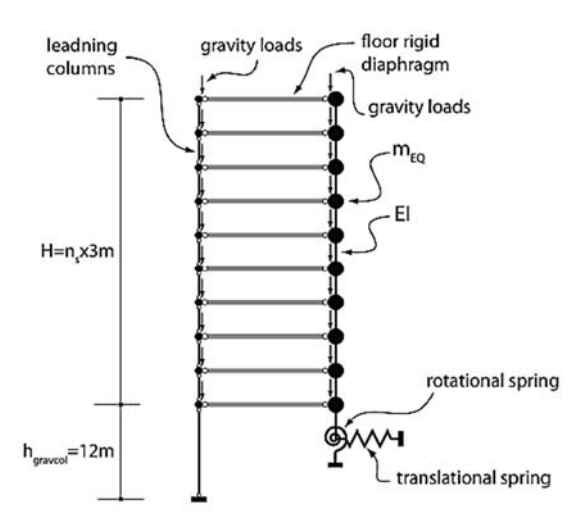


Figure 2-8: Simplified model of the MechRV3D system with a stick-model superstructure [15]

A group of six design parameters was selected to conduct the parametric analyses. These included two superstructure parameters, the fundamental period ( $T_1$ ) and aspect ratio (H/B); one rocking mechanism parameter, the moment reduction factor ( $R_M$ ); and three shear mechanism parameters, the shear reduction factor ( $\mu\nu$ ), relative lateral stiffness of shear mechanism ( $I(K_{b1})$ ), and post-yield stiffness ratio ( $\alpha\kappa$ ). For each parameter, a range of values was chosen to reflect both realistic high-rise buildings application and a spectrum of possible design choices. The parameters related to the superstructure focused on its geometric dimensions. In contrast, the parameters for the MechRV3D mechanisms were limited to stiffness and strength properties, not by the explicit geometry of the components, due to their simplification as springs in the model.

The nonlinear parametric analyses revealed the variation of governing seismic response quantities with the selected design parameters. The analysis results demonstrated a fundamental trade-off between base displacement ( $\Delta_b$ ) and inter-story drift ratio ( $\delta_s$ ), where a stiffer base mechanism reduces base displacement at the expense of increasing inter-story drift ratio in the superstructure, and vice versa. Based on this correlation, design charts were developed for these two response quantities ( $\delta_s$  and  $\Delta_b$ ). A design procedure was recommended using the obtained design charts and range of design parameters to assist in the preliminary design of the proposed system.

In the parametric studies of the MechRV3D system, the mega-columns were not modelled with their actual geometrical properties -particularly their height. This approach introduced two critical limitations for practical design. First, the simplified model provided results in terms of abstract spring properties (e.g., required stiffness). The primary limitation of this approach is its inconvenience for designers, who are left without a direct method to determine the physical component geometries required to achieve those properties. Second, the model could not capture the significant second-order effects generated by the gravity

load (P) acting on the laterally displaced mega-columns ( $\Delta$ ). This P- $\Delta$  effect is critical for assessing the overall stability of the system and was a key uncertainty left unaddressed.

Therefore, the central objective of this research is to develop an explicit design framework by directly investigating the influence of key system-level geometric parameters. While the cross-sectional design of a composite mega-column can follow conventional methods, the mega-column height directly governs the magnitude of the  $P-\Delta$  effect and overall system stability. By treating mega-column height as a primary design variable, this study aims to develop a more practical and direct design procedure for the MechRV3D system.

#### 2.6. Summary

Due to the increasing demand for accommodation in urban areas worldwide, the construction of high-rise buildings has significantly increased as a solution to address this need. Many of these buildings are in regions with high seismicity, making it essential to design them to withstand the challenges posed by significant seismic loads. One of these challenges is the higher-mode effect, which leads to amplified seismic responses in high-rise structures.

To assure more resilient buildings, designers developed some high-performance systems to reduce the impact of seismic excitation. While rocking systems can effectively control damage associated with the fundamental period, they are not efficient to mitigate higher-mode effects. Base isolation systems, on the other hand, are effective in reducing higher-mode effects but they are generally not considered suitable for high-rise building due to their vulnerability to the significant axial loads these structures impose.

A new high-performance dual-mechanism system called MechRV3D system was proposed in 2020. This system decouples shear and flexural responses by employing two separate

mechanisms- rocking and shear - that operate in parallel without interference. In the model used for numerical parametric analyses, some components of the MechRV3D system were represented by nonlinear rotational springs instead of detailed line elements. This simplified model provides a useful starting point for exploring the system's behaviour and conducting initial parametric studies. However, it may not fully capture important structural effects like  $P-\Delta$  effects and negative stiffness, which result from the interaction of gravity loads with lateral displacements due to the system's geometry.

To support the practical application of the MechRV3D system in high-rise, earthquake-resistant buildings, there is a need to further develop and refine the design procedure associated with this system. Introducing mega-columns into the simplified model can help study how different configurations influence  $P-\Delta$  effects and negative stiffness. Updating the parameter ranges can also make the model more representative of practical design cases. These modifications may provide additional insights that can refine the design procedure for improved applicability in practice.

## 3. Methodology

### 3.1. Technical Roadmap

This research aims to develop a preliminary design procedure for the MechRV3D system. The procedure is based on seismic performance spectra, which are developed by conducting a comprehensive suite of nonlinear parametric analyses. The methodology involves the following steps:

- Identify governing design parameters, including newly introduced ones (the height
  of mega-columns and depth of the rocker) that reflect the actual size and role of the
  rocking components. Determine suitable ranges for these parameters based on
  structural behaviour and feasibility.
- Develop a simplified numerical model using OpenSeesPy [48]. The modelling approach remains consistent with the initial study of MechRV3D system, but the current model improves the representation of P–Δ effects and negative stiffness resulted from lateral displacement of mega-columns.
- Select two high-seismicity locations, Los Angeles (USA) and Vancouver (Canada), for input ground motions. Choose and scale ground motion records to the MCE level, following current building codes [18] [49], and high-rise buildings' guidelines [47] [50].
- Perform NLRHAs for the full set of parameter combinations and selected ground motions. Use the results to construct seismic performance spectra that relate design parameters to structural responses.

Based on the seismic performance spectra obtained from this approach, the design procedure is developed in the next chapter. This facilitates a generalized design of the

system by evaluating structural responses and identifying suitable parameter ranges for practical application.

#### 3.2. Design Parameters

#### 3.2.1. Fundamental Period $(T_1)$ of Generic Buildings

The parametric analyses were conducted on a series of generic high-rise buildings in which RC core walls serve as the lateral-force resisting system. The height of these buildings, ranges from 45 m to 360 m, or 15 to 120 stories, assuming a typical story height of 3 m. The fundamental period ( $T_1$ ), a key dynamic characteristic of a structure, is a function of its mass, lateral stiffness and building height.

Code provisions provide empirical  $T_1$ -H formulas for different lateral force-resisting systems which allows for the back-calculation of an effective lateral stiffness when the period and mass are known.  $T_1$  is selected as one of the design parameters in the parametric analyses, serving also as a representative measure of building height.

To establish a realistic relationship between the height and fundamental period for these generic RC core wall buildings, an appropriate empirical formula was required. While the overall design framework of this study is consistent with US practice (ASCE), a direct comparison with measured building data is essential for selecting the most accurate period estimation method.

A study by Ha et al. [51] compared the obtained fundamental period from the ambient vibration measurement to the computed values from the KBC 2009 and ASCE 7-10 empirical formulas. As it can be seen in Figure 3-1, they found that the fundamental periods resulted from KBC 2009 formula are closer to the experimental measurement values [51]. Therefore, despite the study's North American context, the KBC 2009 formula was selected for this research on the basis of its superior, experimentally-validated accuracy. It should

be noted that for the specific case of a reinforced concrete core wall building, the primary formula for *T* in ASCE 7-10 to ASCE 7-22 has not changed [18].

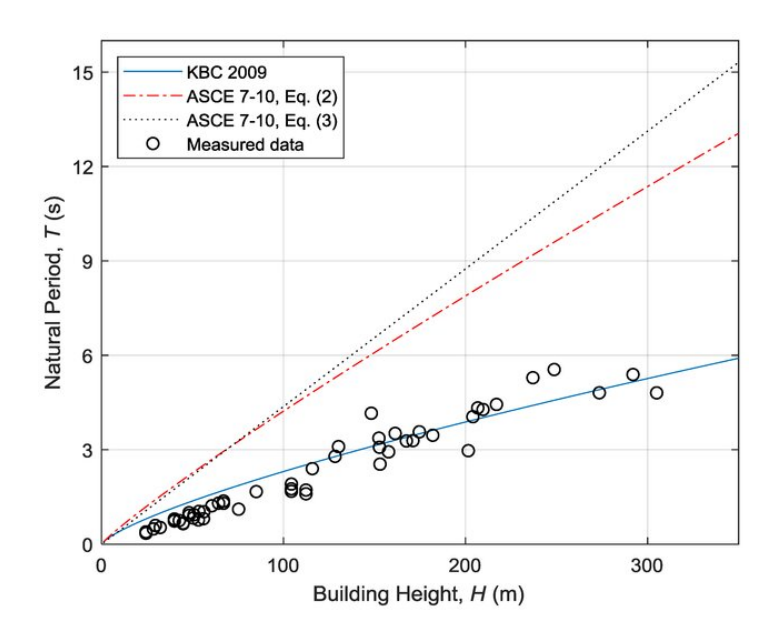


Figure 3-1: Comparison of fundamental periods from KBC 2009 and ASCE 7-10 empirical formulas with measured fundamental periods (*T*) with ambient vibration method [51]

Equation 3-1 shows the KBC 2009 formula to calculate the fundamental period for RC core wall building using the height of the structure,

$$T = 0.073H^{0.75} (3-1)$$

where T is the fundamental period (s), and H is the building height (m).

Table 3-1 shows the approximate fundamental periods calculated for the generic buildings using Equation 3-1. The results confirm that the fundamental periods for the range of building heights considered (15 to 120 stories) fall in the approximate range of 1 to 6 seconds, with each period corresponding to a specific building archetype. For the parametric study, a set of discrete, idealized target periods ( $T_1 = \{1, 2, 3, 4, 5, \text{ and } 6\}$  s) was then selected to define these generic building archetypes. This approach creates a clear, evenly-spaced parameter matrix, which significantly facilitates the development and interpretation of the seismic performance spectra.

Table 3-1: Fundamental periods of generic RC buildings using KBC 2009 formula

Building Height (m)	Number of stories	T <sub>1</sub> (sec)	Selected $T_1(sec)$
45	15	1.27	1
90	30	2.13	2
150	50	3.13	3
210	70	4.03	4
300	100	5.26	5
360	120	6.03	6

#### 3.2.2. Aspect Ratio (*H/B*) of Generic Buildings

The plan dimension, B, expressed through the aspect ratio (H/B) of the buildings, is another design parameter considered in this study. According to previous studies, aspect ratios larger than 7 lead to a significant increase in base shear, base overturning moment and interstory drift ratio. As a result, the design of RC core wall buildings with such high slenderness becomes inefficient and cost-ineffective [52], [53].

Therefore, it is suggested to check the aspect ratio as one of design parameters. In this research, the aspect ratio of the buildings is restricted to a range between 3 and 6 to be theoretically close to the optimal value of the aspect ratio for high-rise building design [54]. For all buildings in this study, the floor plan is like the typical plan shown in Figure 3-2 with the RC core located at the centre of the floor. The plan dimensions (B) are back calculated based on the assigned height of building (H) and aspect ratio (H/B). The resulting B values are close to those commonly used in practical design.

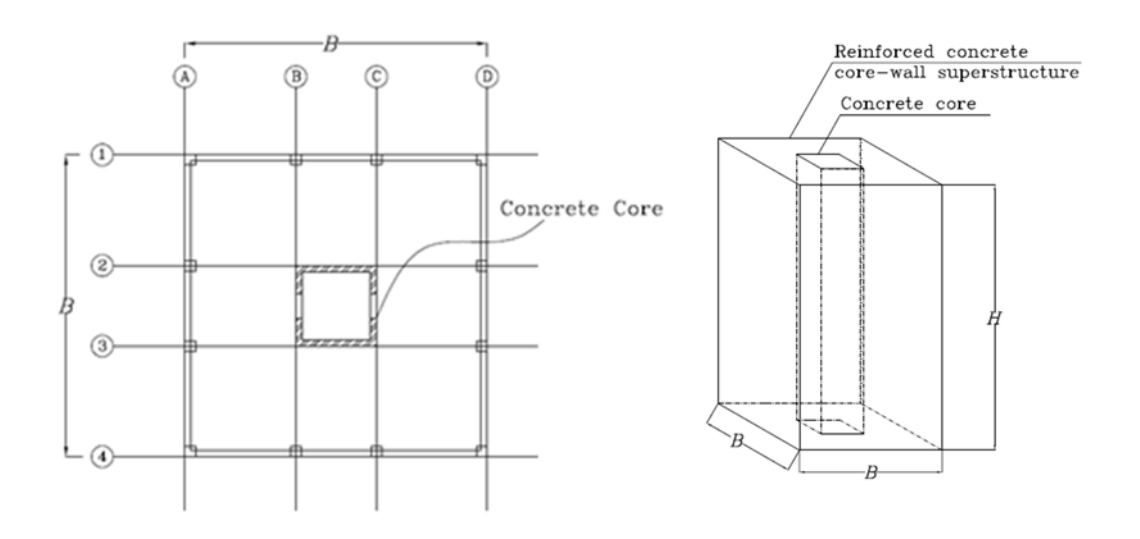


Figure 3-2: Typical floor plan of the generic buildings (left), height and width of a building to calculate aspect ratio, H/B (right)

For each floor, a uniformly distributed area load, w=10 kPa is assumed including dead and live loads according to practical design [50]. Seismic mass,  $m_{EQ}$ , that is lumped at each floor level, is computed based on assumed uniformly distributed load (w) and floor area (B). The parameters for each of the generic buildings in this study, along with the values derived from the preceding assumptions, are summarized in Table 3-2.

Table 3-2: Properties of the generic buildings

Number of stories (n)	Height,  H (m)	Aspect ratio (H/B)	Floor dimension, B (m)	Selected $T_1(s)$	Mass of floor, $m_{\rm EQ}$ (t)	EI (MN·m²)	T <sub>1a</sub> from analysis (s)
15	45	3	15	1	229	1.00×10 <sup>6</sup>	1.04
30	90	4	22.5	2	516	9.01×10 <sup>6</sup>	2.08
50	150	5	30	3	917	5.49×10 <sup>7</sup>	3.09
70	210	5	42	4	1798	2.33×10 <sup>8</sup>	4.11
100	300	6	50	5	2548	8.79×10 <sup>8</sup>	5.13
120	360	6	60	6	3669	1.82×10 <sup>9</sup>	6.16
120	300	<u> </u>		<u> </u>	3009	1.02^10	0.10

For parametric analyses, the superstructure was represented by a simplified stick model with a uniform flexural rigidity (EI) over its height. This uniform value is not a realistic representation of a tapered structure, but an equivalent stiffness calibrated to ensure the model accurately achieves its target fundamental period ( $T_1$ ). This simplification is a standard and computationally efficient method in structural dynamics for capturing the global response needed to evaluate the base mechanism [5]. To find the value of EI (N.m<sup>2</sup>), Equation 3-2 is used,

$$EI = \frac{4\pi^2 H^4 m}{(\beta_1 H)^2 T_1^2} \tag{3-2}$$

where  $T_1$  is the fundamental period (s). H and m are the total height (m) and total mass ( $n \times m_{EQ}$  (kg)), respectively.  $\beta_1 H$  (unitless) is assumed equal to 1.8751 form the initial study for fixed-based conditions that was used in the same theoretical equation to obtain EI [15]. The fundamental periods ( $T_1$ ) used to define the generic building archetypes are based on the effective linear-elastic stiffness of the superstructure in its undamaged state. The target  $T_1$  values were derived from the KBC 2009 empirical formula, which is calibrated against periods measured from real, in-service buildings under low-amplitude ambient vibrations. This measured period implicitly accounts for the effects of existing microcracking and non-structural components [51]. This approach is consistent with the primary design objective of the MechRV3D system, which is to protect the superstructure and ensure it remains essentially elastic, thereby preventing the significant stiffness degradation associated with yielding and large-scale cracking.

With given  $m_{EQ}$  and EI, eigenvalue analyses were conducted for each of the generic buildings using the simplified model of superstructure fixed at the base. The modelling assumptions were consistent with those that will be discussed in Subsection 3.5.1. Accordingly, the value of  $T_{1a}$  (the actual fundamental period) was determined for each

building and is presented in the last column on the right of Table 3-2. As it can be seen, the values of  $T_{1a}$  are close to selected values for  $T_1$ .

The choice to back-calculate EI using a formula based on Euler-Bernoulli (pure flexure) beam theory (Equation 3-2), which neglects shear deformations, is a deliberate and justified simplification appropriate for this study. A more complex Timoshenko beam model would require defining separate flexural and shear rigidities [5], adding unnecessary complexity and assumptions for a parametric study focused on the base mechanism. Moreover, for beams with a length-to-depth ratio up to 5, Euler-Bernoulli beam theory provides a reasonable estimation for the first two natural frequencies [55]. In the present study, the Euler-Bernoulli assumption was used to estimate the fundamental period, and the corresponding slenderness ratio of the modeled buildings was limited to 6. Although this slightly exceeds the recommended limit, it is still considered reasonable for estimating the first mode. Therefore, the standard and widely accepted approach of using a single equivalent stiffness parameter was adopted, where the EI is calibrated to ensure the simplified model matches the target global dynamic response  $(T_1)$ .

#### 3.2.3. Moment Reduction Factor $(R_{\rm M})$

The MechRV3D system is designed for a sequential activation of its two primary mechanisms to optimize seismic performance. For the scope of this study, the research focuses on high-seismicity regions where the seismic design requirements, rather than wind-induced forces, are the primary drivers for the configuration and proportioning of the structural system.

Within this framework, the design philosophy dictates that the superstructure must remain elastic during frequent events. To achieve this, the activation threshold of the rocking mechanism ( $M_{\text{rock}}$ ) is calibrated to be equal to the base overturning moment demand at the

Service Level Earthquake ( $M_{b,SLE}$ ). This provides a predictable flexural fuse that engages only when seismic demands exceed the serviceability level, thereby protecting the mechanism from inelastic damage during frequent earthquakes.

A direct determination of  $M_{b,SLE}$  often requires a site-specific SLE response spectrum, which is not always readily available from standard seismic hazard tools [56], [57]. To create a more direct preliminary design path, this study, following the approach in Tong [15] establishes a Moment Reduction Factor ( $R_{\rm M}$ ). This unitless factor conceptually relates the moment at the Maximum Considered Earthquake ( $M_{\rm b,MCE}$ ), which is readily available from hazard analysis, to the target activation moment ( $M_{\rm rock}$ ) (Equation 3-3):

$$R_M = \frac{M_{b,MCE}}{M_{b,SLE}} \tag{3-3}$$

This  $R_{\rm M}$  factor therefore represents the ratio of the MCE demand to the SLE demand. This approach is supported by guidelines like the CTBUH's "Performance-based Seismic Design for Tall Buildings" [20], which indicates that this ratio typically falls within a range of 4 to 8. This range is consistent with the specific sites considered in this study: the ratio for Los Angeles is approximately 8 [58], while for Vancouver, it is calculated around 4.

It is critical to note that this methodology applies the reduction factor  $R_{\rm M}$  directly to the full MCE-level demand. This is philosophically consistent with the Canadian design approach (NBCC) [28], but differs from the standard prescriptive approach in the United States (ASCE 7), where force reduction factors are typically applied to the Design Basis Earthquake (DBE) demand, defined as 2/3 of the MCE [18]. The direct-to-MCE approach is deliberately adopted for this performance-based procedure because it provides a clearer and more direct relationship between the ultimate seismic hazard and the defined capacity of the protective mechanism.

Based on this framework, for the parametric analyses in this study, the range of moment reduction factor ( $R_{\rm M}$ ) is selected as follow:

$$R_{\rm M} = \{4, 6, 8\}$$

#### 3.2.4. Rocker Depth (D) and Mega-Column Spacing ( $d_{c2c}$ )

In the previous section, the required rocking moment (N.m),  $M_{\text{rock}}$ , was established as the design demand. The next step is to size and configure the physical system to provide sufficient resistance to the expected loads. The moment resistance of rocking mechanism is generated by the self-weight of the structure (weight of the rocker (N),  $W_{\text{rckr}}$ , and the gravity loads tributary to the core wall of the building (N),  $W_{\text{core}}$ ) acting at the lever arm defined by the distance (m) between the pivot point and the centre of gravity of the superstructure when rocking occurs. The pivot point in this system is top of one of the mega-columns. Regarding the symmetry of the model, the lever arm would be the half of the centre-to-centre distance between two mega-columns which is represented by  $d_{c2c}$  (refer to Figure 3-16).

Additionally, as discussed in the initial study,  $M_{\text{rock}}$  would be approximately constant during earthquakes, because 95% of central core loads ( $W_{\text{core}}$ ) originated from the dead load (weight) that is constant [15]. Considering the moment resistance equal to  $M_{\text{rock}}$ , Equation 3-4 can be used.  $W_{\text{core}}$  (assumed as 50% of total gravity load) and  $W_{\text{rckr}}$  are referred to as structural weight ( $W_{\text{SC}}$ ).

$$d_{\rm c2c} = \frac{2 (M_{\rm rock})}{W_{\rm core} + W_{\rm rckr}} = \frac{2M_{\rm rock}}{W_{\rm SC}}$$
(3-4)

The weight of the superstructure is a function of the height of the building, and it can be obtained from the mass of the floors in Table 3-2. Thus, for each of the generic buildings,

it has a designated value. Consequently, the weight of the rocker and the mega-columns spacing ( $d_{c2c}$ ) are variables in Equation 3-4.

To determine  $d_{c2c}$ ,  $M_{rock}$  is substituted by  $M_{b, SLE}$  in a specified site. To calculate  $M_{b, SLE}$ , the time history analyses under 11 scaled ground motion at the MCE level was conducted in a fixed-base condition for each of the generic buildings listed in Table 3-2. From the analysis results, an average of maximum response of base overturning moments ( $M_{b, MCE}$ ) is obtained and  $M_{b, SLE}$  will be determined from dividing  $M_{b, MCE}$  by  $R_{M.}$ 

The remaining variables in Equation 3-4 are the centre- to centre space between megacolumns ( $d_{c2c}$ ), which is part of the geometric dimension of the rocker at the bottom face, and  $W_{rckr}$ , which is a function of the rocker's volume and depends on its dimensions, including the depth of the rocker (D). To satisfy the required  $M_{rock}$  ( $M_b$ , SLE), a set of geometrically feasible dimensions of  $d_{c2c}$  and D must be achieved.

To find a ratio between  $d_{c2c}$  and D, the rocker can be considered as a deep beam placed on mega-columns as its supports. In a deep beam, the ratio of span to the depth should be less than 4 [59], [60]. In this case,  $d_{c2c}$  can be considered as span length of the beam. Thus, the  $d_{c2c}$  is assumed to be less than four times the rocker depth (D) to satisfy the deep beam's practical check and ensure the required rigidity of the rocker block.

This beam is imposed to the applied vertical load ( $W_{core}$ ) acting as shear force and lateral load acting as axial load on it in this context. The rocker is intended to slightly rotate atop of mega-columns, and it is not fixed to them. Therefore, rocker as a deep beam can be designed only for shear and axial loads and there is no need to design it for flexure.

The shape of the rocker is assumed to be an inverted truncated square pyramid (refer to Figure 3-16), where both the top and bottom faces are square. The rocker consists of concrete with steel elements embedded within it [15], and its unit weight ( $\gamma_c$ ) is assumed to

be 24,522 N/m³. Equation 3-5 for volume of an inverted truncated square pyramid (m³) is used:

$$V = \frac{D}{3} \times (A_1 + A_2 + \sqrt{A_1 A_2}) \tag{3-5}$$

where D is the depth of the rocker (m), and  $A_1$  and  $A_2$  represent the areas of the top and bottom faces of the rocker (m<sup>2</sup>), respectively. If the side lengths of the top and bottom square faces are assumed to be  $d_{c2c}+3$  m and  $d_{c2c}$ , respectively, then the weight of the rocker ( $W_{rckr}$ ) can be calculated using Equation 3-6:

$$W_{\text{rckr}} = \gamma_c \times D \times (d_{c2c}^2 + 3d_{c2c} + 3)$$
 (3-6)

The rocker depth (D) is assumed to range from 4 to 12 m (depth values larger than 12 m may not be practical).

$$D = [4, 12] \text{ m}$$

Using Equations (3-3), (3-4), (3-6), and the range assumed for D, the corresponding values of  $d_{c2c}$  for each of the generic buildings are calculated based on the specified values of  $M_{rock}$  ( $M_{b, SLE}$ ) and  $W_{core}$ . The obtained values for  $d_{c2c}$  are shown in Figure 3-3 as a function of D. In this case,  $R_{M}$  was assumed to be 8 and  $M_{b, MCE}$  was calculated for the Los Angeles site.

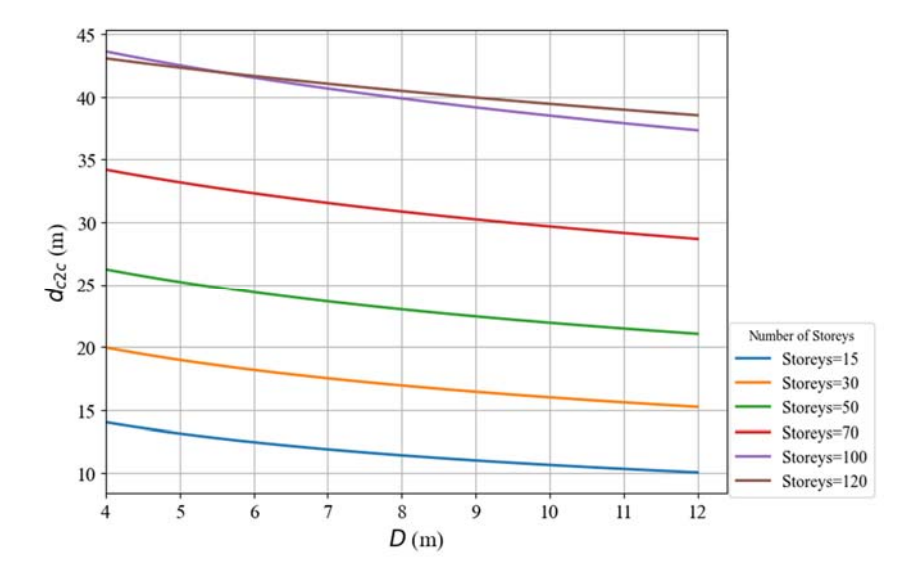


Figure 3-3: The variation of  $d_{c2c}$  with rocker depth (D) for  $R_{\rm M} = 8$ 

To observe the variation in more detail, Figures 3-4 and 3-5 display the graph for 15-and 120-story buildings. When the rocker depth is 4 m, the corresponding value for  $d_{c2c}$  is obtained approximately 9.70 and 22.85 m for 15- and 120-story respectively.

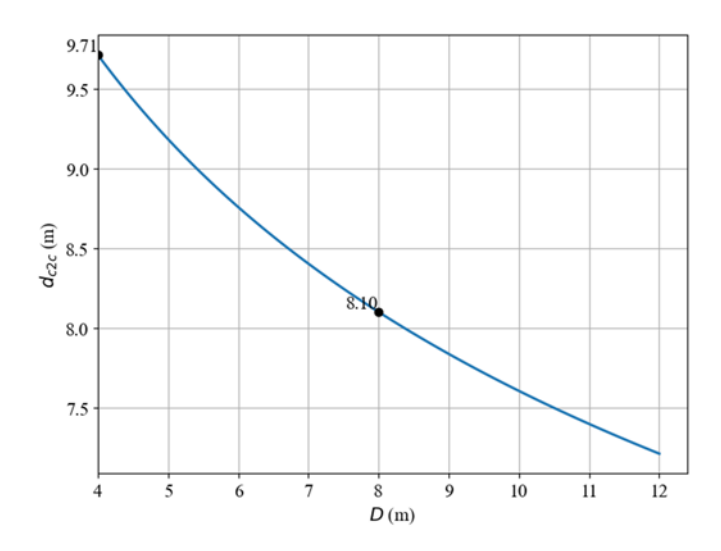


Figure 3-4: The variation of  $d_{c2c}$  with rocker depth (D) for 15-story building,  $R_M=8$ 

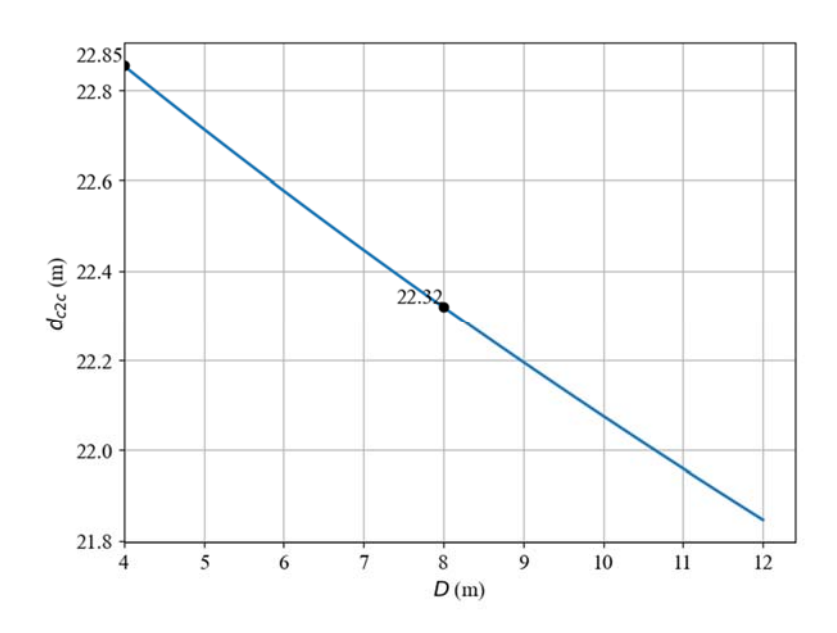


Figure 3-5: The variation of  $d_{c2c}$  with rocker depth (D) for 120-story building,  $R_M=8$ 

The graphs for all generic buildings and all values of  $R_{\rm M}$ , are summarized in Appendix A for both Los Angeles and Vancouver sites. Table 3-3 shows the mega-columns spacing  $(d_{\rm c2c})$  and the rocker depth (D) for each value of  $R_{\rm M}$  at the Los Angeles site as they should

be considered in parametric analyses. All  $(d_{c2c}/D)$  values are less than 4, as expected, consistent with the deep beam assumption.

Table 3-3:  $d_{c2c}$  and D values of the rocker for different values of  $R_{\rm M}$  for Los Angeles site

Number of stories (n)		$R_{\rm M} = 4$			$R_{\rm M} = 6$			$R_{\rm M} = 8$	
	$d_{ m c2c}$ (m)	<i>D</i> (m)	$d_{c2c}/D$	d <sub>c2c</sub> (m)	<i>D</i> (m)	$d_{c2}$ / $D$	d <sub>c2c</sub> (m)	<i>D</i> (m)	$d_{c2}$ / $D$
15	14.0	4.0	3.5	11.4	4.0	2.8	9.7	4.0	2.4
30	20.0	5.0	4.0	15.5	5.0	3.1	12.2	5.0	2.4
50	24.0	6.5	3.7	19.6	5.0	3.9	15.2	5.0	3.0
70	31.0	8.0	3.9	23.8	6.0	4.0	18.8	5.5	3.4
100	38.5	10.0	3.8	29.5	8.0	3.7	23.5	6.0	3.9
120	39.0	11.0	3.5	29.0	7.5	3.9	22.5	6.5	3.5

It should be considered that vertical ground acceleration may cause  $M_{\text{rock}}$  to fluctuate by 25% to 30% around the constant component created by gravity loads (N),  $W_{\text{SC}}$  [15]. This estimated range is consistent with established seismic design principles [18]. To account for this fluctuation, the obtained values(m) for  $d_{\text{c2c}}$  could be increased accordingly. However, in the current study, the vertical effect of earthquakes is not considered. Therefore, this increase is not applied in the values of  $d_{\text{c2c}}$  in Table 3-3.

Considering the different values (m) of D and  $d_{c2c}$  corresponding to each  $R_M$  values in Table 3-3, the rocker weights ( $W_{rckr}$ ) also change accordingly. The different values of the rocker weight ( $W_{rckr}$ ) can be expressed as a ratio to the weight of the core stick ( $W_{core}$ ), which remains constant in each case. Table 3-4 summarizes these ratios corresponding to different  $R_M$  values at the Los Angeles site for all generic buildings.

Table 3-4: The ratio of weight of the rocker to the weight of the core stick for different  $R_{\rm M}$  values at the Los Angeles site

Number of stories (n)	M (MNI)	H/ (MN)	Wrckr /Wcore (%)			
	$M_{ m b,MCE}({ m MN}\cdot{ m m})$	$W_{\rm core}$ (MN)	$R_{\rm M}=4$	$R_{\rm M}=6$	$R_{\rm M}=8$	
15	1,138	16.8	140	97	73	
30	4,832	75.9	75	47	30	
50	15,760	225.0	42	24	15	
70	50,756	617.4	28	15	9	
100	126,462	1250.0	24	13	7	
120	202,791	2160.0	15	7	4	

The choice of such a large upper limit value of 12 m for rocker depth was included in the parametric study not as a practical design recommendation, but to fully explore the theoretical design space and understand the system's sensitivity. While likely impractical due to cost and constructability, its inclusion was methodologically necessary to define the complete relationship between the rocker depth (D) and the required mega-column spacing  $(d_{c2c})$ . The rocker depth indirectly influences the seismic response by controlling this critical geometric relationship, forcing the designer to make a practical trade-off between a deeper, heavier rocker and a wider, potentially more intrusive mega-column layout.

#### 3.2.5. Mega-Column Height (h<sub>c</sub>)

The height of mega-columns is introduced as a new design parameter, which was not considered in the previous study [15]. The rocking mechanism is designed such that no tensile forces are transferred to the mega-columns when the rocker uplifts from their tops. This prevents the mega-columns from being pulled out of their foundations. Therefore, the

mega-columns are expected to carry only axial compression under vertical loading. The maximum compressive force in each mega-column corresponds to  $W_{\rm SC}$  ( $W_{\rm core} + W_{\rm rckr}$ ) assuming all vertical loads are carried by a single mega-column when uplift occurs at the top of the other columns.

Additionally, the mega-columns are not subjected to horizontal shear forces or bending moments, which is achieved through a special end connection - pipe-pin rolling joints - at their ends, as will be discussed in Subsection 3.5.2. When a lateral load is applied, the mega-columns sway and roll at these joints instead of bending. To control the horizontal displacement at the top of the mega-columns — which affects their stability and the seismic behaviour of the whole system — their height must be carefully selected.

Design of mega-columns includes prevent buckling (loss of stability) and axial compressive resistance under any circumstances. The mega-columns need to have different cross-sectional areas corresponding to the  $W_{SC}$  of each generic building. They should continue to serve as the supports for the entire structure while they remain in their elastic range. If they enter the inelastic range and experience plastic deformation along their height ( $h_c$ ), they will need to be replaced for future use, which is neither economical nor feasible, especially since they must continuously carry significant gravity loads.

A steel-reinforced concrete (SRC) section is assumed for designing the mega-columns (Figure 3-6). Eurocode 4 [61] was selected to design this section which is consistent with initial study [15], and its provisions are well-suited for unconventional, heavily reinforced composite sections. The mega-column section in this design is composed of several components. The main body consists of concrete encased in multiple steel tubes, along with additional reinforcing elements. Each part of the steel reinforcement in these columns is designed to perform a specific function, as explained in detail in the initial study [15].

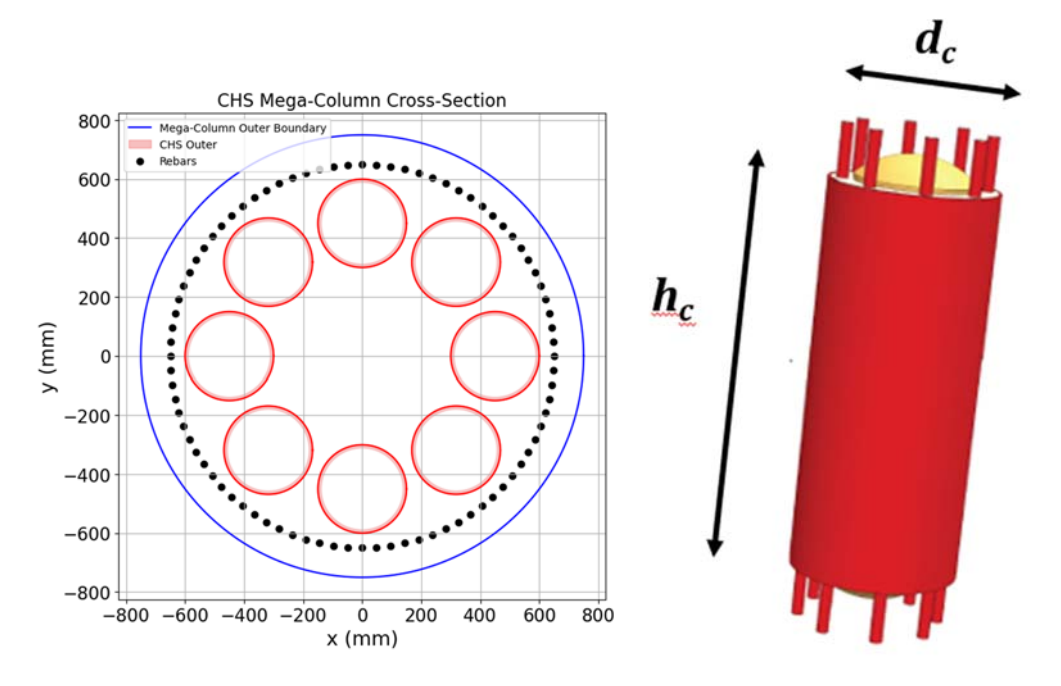


Figure 3-6: Modelling the cross-sectional area of mega-columns,  $d_c$ =1500 mm (left), dimensions of mega-columns [15] (right)

The yielding stresses for the structural steel and longitudinal bars are assumed to be 450 MPa and 500 MPa, respectively. The specified compressive strength of concrete is 60 MPa. Material strength unitless reduction factors of 0.9, 0.85, and 0.65 are applied for steel, reinforcement and concreter material of mega-columns respectively [61]. Based on the Eurocode 4, the number of Circular Hollow Steel sections (CHS), their wall thickness, diameter, and other geometric properties of the steel components (mm) can be determined for a SRC section [61].

To calculate the flexural rigidity of the mega-columns ( $EI_{eff}$ ), a unitless concrete creep coefficient of 0.5 was assumed to account for the long-term effects of sustained loads on concrete stiffness. Additionally, a unitless reduction factor of 0.6 was applied to account for concrete cracking addressing the effects of secondary moments induced by deformation, imperfections, and lateral displacements [61].  $EI_{eff}$  is also essential for determining the Euler buckling load, which is used to calculate the factored total resistance considering buckling ( $N_{pl,b,Rd}$ ) in MN. The factor used in this calculation ( $\chi$ ) was adopted from Eurocode

3 [62] because its methodology is seamlessly integrated with the composite design rules of Eurocode 4.

To maintain an efficient and economical design, a range of diameters  $\{1000, 1500, 2200, 3500, 5000, and 6400\}$  mm was assumed for the mega-columns. The application of such large-scale columns is exemplified by iconic structures such as the Shanghai Tower [63], which utilizes composite mega-columns approximately 5 m in diameter at its base. These values were selected to provide adequate space for the various components of the multiple steel sections while minimizing the column diameter ( $d_c$ ) as much as possible, considering the strength demand. Each value in this range can be assigned to one of the generic buildings. However, the final choice of mega-column diameter for each generic building should be based on a comparison between the applied gravity load and the load-bearing capacity of each case.

Subsequently, a series of analyses was conducted to determine design demands of mega-column, treating the mega-column height ( $h_c$ ) as a variable while keeping the cross-sectional properties, including the mega-column diameter,  $d_c$ , constant to assess the influence of  $h_c$  on design demands. This process resulted in a range of feasible mega-column heights ( $h_c$ ) corresponding to specified diameters for each of the generic buildings. To ensure sufficient space for the shear mechanism underground at the base of superstructure (the shear mechanism is assumed to be BRBFs in this study), a minimum  $h_c$  of 2.5 m was set as the lower bound of mega-column height, corresponding to the typical height of a one-story basement. The upper bound was set at 33 m, that is greater than the allowable slenderness ratio obtained for the mega-columns in the case of a 120-story superstructure (29 m). However, from a practical perspective, this large upper bound will not be adopted as the recommended limit for the parametric analysis of the MechRV3D system.

Figures 3-7 and 3-8 illustrate the axial compression capacity (factored total resistance considering buckling,  $N_{\rm pl,b,Rd}$  in MN) for each specified diameter at different mega-column heights. The applied load was considered with 10 percent increase to account for some possible changes in the construction of the rocker. Using these graphs, designers can determine the required mega-column height based on the given diameter ( $d_c$ ) and the expected applied vertical load that should be compared to ( $N_{\rm pl,b,Rd}$ ). Figure 3-7 presents the full range of results, while Figure 3-8 focuses on smaller diameters, whose variations with height are less distinguishable in Figure 3-7.

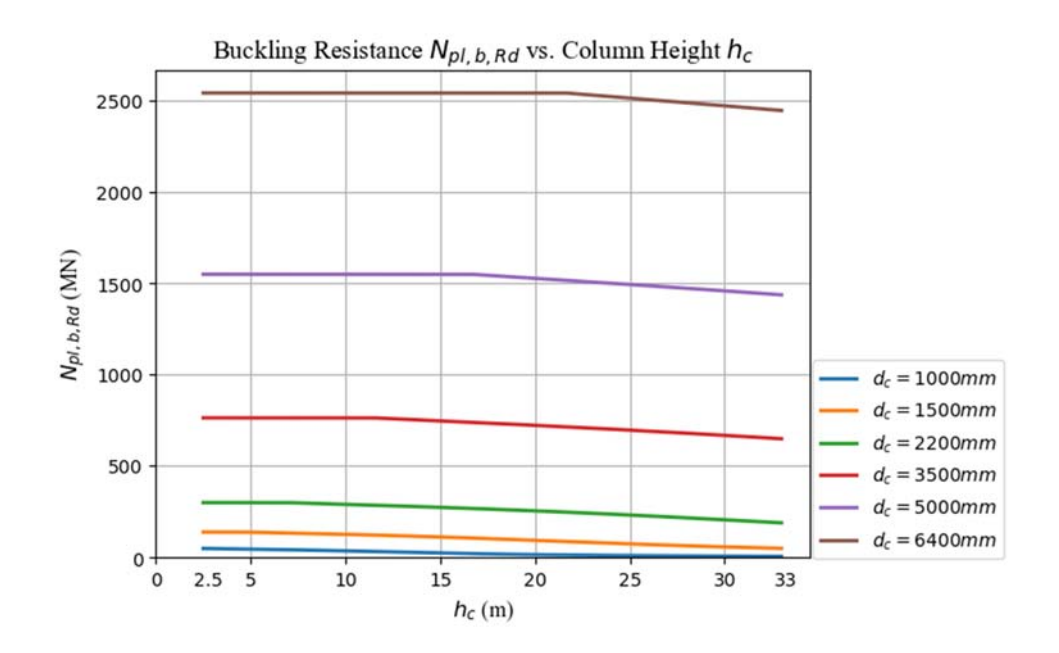


Figure 3-7: Results of analyses to design mega-columns (diameters: 1000-6400 mm)

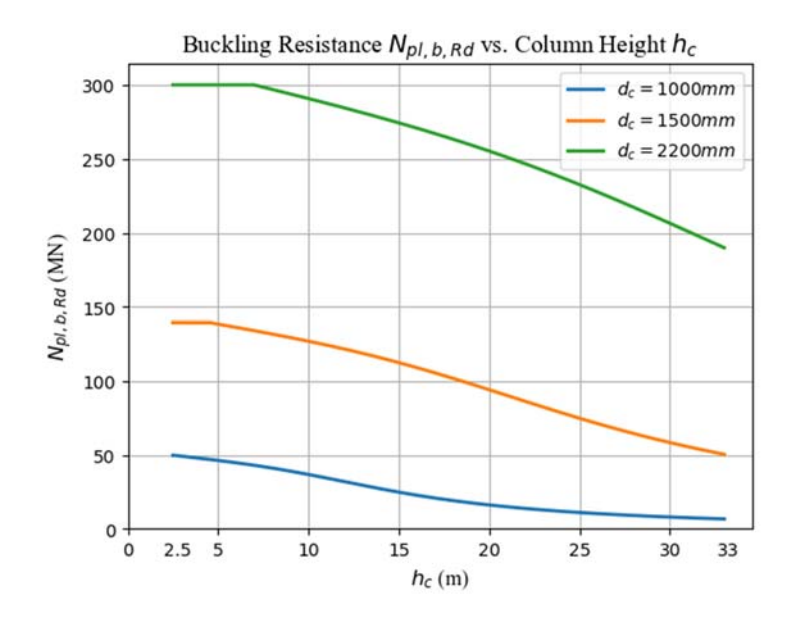


Figure 3-8: Results of analyses to design mega-columns (lower diameters: 1000-2200 mm)

In these graphs, the maximum buckling resistance ( $N_{\rm pl,b,Rd}$ ) corresponds to the minimum height (2.5 m) for each specified diameter. As observed, increasing the height ( $h_{\rm c}$ ) leads to a reduction in axial compression capacity or buckling resistance. However, this reduction is not uniform across all diameters; for larger diameters, the decrease in buckling resistance occurs more rapidly.

Figures 3-9 to 3-14 provide a tool for determining the upper bound (maximum allowable) of mega-columns height with diameters of 1000 mm, to 6400 mm. The red line in each figure represents the expected vertical load ( $W_{SC}$ ) corresponding to one of the generic buildings with 10 percent increase (1.1  $W_{SC}$ ).  $W_{SC}$  in these graphs are calculated based on  $W_{core}$  listed in Table 3-4 and  $W_{rekr}$  corresponding to  $R_{M}$ =8 for the Los Angeles site. In each graph, the minimum required diameter from the assumed list was assigned to each generic building. The green lines denote the maximum applicable height ( $h_c$ ) that satisfies the buckling resistance requirements for the corresponding applied  $W_{SC}$ .

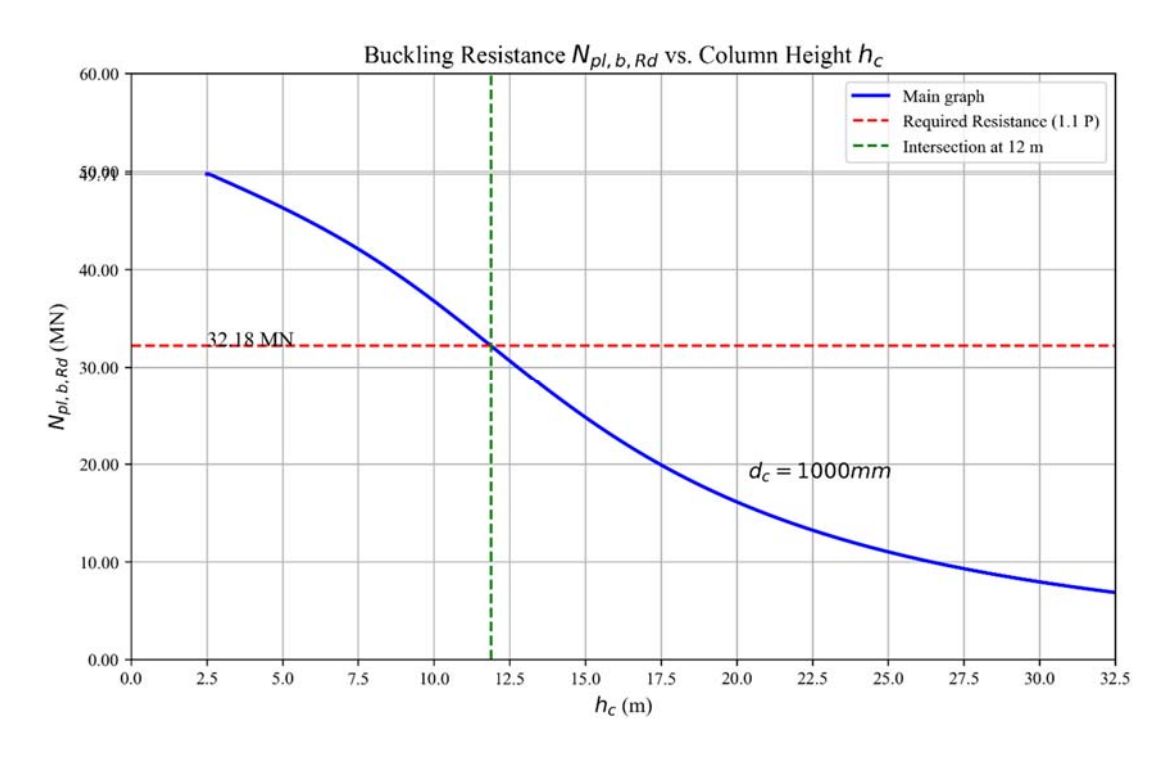


Figure 3-9: Maximum height of mega-column suggested for 15-story building, column diameter =1000 mm

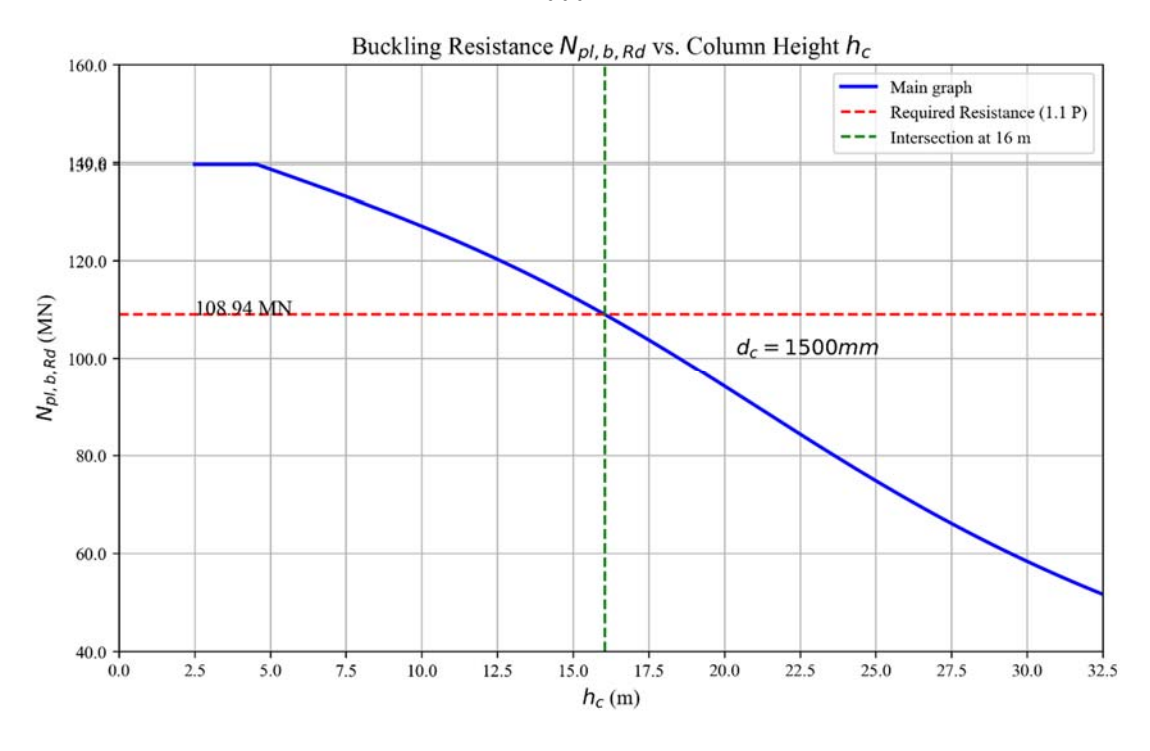


Figure 3-10: Maximum height of mega-column suggested for 30-story building, column diameter =1500 mm

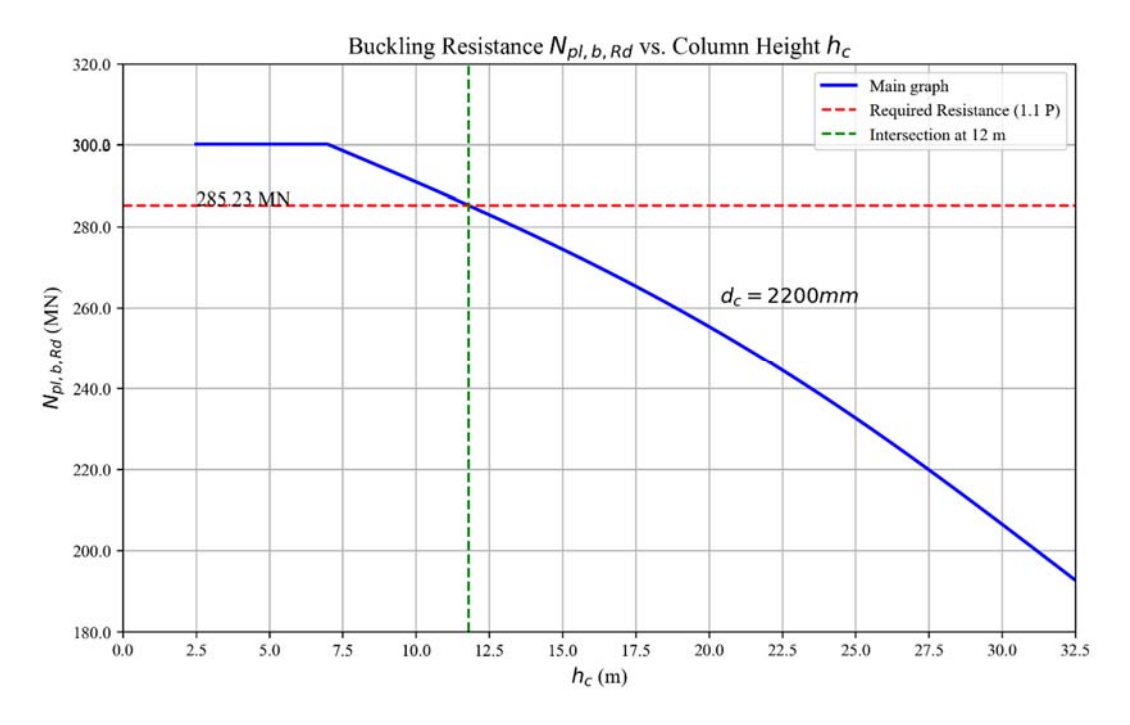


Figure 3-11: Maximum height of mega-column suggested for 50-story building, column diameter =2200 mm

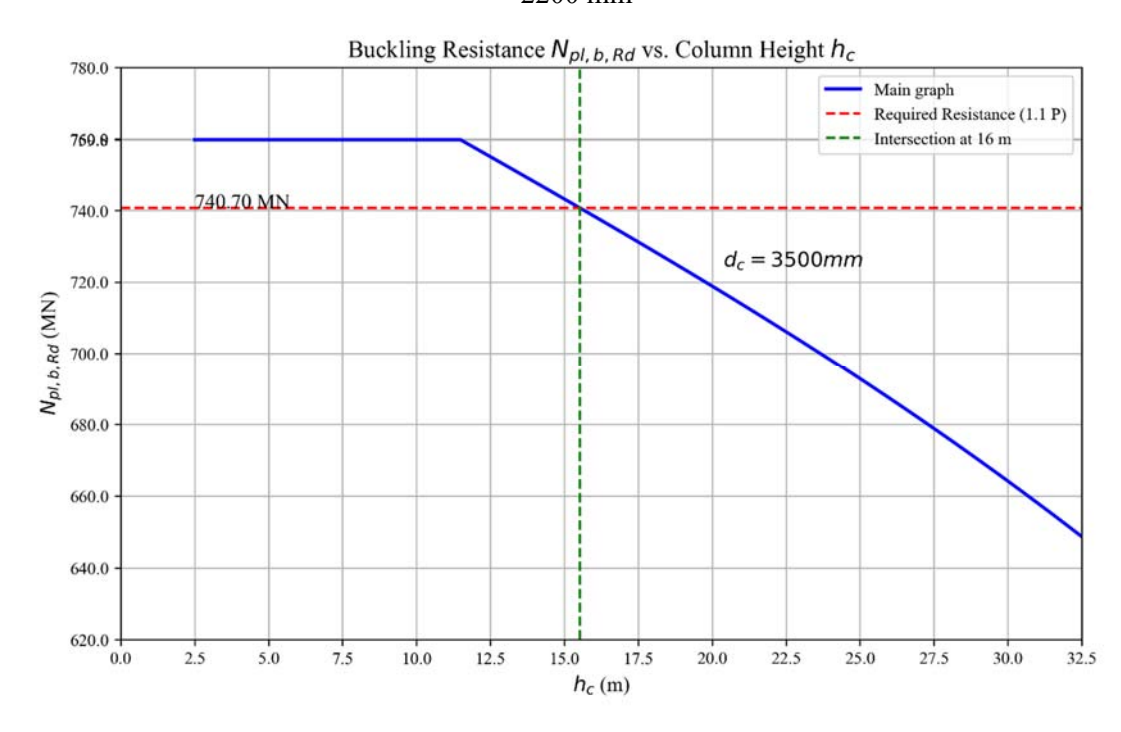


Figure 3-12: Maximum height of mega-column suggested for 70-story building, column diameter =3500 mm

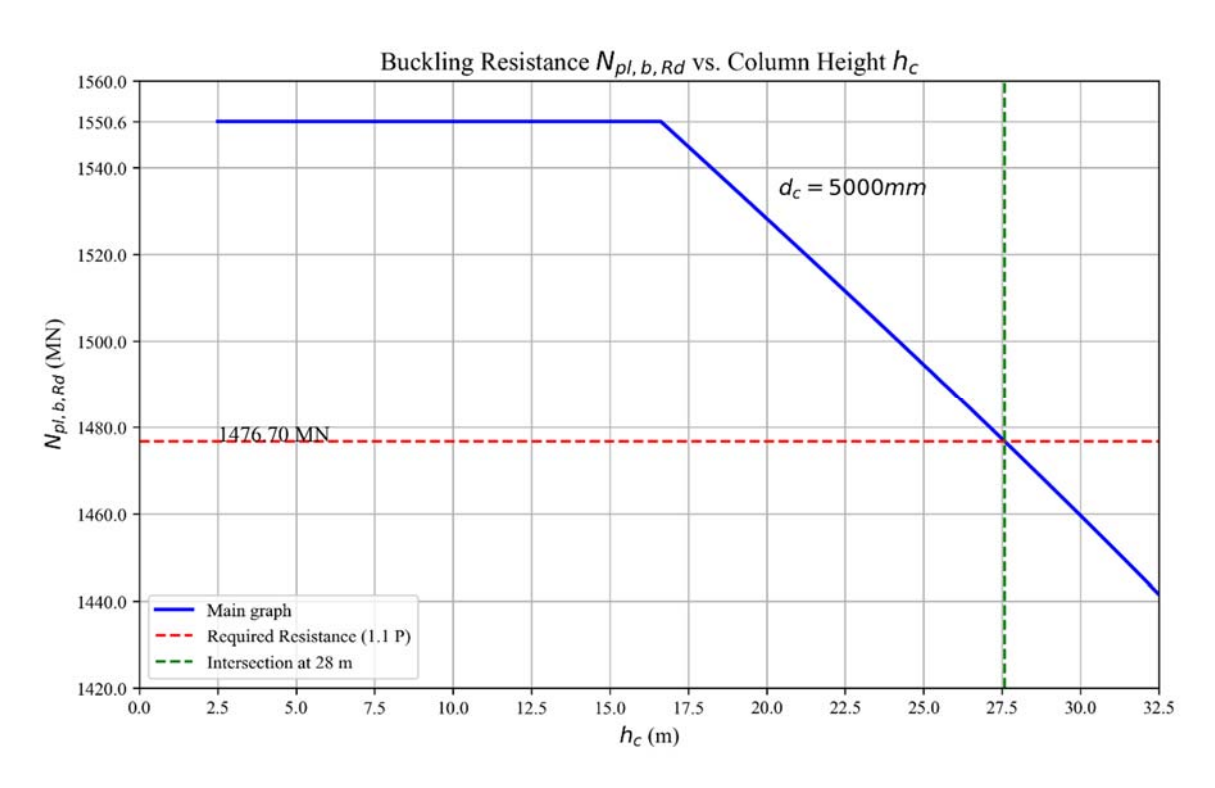


Figure 3-13: Maximum height of mega-column suggested for 100-story building, column diameter =5000 mm

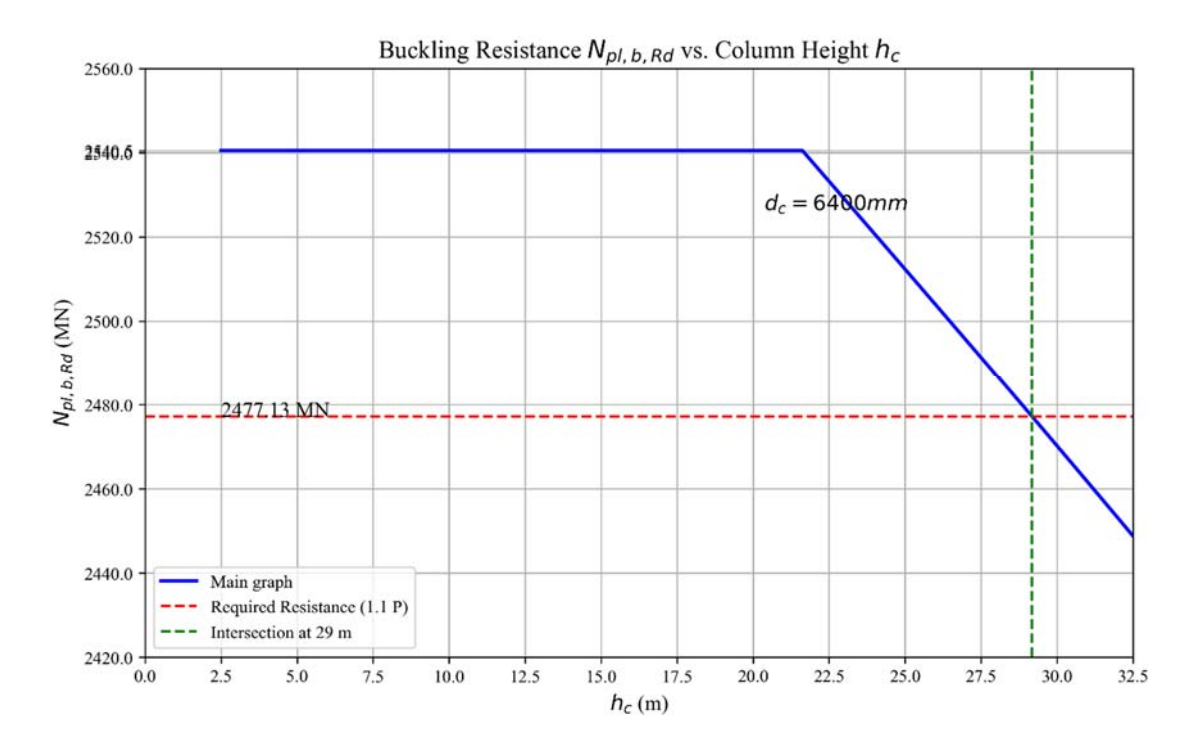


Figure 3-14: Maximum height of mega-column suggested for 120-story building, column diameter =6400 mm

The obtained values of mega-column properties required for all generic buildings and column diameters for Los Angeles site are summarized in Table 3-5. The applied vertical

load ( $W_{SC}$ ) does not account for the additional demand induced by vertical seismic excitation. However, to accurately determine the vertical earthquake response, the vertical component of the earthquake should be incorporated into the analyses, which was not considered in this study.

Table 3-5: Design properties of mega-column for specified height of building

Number of stories (n)	Diameter of mega- column (mm)	Maximum axial load (MN)	W <sub>SC</sub> (MN)	Maximum allowable (hc) for recommended story (m)	EI <sub>eff</sub> of mega- column (N·mm²)	Maximum assumed height, h <sub>c</sub> (m)
15	1000	50	29	12	$1.1 \times 10^{15}$	12
30	1500	139	99	16	$9.4 \times 10^{15}$	12
50	2200	273	259	12	$4.8 \times 10^{16}$	12
70	3500	760	673	16	$3.2 \times 10^{17}$	12
100	5000	1534	1342	28	$1.4 \times 10^{18}$	12
120	6400	2711	2252	29	$3.8 \times 10^{18}$	12

According to ASCE/SEI 7-22 [18], the vertical earthquake response can be assumed as  $0.12S_{\rm MS}W_{\rm SC}$ . For the Los Angeles site, where  $S_{\rm MS}=2.3$  [56], it results in a vertical earthquake response of approximately 0.276 times  $W_{\rm SC}$ . To account for this response, the graphs in Figure 3-7 (or one of Figures 3-9 to 3-14) can be used. Considering the vertical load assumed as 1.276  $W_{\rm SC}$ , a suitable diameter ( $d_{\rm c}$ ) and its corresponding height of megacolumn ( $h_{\rm c}$ ) can be selected from one of the listed values.

However, the composite column section exhibits greater resistance in experimental tests than what is predicted by code provisions, due to the concrete's confinement effect. This increased resistance is recommended to be considered as a 30% enhancement [64]. Considering this increase, the specified diameter in each case would also be enough to

accommodate the vertical earthquake response. In general, the graphs remain valid for different  $W_{SC}$  values and site locations. The only variation is the assignment of a suitable generic building to each graph, based on engineering judgment.

From the mega-column design procedure, the maximum allowable height for each specified diameter can be variable and in the maximum value for 120-story building, it can reach to around 33 m. However, this upper-bound does not seem to be practical or feasible. To meet the other criteria for the construction, the maximum range is restricted to 12 m. The minimum of the applicable range is also selected as 2.5 m. Therefore, the range of height of mega-columns is defined as:

$$h_c = \{2.5, 6, 12\} m$$

Table 3-5 includes the maximum allowable values governed by buckling resistance for the mega-column heights ( $h_c$ ); any shorter column would offer greater strength and is therefore acceptable from a structural standpoint. For the parametric study, a conservative upper bound of 12 m was selected for  $h_c$  to reflect a practical limit for deep basements applicable across all building models.

#### 3.2.6. Shear Reduction Factor ( $\mu_{\rm V}$ )

Determining the design shear strength ( $V_y$ ) is a key step in designing the shear mechanism, as its strength directly influences its capacity and activation sequence of mechanisms in MechRV3D system. The lower bound of the shear mechanism strength is set slightly above the base shear demand expected at the onset of rocking action. This approach ensures that the rocking mechanism is effectively engaged during the seismic events as intended. If the lateral yielding strength falls below this shear limit, there is a possibility that the shear mechanism may be activated before the rocking action occurs. Then, system would fail to

behave as a dual-mechanism system and would instead behave like a simple base-isolated system, which defeats the entire design purpose [15].

A higher shear mechanism strength more effectively controls horizontal displacement at the base of the superstructure which may lead to reduce base displacement but an increased inter-story drift ratio (IDR) in the superstructure. Conversely, a lower shear mechanism strength reduces the shear transmitted to the superstructure, potentially decreasing the IDR, enhancing energy dissipation at the base through the shear mechanism, and mitigating the effects of higher mode responses [15]. To achieve a balanced design, Equation 3-7 — adopted from the initial study —is used to consider different possible values for shear strength  $(V_y)$  [15].

$$V_{y} = \frac{M_{\text{rock}}}{H_{\text{eff}}} + \mu_{V} \left( V_{\text{b,1MOV}} - \frac{M_{\text{rock}}}{H_{\text{eff}}} \right)$$
(3-7)

Lower-bound of the shear mechanism strength can be determined using  $M_{\text{rock}}$  /(0.726H), where  $M_{\text{rock}}$  is assumed as  $M_{\text{b,SLE}}$  and 0.726H represents the effective modal height for the first mode of a superstructure with total height (H) [5]. Using 0.726H, rather than directly using the base shear from fixed-base building analysis results, implies that this shear strength value is primarily associated with the first-mode base shear response. Consequently, it does not account for the contributions of higher modes to the base shear. This distinction is evident in Table 3-6, where the values of  $V_{\text{b, SLE}}$  (corresponding shear demand at the base of superstructure under SLE level) and the lower bound of shear strength differ.

Table 3-6: Lower- and upper-bound of shear mechanism strength  $(V_y)$ 

Number of stories (n)	$M_{ m b,  SLE}$ (MN·m), $R_{ m M}$ =8	V <sub>b, SLE</sub> (MN)	Lower-bound, $M_{\rm b,  SLE}/H_{\rm eff}$ (MN)	Upperbound, $V_{ m b,1M0V}$ (MN)
15	142.3	5.5	4.4	44.5
30	604.0	18.9	9.2	65.0
50	1970.0	39.3	18.1	357.5
70	6344.5	116.7	41.6	757.6
100	15807.7	212.5	72.6	1367.9
120	25348.9	324.7	97.0	2160.0

Upper-bound strength limits for the shear mechanism are examined through a special case scenario in which the rocking action is designed to be activated as intended, while the shear mechanism is intentionally kept elastic under all loading conditions. In this scenario, the proposed dual-mechanism system effectively becomes a rocking-only system, and under this condition, the lateral demand referred to as  $V_{b,1M0V}$  as it was discussed in the initial study [15].  $V_{b,1M0V}$  represents the mean base shear response obtained from nonlinear response history analyses (NLRHAs) at the MCE level. These lower-bound and upper-bound shear limits establish the permissible range for selecting the design value of lateral resistance ( $V_y$ ) for the shear mechanism in the MechRV3D system. The obtained values for all the generic building were summarized in Table 3-6.

To achieve a balanced design, an appropriate yield strength ( $V_y$ ) for the shear mechanism must be selected from within the established lower and upper bounds. To facilitate this design choice, in Equation 3-7, a shear reduction factor ( $\mu_V$ ) was introduced. This factor helps determine an appropriate value for  $V_y$  within the defined lower and upper bounds.  $\mu_V = 0$  corresponds to the lower-bound strength, while  $\mu_V = 1$  corresponds to the upper-

bound (rocking-only) case. The discrete values for  $\mu v$  used in this study are defined as follows:

$$\mu_V = \{0, \quad 0.2, \quad 0.5, \quad 0.8, \quad 1\}$$

#### 3.2.7. Initial Stiffness Factor for the Shear Mechanism ( $r K_{b1}$ )

To determine the initial stiffness of shear mechanism,  $K_{b1}$ , the maximum base shear that cause shear yielding ( $V_y$ ) and the corresponding displacement at this point are required. Assuming the shear fuses behave like a buckling-restrained braced frame (BRBF), its force-deformation response is illustrated in Figure 3-15. While other damper types may also be used as shear fuses, the method presented in the following paragraphs remains applicable to their corresponding behaviour.

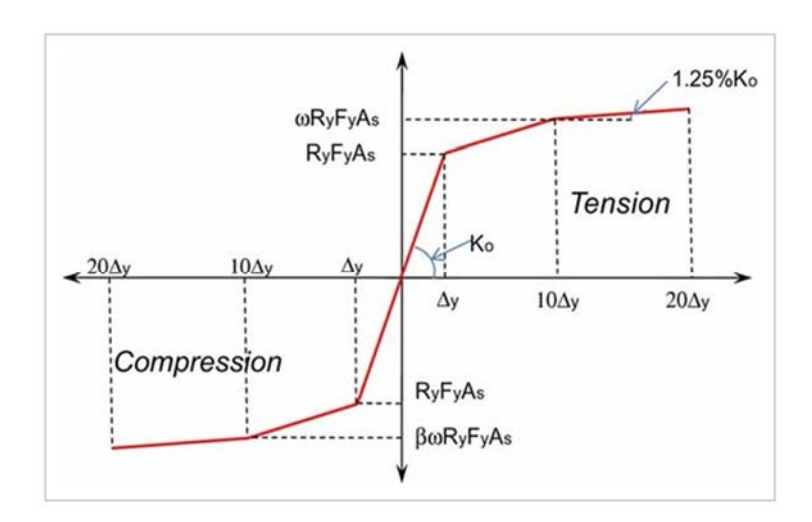


Figure 3-15: A modelled BRBF with deformation ( $\Delta_y$ ) in yielding point and  $20\Delta_y$  in ultimate strength [65]

According to the backbone curve in Figure 3-15, the ultimate deformation in the post-yielding zone can be up to 20 times the deformation in the yielding point  $(\Delta_y)$ . The maximum value of  $\Delta_{rckr}$  ( $\Delta_b$ ) can be assumed the same as ultimate deformation of shear mechanism (20  $\Delta_y$ ). Therefore, the yielding deformation at the onset of rocking activation

can be assumed to be 1/20 of the maximum allowed base displacement ( $\Delta_{b, max}$ ) in this case. This assumption leads to Equation 3-8.

$$V_y = K_{b1} \times (\frac{\Delta_{b,max}}{20}) \tag{3-8}$$

The values of  $K_{b1}$  for all generic buildings at the Los Angeles site —based on a deformation of  $1/20 \, \Delta_{b,max}$  at the activation of the rocking mechanism— are summarized in Table 3-7. The same procedure is used for the Vancouver site, with  $V_{b,SLE}$  determined according to the seismicity specific to that location. In this approach,  $\Delta_{b,max}$  is assumed to be 800 mm consistent with the assumption by Calugaru [42], who examined a high-rise dual-mechanism system and explicitly discussed large base shear deformations, with a reported mean value of 830 mm. The shear yielding  $(V_y)$  is assumed to be  $V_{b,SLE}$ , which is slightly greater than the lower-bound of shear mechanism strength.

Table 3-7: Initial stiffness for shear mechanism based on  $\Delta_{b,max}$  =800 mm at the base for all generic buildings at the Los Angeles site

$\Delta_{ m rckr}$ (mm)	$V_{ m b,SLE}( m MN)$	$K_{b1}$ (N/mm)
40	4.4	1.087×10 <sup>5</sup>
40	9.2	2.310×10 <sup>5</sup>
40	18.1	4.522×10 <sup>5</sup>
40	41.6	1.040×10 <sup>6</sup>
40	72.6	1.814×10 <sup>6</sup>
40	97.0	2.425×10 <sup>6</sup>
	40 40 40 40 40	40     4.4       40     9.2       40     18.1       40     41.6       40     72.6

Using this method, the initial stiffness is directly related to the intended initial displacement  $(\Delta_y)$ . Results from the nonlinear response history analyses showed that using tabulated  $K_{b1}$ , and even twice that value, led to horizontal displacements exceeding the maximum allowable limit (greater than 800 mm) due to the negative stiffness of the mega-columns.

Moreover, this displacement can occur in the direction opposite to the applied load, indicating that the mega-column may sway in the reverse direction when the initial stiffness of the shear mechanism is less than twice the  $K_{b1}$  values in Table 3-7. In such case, the mega-columns become the primary source of lateral stiffness and may experience premature failure due to buckling or excessive lateral displacement. As will be discussed in Subsection 3.3, there is a trade-off between the stiffness of the shear fuses and that of the mega-columns. This study assumes that the shear fuses are designed to serve as the primary source of lateral stiffness, in order to control lateral demand on the mega-columns and prevent premature failure.

To maintain this assumption, it was found that the initial stiffness of shear mechanism must exceed four times the basic initial stiffness ( $K_{b1}$ ). This requirement is expressed by multiplying  $K_{b1}$  by factors greater than 4. These unitless multipliers are referred to as the initial stiffness factor ( $r_K_{b1}$ ), and they are assigned discrete values ranging from 4 to 8, as follows:

$$r_{K_{b1}} = \{4, 6, 8\}$$

The minimum of this range was chosen to be 4 because, in the initial parametric analysis, buildings taller than 70 stories, showed divergent results due to the instability in the 12m mega-columns when  $r_{Kb1}$  values lower than 4 were used. On the other hand, values above 8 were deemed impractical due to the difficulty of sourcing materials and elements with such high initial stiffness, which would also significantly increase costs. Referring to upperbound values listed in Table 3-6 for shear strength, these are approximately 8 times the lower-bound shear strength for buildings up to 30-story, and more than 18 times the lower-bound for 50-story buildings and taller. This justifies the need to assume a variable range of  $r_{Kb1}$  for the shear mechanism, since shear strength itself is not constant and initial stiffness must be adjusted to account for the variation in  $V_y$  in Equation 3-8. Table 3-8 lists

the initial stiffness values of the shear mechanism at the Los Angeles site, incorporating the applied factor r  $K_{b1}$ :

Table 3-8: Initial stiffness values of shear mechanism for all generic buildings at Los Angeles site

Number of stories (n)	Basic initial stiffness, K <sub>b1</sub> (N/mm)	<i>K</i> <sub>b1</sub> with <i>r- K</i> <sub>b1</sub> =4	$K_{\rm b1}$ with $r$ - $K_{\rm b1}$ =6	<i>K</i> <sub>b1</sub> with <i>r</i> − <i>K</i> <sub>b1</sub> =8
15	1.087×10 <sup>5</sup>	4.348×10 <sup>5</sup>	6.522×10 <sup>5</sup>	8.696×10 <sup>5</sup>
30	2.310×10 <sup>5</sup>	9.240×10 <sup>5</sup>	1.386×10 <sup>6</sup>	1.848×10 <sup>6</sup>
50	4.522×10 <sup>5</sup>	1.808×10 <sup>6</sup>	2.713×10 <sup>6</sup>	3.616×10 <sup>6</sup>
70	1.040×10 <sup>6</sup>	4.160×10 <sup>6</sup>	6.240×10 <sup>6</sup>	8.320×10 <sup>6</sup>
100	1.814×10 <sup>6</sup>	7.256×10 <sup>6</sup>	1.088×10 <sup>7</sup>	1.451×10 <sup>7</sup>
120	2.425×10 <sup>6</sup>	9.700×10 <sup>6</sup>	1.455×10 <sup>7</sup>	1.940×10 <sup>7</sup>

#### 3.2.8. Post-yield Shear Stiffness ( $\alpha_K$ )

Assuming buckling restrained braced frame (BRBF) as the shear fuses in this study, the accessible properties for this type of element dictate the value of the parameter  $\alpha$  for the ratio of post-yielding stiffness to pre-yielding stiffness. In the initial study, it was assumed 0.02 for BRBFs [15]. However, considering an element with the properties shown in Figure 3-15, it is assumed to be 0.025 in the current study.

While this property can vary slightly between different BRBF products, it is considered a secondary parameter with less influence on peak seismic demands compared to yield strength or initial stiffness. Therefore, to maintain a focused and manageable parametric study,  $\alpha_K$  was held constant in this research.

# 3.3. Initial Stiffness of the Base Mechanisms (K<sub>base\_initial</sub>) and Mega-Column's Negative Stiffness

The initial stiffness of the MechRV3D system's base is not determined by the shear mechanism alone, but is a complex combination of several interacting components. At very small displacements, before the shear fuse has yielded, the total initial stiffness ( $K_{\text{base\_initial}}$ ) is the sum of all components (three distinct contributions) acting in parallel and can be conceptualized as Equation 3-9:

$$K_{base\_initial} = K_{b1} + K_{mega-columns} - K_{P-Delta}$$
 (3-9)

- Shear Mechanism Stiffness ( $K_{b1}$ ): This is the primary source of positive, restoring stiffness. It is provided by the shear fuses (e.g., BRBFs) and is controlled in this study by the initial stiffness factor, r  $K_{b1}$ .
- Mega-Column Primary Stiffness ( $K_{\text{mega-columns}}$ ): The mega-columns themselves provide a positive contribution to the lateral stiffness as they resist sway. This stiffness is highly dependent on the mega-column height ( $h_c$ ), with taller, more flexible columns providing significantly less stiffness than shorter ones. In this initial elastic range, the stiffness of the mega-columns can be a significant fraction of the total stiffness, especially if a soft shear fuse is used. The mega-columns are modeled as elastic beam-column elements with pinned ends. Their primary contribution (for two mega-columns) to the lateral base stiffness is given by  $K_{\text{mega-columns}} = 6EI_{\text{eff}} / h_c^3$ , where  $EI_{\text{eff}}$  is the effective flexural rigidity of a single mega-column. When uplift occurs at the top of one column, 6 in this formula will decrease to 3.
- Mega-Column P-Delta Stiffness ( $K_{\text{P-Delta}}$ ): The gravity load ( $W_{\text{SC}}$ ) acting on the laterally displaced mega-columns induces a secondary P-Delta effect. This effect manifests as a destabilizing negative stiffness, which is inversely proportional to the mega-column height ( $K_{\text{P-Delta}} = W_{\text{SC}}/h_{\text{c}}$ ).

The overall stability and performance of the base mechanism depend on the balance between these competing positive and negative stiffness contributions. The loss of primary stiffness in taller, more flexible mega-columns ( $K_{\text{mega-columns}}$  decreases) is the dominant geometric effect. Furthermore, the P-Delta negative stiffness can become very large for configurations with short mega-columns or very heavy superstructures. For the system to be stable, the positive stiffness provided by the shear mechanism ( $K_{\text{b1}}$ ) must be sufficiently large to counteract these effects and ensure that the total base stiffness ( $K_{\text{base\_initial}}$ ) remains robustly positive. This principle was the fundamental basis for the selection of the initial stiffness factor ( $K_{\text{b1}}$ ) in the subsequent parametric study.

### 3.4. Ultimate Strength of Shear Mechanism ( $V_u$ )

The ultimate shear resistance provided by the MechRV3D system at the base of the superstructure is denoted as  $V_{\rm u}$ . This maximum base shear occurs when the shear mechanism, it was assumed to be BRBF, develops its ultimate shear strength,  $V_{\rm u,f}$ . As noted by Tong [15], the shear mechanism (or BRBF) also provides a simultaneous buttressing force,  $V_{\rm u,c}$ , to the rolling mega-column. The total ultimate shear resistance,  $V_{\rm u}$  can be calculated using Equation 3-10 [15].

$$V_{\rm u} = V_{\rm u,f} + V_{\rm u,c} \rightarrow V_{\rm u,f} = V_{\rm u} - V_{\rm u,c}$$
 (3-10)

The ultimate shear strength,  $V_{\rm u,f}$ , is used to design the shear mechanism. The buttressing force,  $V_{\rm u,c}$  multiplying by the height of mega-column ( $h_{\rm c}$ ), counteracts the overturning moment induced by the total gravity,  $W_{\rm SC}$ , as the mega-columns undergo lateral displacement ( $\Delta_{\rm b}$ ).  $V_{\rm u,c}$  can be determined according to Equation 3-11:

$$V_{\rm u,c} = \frac{W_{\rm SC} \, \Delta_b}{h_c} \tag{3-11}$$

where  $h_c$  and  $\Delta_b$  have the same units. This approach is also applicable to the shear force at the base prior to reaching the ultimate resistance. Assuming the maximum base displacement ( $\Delta_{b,max}$ ) of 800 mm, the corresponding buttressing force provided by the mega-columns is calculated using Equation 3-11. These values, derived based on the previously stated assumptions, are summarized in Table 3-9.

Table 3-9: Buttressing force,  $V_{u,c}$  provided by mega-columns at 800 mm displacement for the Los Angeles site

Number of stories (n)	$\Delta_b$ (mm)	W <sub>SC</sub> (MN)	$h_c(m)$	$W_{\rm sc}/h_{\rm c}$ (N/mm)	$V_{\mathrm{u,c}}(\mathrm{MN})$
15	800	29.2	12	$2.43 \times 10^{3}$	1.9
30	800	99.0	12	8.25× 10 <sup>3</sup>	6.6
50	800	259.3	12	2.16× 10 <sup>4</sup>	17.3
70	800	673.3	12	5.61× 10 <sup>4</sup>	35.9
100	800	1342.4	12	1.12× 10 <sup>5</sup>	71.6
120	800	2251.9	12	1.87× 10 <sup>5</sup>	120.1

Once the shear fuse yields, its stiffness drops dramatically to its post-yield stiffness ( $\alpha_K \times K_{b1}$ ). The vast majority of the inelastic deformation and energy dissipation is concentrated in the shear fuse. The very stiff mega-columns will attract very little additional force as the displacement increases further. The primary role of the mega-columns is to handle gravity and provide a pivot. Their contribution to the ultimate lateral strength is secondary to the shear fuse, which is the dedicated energy-dissipating element. For a preliminary design procedure, simplifying the ultimate strength equation to  $V_u$  in Equation 3-10 (without considering  $K_{mega-columns}$ ) is a standard and justifiable approach.

#### 3.5. Summary of Parameters and Rationale for Their Ranges

1- Fundamental Period ( $T_1 = \{1, 2, 3, 4, 5, 6\}$  s):

Parameter  $T_1$  represents the fundamental period of the building—which depends on its height—and is used to back-calculate the stiffness of the superstructure, which significantly affects the seismic response of the system. This parameter is also used to define the period range within which the ground motions are scaled and applied in the analyses.

This range was chosen to represent the range of high-rise buildings considered in practice for RC core wall buildings, from a relatively stiff 15-story structure to a very flexible 120-story structure. The specific integer values were selected to create a clear, evenly-spaced parameter matrix for the study. The correspondence to real building heights was established and validated using the KBC 2009 empirical formula to have a strong correlation with measured data for this building type.

#### 2- Aspect Ratio (H/B):

This parameter reflects one of the architectural limitations of high-rise buildings, as well as the effect of building width (B) on the mass of the superstructure and its slenderness. The range was selected based on statistical data provided by CTBUH from previously constructed high-rise buildings worldwide, which also indicate a practical range for this parameter.

#### 3- Moment Reduction Factor ( $R_M = \{4, 6, 8\}$ ):

This factor represents the ratio of the MCE demand to the SLE demand and eliminates the need for a direct calculation of the base moment at SLE (as rocking threshold), whose value is not well-defined in some design codes.

The selected range of 4 to 8 is directly supported by performance-based design guidelines (e.g., CTBUH). Furthermore, the range is consistent with site-specific hazard analyses for the two locations studied: the ratio for the high-seismicity Los Angeles site is

approximately 8, while for the moderate-to-high seismicity Vancouver site, it is approximately 4.

4- Shear Reduction Factor ( $\mu_V = \{0, 0.2, 0.5, 0.8, 1\}$ ):

This factor represents the variation in the yielding shear strength of the shear mechanism, which governs the sequence of engagement of the base mechanisms and the activation of both uncoupled mechanisms, thereby affecting the overall system response. This range was chosen to explore the full spectrum of possible shear mechanism yielding strength.

- $\mu v = 0$ : Represents the softest, most ductile design of shear mechanism, where the shear fuse yields immediately after rocking begins (the lower-bound strength), , ensuring that the shear mechanism is not engaged before the activation of the rocking mechanism.
- $\mu_{V}$  = 1: Represents the strongest, stiffest design of shear mechanism, where the shear fuse is designed to remain elastic up to the maximum credible shear demand (the "rocking-only" case).

The intermediate values (0.2, 0.5, 0.8) were selected to provide a reasonable discretization of the design space between these two extremes, capturing the effect of its variation on the seismic response without making the analyses excessively numerous, long, or repetitive.

5- Initial Stiffness Factor of the Shear Mechanism  $(r_K_{b1} = \{4, 6, 8\})$ :

For high-rise buildings integrated with base shear systems (such as base isolation), selecting appropriate values for the base mechanism's shear strength and stiffness can lead to improved seismic performance of the system. This parameter reflects the role of the base shear mechanism's stiffness. This range was determined based on stability considerations.

• Lower Bound (4): Preliminary analyses revealed that for stiffness factors less than 4, the system became unstable for taller buildings due to the negative stiffness from

the mega-columns' P-Delta effect. A value of 4 was therefore established as the minimum required to ensure a stable response.

Upper Bound (8): Values significantly higher than 8 were deemed to represent an
impractically high initial stiffness for the shear mechanism, which would be
difficult and costly to achieve in practice.

## 6- Post-Yielding Stiffness Ratio for Shear Mechanism ( $\alpha_K = 0.025$ ):

It was necessary to consider this parameter because, as highlighted in the literature review, the post-yielding stiffness of the base shear mechanism influences the performance of such systems. However, it was treated as a constant value (0.025) because, for BRBFs, the practical values of this parameter are relatively close to each other, and the results indicated that small variations of this parameter do not significantly affect the seismic responses.

# 7- Mega-Column Height ( $h_c = \{2.5, 6, 12\}$ m):

Mega-column height is an important design parameter in the developed model, as it is critical for the system's overall stability due to the negative stiffness that these columns introduce, which directly affects the system's behavior. This range is bounded by practical and structural constraints.

- Lower Bound (2.5 m): This was selected as a practical minimum height to provide sufficient vertical clearance for the installation and function of the shear mechanism's components (e.g., BRBFs), corresponding to a typical single-story basement.
- Upper Bound (12 m): This was selected as a practical upper limit representing a deep, multi-level basement (e.g., 3-4 stories). While buckling calculations showed that taller columns could be feasible for some configurations, 12m was chosen as a conservative and consistently applicable upper bound for the parametric study.

# 8- Rocker Depth (D = [4, 12] m):

Parameter D plays an important role in determining the size of the rocker in the developed model. Specifying the rocker dimensions during the design process is crucial, as it ensures that the required rigidity of the rocker is achieved from the outset. Moreover, the size of the rocker can directly influence the ability to meet the restoring moment demand during rocking activation. From two dimensions of the rocker, D represents a more fundamental practical constraint in real-world applications, as it is dictated by the number of the basement levels and involves a trade-off with mega-column height in terms of available underground space. This is a continuous range from which a specific value is derived, but the bounds themselves are based on practical considerations.

- Lower Bound (4 m): A depth of less than 4 meters was considered insufficient to
  ensure the rocker would behave as a deep beam and possess the required rigidity
  and strength for taller, heavier buildings.
- Upper Bound (12 m): This corresponds to the practical limit of a deep basement
   (h<sub>c</sub>), as the rocker depth cannot exceed the available vertical space.

The range of parameters obtained in this chapter and used to generate the parametric analysis results is summarized in Table 3-10 for convenient reference.

Table 3-10: Range of parameters of MechRV3D system to conduct parametric analyses

No.	Parameter	Range
1	Fundamental period $(T_1)$	{1, 2, 3, 4, 5, 6} Sec
2	Aspect ratio (H/B)	{3, 4, 5, 5, 6, 6} m
3	Moment reduction factor, $R_{\rm M}$	{4, 6, 8}
4	Shear reduction factor, $\mu_{\rm V}$	{0, 0.2, 0.5, 0.8, 1}
5	Initial stiffness factor of shear mechanism, $r_{K_{b1}}$	= {4, 6, 8}
6	Post-yielding stiffness ratio for shear mechanism $(a_K)$	0.025
7	Height of mega-columns (hc)	{2.5, 6, 12} m
8	Depth of rocker (D)	[4, 12] m

To conduct the parametric analyses, a numerical model is developed for each value of parameter T (1 to 6 s), with parameter H/B specific to each corresponding T. As discussed previously in Subsection 3.2.4, parameter D—the depth of the rocker—is not entirely independent of  $R_{\rm M}$ ; therefore, a specific D is assigned to each  $R_{\rm M}$ . The parameter  $\alpha_{\rm K}$  is held constant at 0.025, as it was found to have negligible influence on the results. The remaining parameters are treated as variables: three levels for  $R_{\rm M}$ , three for  $r_{\rm L}K_{\rm b1}$ , five for  $\mu_{\rm V}$ , and three for  $h_{\rm c}$ . This results in 135 unique parameter combinations per generic building, totaling 810 models.

#### 3.6. Numerical Model

For parametric analyses, the system is represented by a two-dimensional model that includes two of the four mega-columns and the shear mechanism on one side of the rocker to represent the in-plane behaviour in a simplified way. This two-dimensional model captures the structural behaviour of the system with sufficient accuracy while remaining

simple enough to avoid unnecessary complexity. By incorporating more detailed components compared to the model used for parametric analyses in the initial study (Figure 2-8), this model can more accurately reflects the real-world behaviour of the MechRV3D system and the potential limitations in practical design.

The model is developed using OpenSeesPy. OpenSees [48] is an open-source software framework to simulate structural behaviour under various loading conditions, including seismic loads. In this study, Python is used as a platform for conducting the parametric analyses, with OpenSees integrated as a library.

#### 3.6.1. Stick Model of the Superstructure

The building's plan is the same as shown in Figure 3-2. To simplify the modelling, only the central RC core-walls of the buildings is included. This core is represented using an elastic stick with lumped masses at each floor level, assuming the superstructure remains elastic when the MechRV3D system is integrated. ElasticBeamColumn elements, assigned a flexural rigidity (*EI*) and a gross cross-sectional area equivalent to that of the core, are used to model the core stick. Seismic inertial masses are lumped at each story level (*m*EQ). Only horizontal masses are considered, consistent with the two-dimensional modelling approach. Accordingly, the rotational inertia about horizontal axis and vertical axis are not considered. All assigned properties were summarized in Table 3-2.

The number of stories (n) varies corresponding to all generic buildings. The height of each story is assumed as 3 m. The core stick is fixed at the ground level to the centre of the top face of the rocker. Additionally, the model incorporates P- $\Delta$  effects to account for second-order deformations in the analysis by assigning a P- $\Delta$  geometric transformation to all vertical beam-column elements representing the superstructure core. The developed model is shown in Figure 3-16.

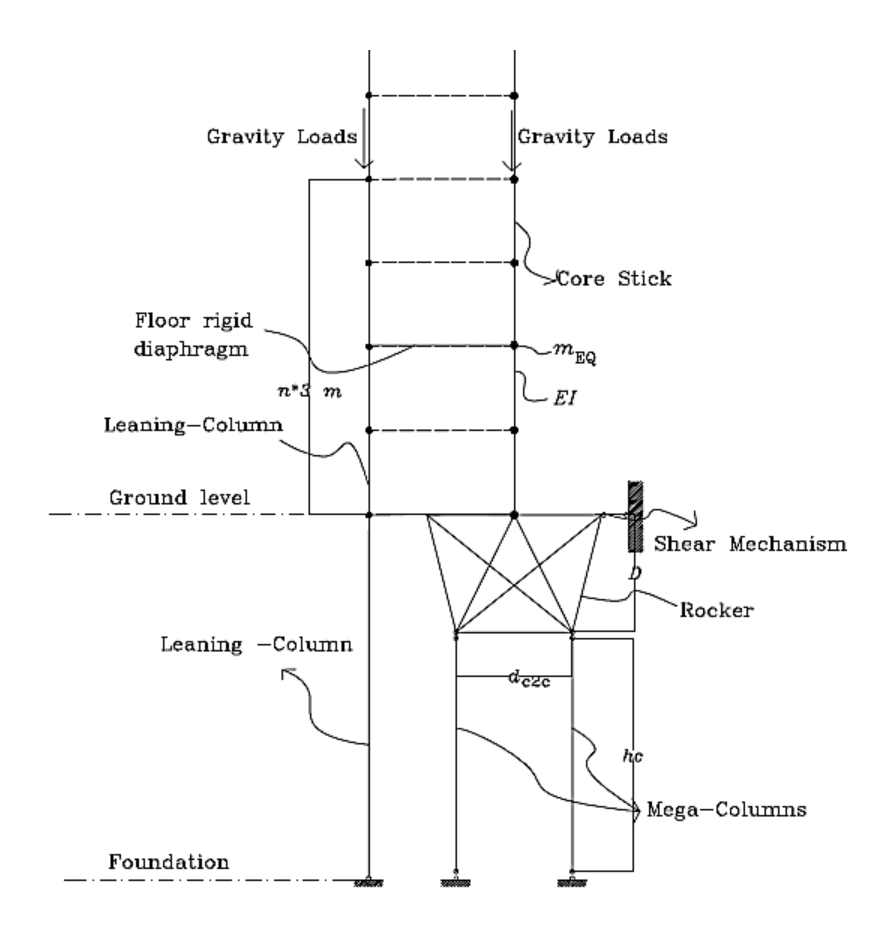


Figure 3-16: Two-dimensional model of the MechRV3D system incorporated into the core-stick superstructure

#### 3.6.2. Rocking Mechanism Components

According to the initial study's description for physical embodiment and case study of the MechRV3D system [15], the rocker was modelled using interconnected frame elements with large axial and flexural rigidities to simulate its negligible deformability. The same approach is adopted here to keep the consistency with the initial research and avoid the need to validate the rigidity of the rocker through another case study. Similarly, in the current study, all rocker elements are modelled using ElasticBeamColumn elements in OpenSeesPy. Large axial and flexural rigidities are assigned to them.

Furthermore, the current research aims to evaluate the negative stiffness induced by the mega-columns within the overall system. To achieve this, the mega-columns are modelled as line elements at the bottom face of the rocker with height of  $h_c$ . The mega-columns are

modelled using ElasticBeamColumn elements, with their determined gross cross-sectional area and height calculated previously using Eurocode 4 in Subsection 3.2.5. This approach ensures that the stiffness of the mega-columns is realistically incorporated into the analysis. At both ends of each mega-column, a pair of nodes with identical coordinates was defined to enable rocking at the top and to implement the support boundary condition at the base. As shown in Figure 3-17, in the top connection, one node is assumed to be attached to the bottom face of the rocker, while the other is at the top of the mega-column. Each pair of nodes was constrained to move horizontally together but were allowed to move vertically relative to each other. This assumption allows the free uplifting of the rocker above the mega-columns. Due to the rigidity of the rocker, the top nodes in each pair of top connection, experience identical horizontal displacements.

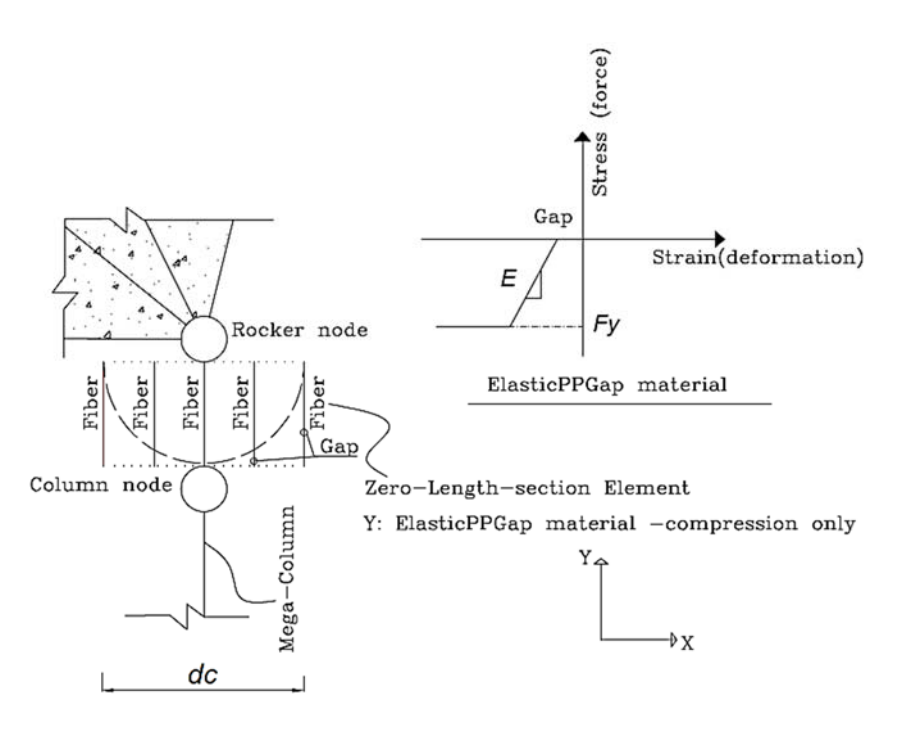


Figure 3-17: Modelling of the connection between mega-column and rocker at the top (left), and the material model used for simulation, selected from the OpenSees library (right)

To model rocking contact surface, the same approach proposed by Vassiliou et al. [34] in OpenSees was applied here to capture the response of in-plane rocking systems [32]. Each pair of nodes was linked using a zero-length-section element, consisting of five fibers

oriented vertically. Five fibers provide a reasonable level of discretization for a two-dimensional line-section. It allows for a central fiber and two fibers on either side, which can capture the gradual shift of the compressive force towards the edge as the column rocks. Each fiber is assigned an area equal to 1/5 of the mega-column's cross-sectional area.

These nonlinear fibers were modelled with no tensile resistance but a high compressive rigidity. The central fibers used the elastic-no-tension (ENT) uniaxial material in OpenSeesPy, while the four surrounding fibers employed the ElasticPPGap material to simulate compression-only behaviour with predefined gaps. These gaps increased in size from the centre outward (Figure 3-17), enabling sequential, stepwise engagement of the fibers while the rocker rotates atop a mega-column as its pivot point. This configuration simulates the curved contact surface at the end of the mega-columns, allowing smooth rolling rotation as developed in the physical embodiment of the MechRV3D system [15]. With no tensile resistance, the fibers allow the rocker to uplift freely above a mega-column while rotating atop another as its pivot. At the same time, to simulate high compressive rigidity in fibers, the Young's Modulus (E) of the fiber material is set to ten times the effective Young's Modulus ( $E_{eff}$ ) of the mega-column. Rigid elastic shear is aggregated into the fibers to prevent sliding at the rocking surface. No Rayleigh damping is applied to these nonlinear fibers, as they are expected to undergo abrupt changes in stiffness. Including abrupt stiffness change introduce artificial energy dissipation, which corrupts the dynamic response. A rigid elastic shear component is aggregated with the fiber sections to restrain sliding at the rocking surface.

The pair of nodes at the bottom of the mega-columns, as shown in Figure 3-18, were constrained to move vertically together, ensuring that the uplift action is confined to the top connection. The bottom nodes were fixed to the foundation to maintain a stable support condition. The same material and element assumptions used for the top pair of nodes were

also applied to the bottom pair. This modelling approach ensures that the rocking mechanism behaves as intended during both the uplift and rotation of the rocker atop the mega-columns, while maintaining the appropriate boundary conditions (no uplift, no sliding, moment-free) at the base of the mega-column.

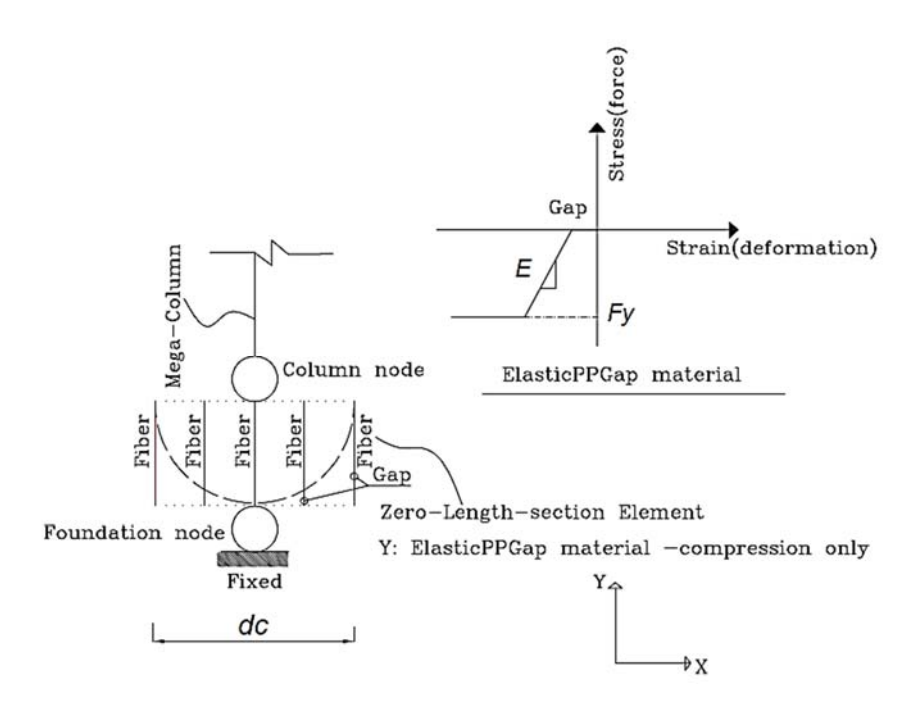


Figure 3-18: Modelling of the connection between mega-column and foundation at the bottom (left), and the material model used for simulation, selected from the OpenSees library (right)

## 3.6.3. The Gap Size in the End Connections of Mega-Columns

The predefined compressive gaps (g) in the zero-length-section fibers are a critical modelling parameter, designed to simulate the smooth kinematics of the physical megacolumns' end connections. The gap size for the outermost fiber must be large enough to accommodate the combined geometric effects of both the mega-column's own sway and the rocker's rotation. The total required gap, g, is therefore calculated as the sum of two components, as shown in Equation 3-12:

$$g = \Delta_{v1} + \Delta_{v2} \tag{3-12}$$

where  $\Delta_{y1}$  is the uplift (mm) caused by the mega-column's rotation ( $\theta_m$ ), in radians, and  $\Delta_{y2}$  is the uplift (mm) caused by the rocker's rotation ( $\theta_{rocker}$ ), in radians, about its pivot point. The lateral displacement of the mega-column is assumed to be equal to the lateral base displacement ( $\Delta_b$ ). Thus, mega-column rotation ( $\theta_m$ ) is a direct function of the base displacement ( $\Delta_b$ ) and the mega-column height ( $h_c$ ). For calculating the gap size required at the onset of rocking, the base displacement is taken as  $\Delta_b = 40$  mm, as established in Section 3.2.7. The resulting rotation  $\theta_m$  is calculated using Equation 3-13:

$$\theta_{\rm m} = \tan^{-1} \frac{\Delta_{\rm b}}{h_c} \tag{3-13}$$

The maximum rocker rotation is a key performance parameter that must be controlled to ensure system stability. For this study, a target maximum rotation of 0.015 radians (1.5%) is selected. This value represents a rational and conservative upper-bound performance target for rocking systems under MCE-level events, ensuring that second-order effects remain manageable [13], [31]. Then, according to Figure 3-19, the combined effect of the two rotations,  $\theta_{\rm m}$  (mega-column rotation) and  $\theta_{\rm rocker}$  (rocker rotation), determine the required gap for the outermost fiber (g), Equation 3-14:

$$g = \Delta_{y1} + \Delta_{y2} = h_c (1 - \cos\theta_m) + \frac{d_c}{2} \sin\theta_{\text{rocker}}$$
 (3-14)

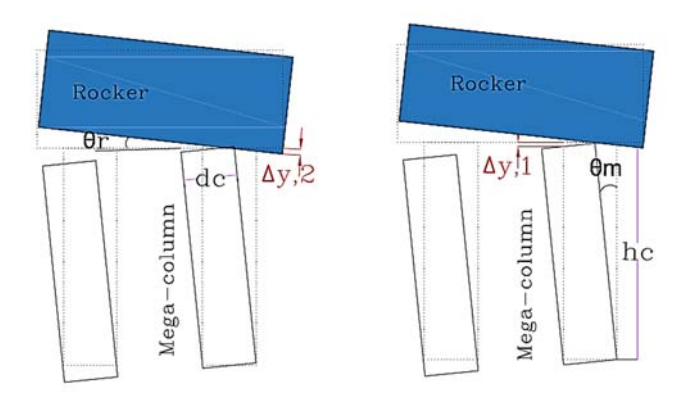


Figure 3-19: The rotation in the rocker,  $\theta_{\text{rocker}}$  (left), the rotation in the mega-column,  $\theta_{\text{m}}$  (right) when the mega-columns sway in the opposite direction of the applied force

As illustrated in the geometry of Figure 3-19,  $\Delta_{y2}$ , cannot exceed the rise created by the curved shape of the mega-column's end connection, which is directly related to the rocker's rotation angle ( $\theta_{\text{rocker}}$ ) and the radial distance from the pivot point to the fiber, equal to half the mega-column diameter taken as  $d_c/2$  (mm). This relationship is shown in Equation 3-14. The gap distance for the second and fourth fibers in Figures 3-17 and 3-18 is assumed to be approximately half of g. No gap is needed to be assigned to the central fiber. In Figure 3-19, the assumption was that the mega-column sway in the opposite direction of the applied load. However, as discussed in Subsection3.2.7, using the determined initial stiffness (multiplied by  $r_{-}K_{b1}$ ) for the shear mechanism, the mega-columns sway in the same direction of the applied force. Therefore, the rotation of the mega-column would occur in the same direction as that of the rocker as shown in Figure 3-20, and the gap distance would be solely related to  $\Delta_{y2}$  in Equation 3-14.

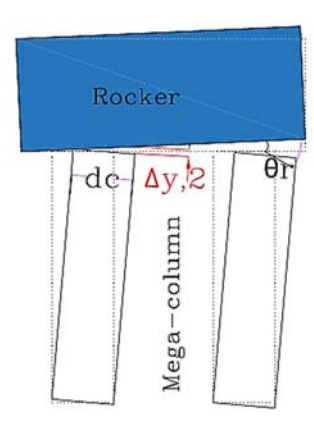


Figure 3-20: Rotation in the rocker ( $\theta_{\text{rocker}}$ ) that affect the gap distance when the mega-columns sway in the same direction of the applied force

Based on this assumption, the gap distance for all generic buildings is calculated using Equations 3-12 to 3-14, with  $\Delta_b$ =40 mm at the activation of the rocking mechanism. The results are presented in Table 3-11.

Table 3-11: Gap distance values for different height of building with  $\Delta_b = 40 \text{ mm}$ 

	Height of						
Number of stories (n)	mega- column, $h_c(\mathbf{m})$	Diameter of mega-column, $d_c$ (mm)	Rotation of mega-column, $\theta_{\rm m}({ m rad})$	Rotation of rocker, $ heta_{ m rocker}$ (rad)	Д <sub>у1</sub> (mm)	$\Delta_{y2}$ (mm)	Gap distance, g (mm)
15	12	1000	3.3×10 <sup>-3</sup>	1. 5× 10 <sup>-2</sup>	6×10 <sup>-2</sup>	7.5	7.6
30	12	1500	3.3×10 <sup>-3</sup>	1. 5×10 <sup>-2</sup>	6×10 <sup>-2</sup>	11.3	11.3
50	12	2200	3.3×10 <sup>-3</sup>	1. 5×10 <sup>-2</sup>	6×10 <sup>-2</sup>	16.5	16.6
70	12	3500	3.3×10 <sup>-3</sup>	1. 5×10 <sup>-2</sup>	6×10 <sup>-2</sup>	26.3	26.3
100	12	5000	3.3×10 <sup>-3</sup>	1. 5×10 <sup>-2</sup>	6×10 <sup>-2</sup>	37.5	37.6
120	12	6400	3.3×10 <sup>-3</sup>	1. 5×10 <sup>-2</sup>	6×10 <sup>-2</sup>	42.4	42.4

## 3.6.4. Shear Mechanism Components

The shear fuse elements in the shear mechanism were represented using a nonlinear zero-length translational spring. This spring is modelled using a zero-length element between a pair of nodes that have identical coordinates, located on the right side of the rocker as it was shown in Figure 3-16. One node is attached to the top corner of the rocker, while the other is fixed to the basement wall. Figure 3-21 illustrates the components of the shear mechanism in the current study's model.

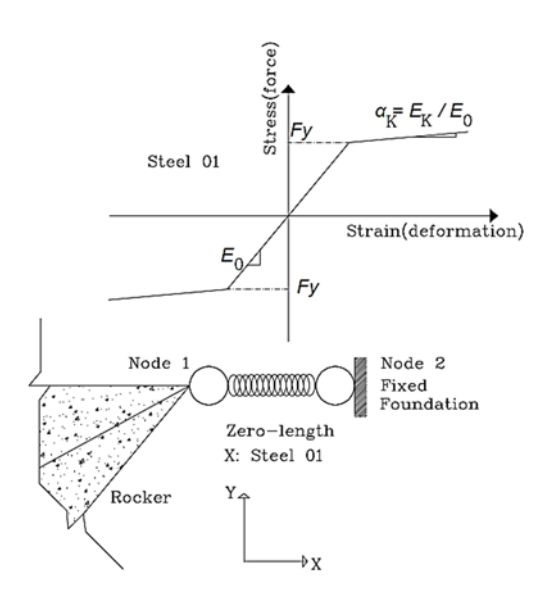


Figure 3-21: Modelling of shear mechanism as a translational spring (bottom), and the material model used for simulation, selected from the OpenSees library (top)

To capture both compression and tension, a zero-length element with Steel01 was assumed and, a uniaxial nonlinear material from the OpenSeesPy library, was assigned. The Steel01 model is a bilinear hysteretic material with kinematic strain hardening. This formulation was selected because it effectively captures the most critical performance characteristic of a BRB: a stable, symmetric hysteretic loop that yields in both tension and compression without degradation [66]. The initial stiffness and yielding strength of this material were determined for each of the generic buildings, as it was discussed in Subsections 3.2.6 and 3.2.7.

By assigning zero stiffness to the vertical and rotational degrees of freedom, the element can only transmit a shear force. This modelling technique provides a computationally efficient way to represent the combined function of both the shear fuse (the BRBFs) and the shear transmitter. It correctly enforces the intended kinematics—transferring lateral load while allowing free vertical and rotational movement—without the need to explicitly model the shear transmitter as a separate physical component. This behaviour is consistent with the intended function of the shear transmitter in this part of the MechRV3D system, as described in the initial study [15].

## 3.6.5. Leaning Columns

To account for the P- $\Delta$  effect from the gravity system, all columns outside the core are represented by a single leaning column element. This element is assigned the full tributary gravity load (P) but modelled with zero lateral stiffness, ensuring its sole function is to introduce the secondary overturning moment ( $M = P \times \Delta$ ) from the building's sway. In this study leaning columns are modelled using corotational truss elements in OpenSeesPy, a type of element that is specifically formulated to handle large geometric displacements and rotations accurately (refer to Figure 3-16). The cross-sectional area assigned to the leaning columns was set equal to the sum of the gross cross-sectional areas of all gravity columns outside the core. The element was assigned a Young's Modulus (E) consistent with the material used in the physical columns.

The leaning columns were connected to the foundation with a pinned boundary condition, which is an intrinsic property of the corotational truss element used in the model. Corotational truss elements in OpenSeesPy is formulated to carry only axial loads and cannot transfer moments. Above the ground level, the leaning columns are constrained to the core stick at each level by truss elements, which simulate the floor rigid diaphragms. At the ground level, the leaning column were slaved to the top nodes of the rocker as part of the horizontal rigid diaphragm (skirt diaphragm), capturing the effect of the swaying of these columns in response to the horizontal movements of the rocker.

A key consideration is the kinematic compatibility between the central rocking core and the peripheral gravity columns that the leaning column represents. The physical gravity columns are supported on the skirt diaphragm, not the rocker. The shear transmitters are designed to transfer horizontal displacement ( $\Delta$ <sub>b</sub>) from the rocker to the skirt but are detailed to accommodate the rocker's rotation and uplift without transferring these motions. Consequently, the bases of the gravity columns experience a large horizontal translation

 $(\Delta_b)$  but do not tilt or uplift. To ensure this compatibility in a real structure, the first-story gravity columns and their connections must be designed to be flexible enough to accommodate this large lateral drift without failing or resisting a significant amount of lateral force, which would interfere with the primary shear fuses.

The leaning column's model used in this parametric study accurately captures this intended behavior. By connecting the leaning column to the core with pin-ended truss elements at each floor, the model correctly simulates a gravity system that sways along with the core but provides no primary lateral resistance. This validates the use of this simplified modeling approach for the objectives of this study. While the development of the physical connection details is a complex design challenge identified for future research, the conceptual basis for both the real system's compatibility and the model's simplification is sound.

## 3.6.6. Damping in the Model

Inherent energy dissipation in the superstructure, separate from the hysteretic action of the primary mechanisms, was modelled using Rayleigh damping. This is a common approach in nonlinear dynamic analysis where the damping matrix is defined as a linear combination of the mass and stiffness matrices. A target damping ratio of 2.5% was selected, which is a standard value recommended in performance-based design guidelines for tall buildings, such as the PEER TBI [29] and LATBSDC [47], for representing the inherent damping in a structure at the onset of significant damage.

To define the Rayleigh damping coefficients ( $\alpha$  and  $\beta$ ), the 2.5% damping ratio was anchored at two key periods: the first mode period ( $T_1$ ) and a higher mode period, depending on which controlled the 90% mass participation. This two-point fit ensures that the damping is reasonably controlled across the most significant modes of response,

preventing overdamping of higher modes which can be a significant issue in tall buildings [5].

A critical aspect of this implementation was the explicit exclusion of Rayleigh damping from certain elements. To avoid unintended damping, no Rayleigh damping is applied to the zero-length elements, as these may encounter abrupt changes in stiffness. This careful application of damping ensures that the energy dissipation is realistically represented and that the analysis results are not corrupted by numerical artifacts.

#### **3.6.7. Loading**

The gravity loads were applied separately to the leaning columns and the core stick at each floor level, based on their respective tributary areas. The gravity loads were distributed equally, with 50% assigned to the core stick and 50% to the leaning column. This 50/50 allocation is a rational assumption for a generic high-rise model and is further supported by established research models, such as the PEER Tall Buildings Initiative (TBI) benchmark building [50]. In terms of lateral loads, this research is focused on high-rise buildings in high-seismicity regions, and therefore assumes that seismic demands, rather than wind loads, govern the design of the lateral force-resisting system.

In the next step, the model was first evaluated using the pushover analysis method to verify that each mechanism was properly engaged as intended. Subsequently, modal analysis was conducted on fixed-base buildings—having the same superstructure as shown in Figure 3-16 but without the mechanisms—to determine their fundamental periods and to assess the contribution of each mode to the overall dynamic response.

## 3.7. Pushover Analysis

Before conducting the comprehensive suite of dynamic analyses, a series of static pushover analyses was performed. It is critical to note that this simplified, static procedure is not intended to capture the complex, dynamic influence of higher-mode effects; that is the explicit purpose of the NLRHA detailed in Section 3.9. Instead, the pushover analyses serve a distinct and limited purpose: to verify that the key nonlinear mechanisms of the numerical model are behaving as intended under simple, well-defined static loading patterns. A first-mode-dominant loading pattern was used to verify the activation of the rocking mechanism, while a separate loading pattern was used to verify the yielding of the shear mechanism.

The 15-story generic building was selected as a representative example for the pushover analysis. This structure was modelled using the general framework shown in Figure 3-16. The rocker depth (D) was set to 4 m, the lower bound of its practical range, while the megacolumn height  $(h_c)$  was set to 8 m, a realistic mid-range value from the range in Subsection 3.2.5. The diameter of the mega-columns was set at 750 mm, which is slightly smaller than the value determined for the 15-story case, yet remains adequate for structural performance. The centre-to-centre distance between the mega-columns in this model was specified as 4985 mm. The weight of superstructure was considered according to  $W_{core}$  in Table 3-4 with weight of the rocker as 10% if the  $W_{core}$ . The other properties of core stick were selected from Table 3-2.

The pushover analysis was conducted in a displacement-controlled manner, with lateral drift measured at the roof level,  $\Delta_{\text{roof}}$ . This displacement was assumed to start from the atrest position and reach 1.5% of the total height of the superstructure (H) above the ground as the target lateral displacement. This target drift was selected as it represents a significant level of lateral deformation, consistent with the life safety performance objective for this type of structure under a design-level earthquake [29]. The lateral displacement at the roof level ( $\Delta_{\text{roof}}$ ) was incrementally increased in a series of small, discrete steps until the target roof drift of 1.5% was achieved.

A first-mode-dominant loading pattern was used primarily to verify the rocking mechanism activates at the prescribed overturning moment and that the model accurately captures the subsequent rigid-body rotation. A separate, shear-dominant loading pattern was then used to verify the shear mechanism, confirming that it yields at its design strength and provides the intended ductile, force-limiting behaviour.

To simulate first-mode dominance, the resultant of the lateral forces was applied as a point load at 2/3H above ground level when the lateral forces forming an inverted triangle over the building height, as shown in Figure 3-22.

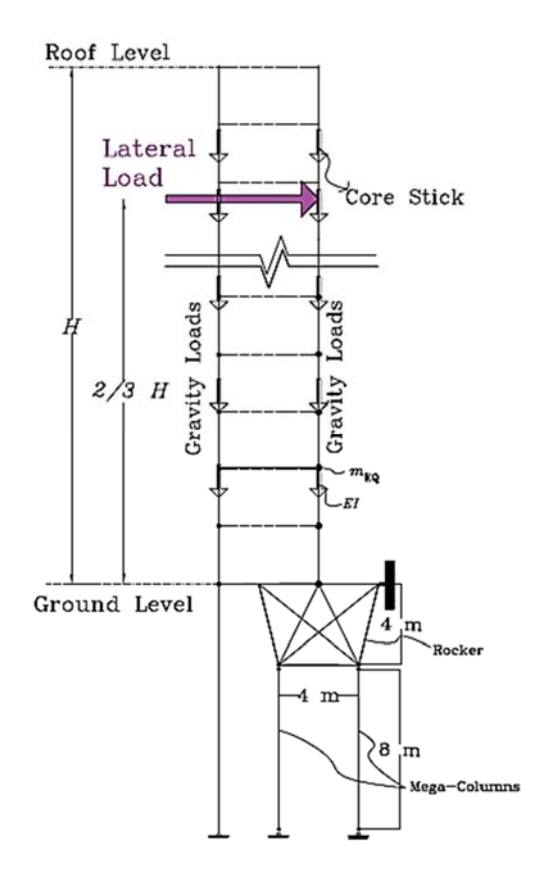


Figure 3-22: Loading profile for pushover analysis to activate rocking mechanism

#### 3.7.1. Activation of the Rocking Mechanism

A capacity curve obtained from the first-mode pushover analysis is plotted in black line in Figure 3-23. This graph shows the relation between the applied lateral force (F), shown as a ratio of it to the seismic weight of the structure  $(W_{EQ})$  and the rotation at the roof level,

 $\theta_{\text{roof}}$  that was considered as a ratio of  $\Delta_{\text{roof}}$  to H. The other graph in blue colour shows the variation of the  $\theta_{\text{rocker}}$  (rotation at the base of the rocker) with  $\theta_{\text{roof}}$ .

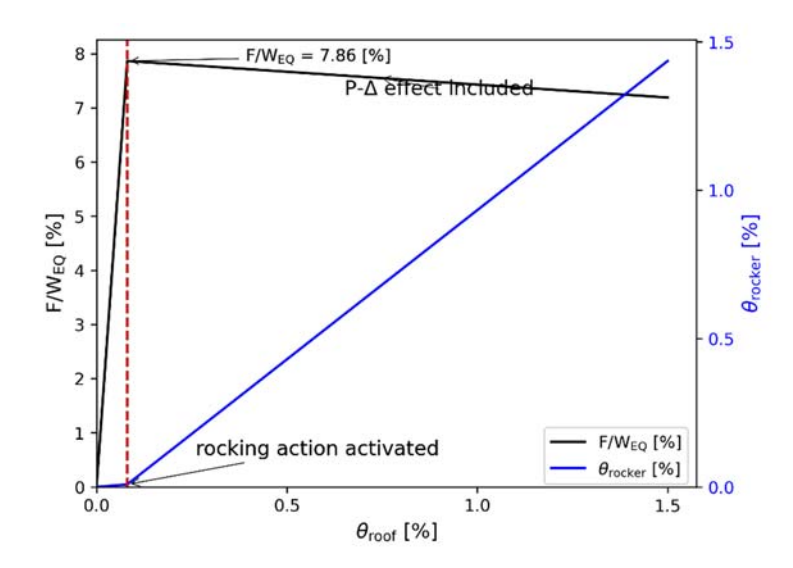


Figure 3-23: Lateral capacity curve and base rocking rotation, using the 15-story building as a representative example at Los Angeles site

From Figure 3-23, it can be observed that initially, no uplifting occurs at the base of the rocker ( $\theta_{\text{rocker}}$ =0), and as the applied force increases, the roof rotation remains relatively small. In this stage, the roof rotation, representing the lateral displacement at the roof level, is primarily contributed by the elastic deformation of the superstructure. When the applied force (F) reaches a threshold (varies due to gravity load and  $d_{c2c}$ ), the rocking mechanism is activated.

As the core is pushed further, the roof rotation increases when the rocker's rotation increases, such that the slope of the  $\theta_{\text{roof}}$ - $\theta_{\text{rocker}}$  curve approaches unity, as seen in the blue graph. Simultaneously, the applied force no longer increases; instead, it begins to decrease (black-colour graph), contrary to the typical behaviour of a capacity curve. This behaviour highlights the contribution of P- $\Delta$  effects due to the rocking action, which induces negative stiffness, leading to a reduction in the capacity curve.

In the first-mode pushover, the shear mechanism remained within its linear elastic range and did not yield. Therefore, the relationship between the base shear ( $V_b$ ), shown as a ratio

of the base shear to the seismic weight of the structure ( $W_{EQ}$ ), and the horizontal displacement of the rocker ( $\Delta_b$  or  $\Delta_{skirt}$ ) remains linear, indicating that the shear mechanism stays within its elastic range, as shown by the red-colour graph in Figure 3-24.

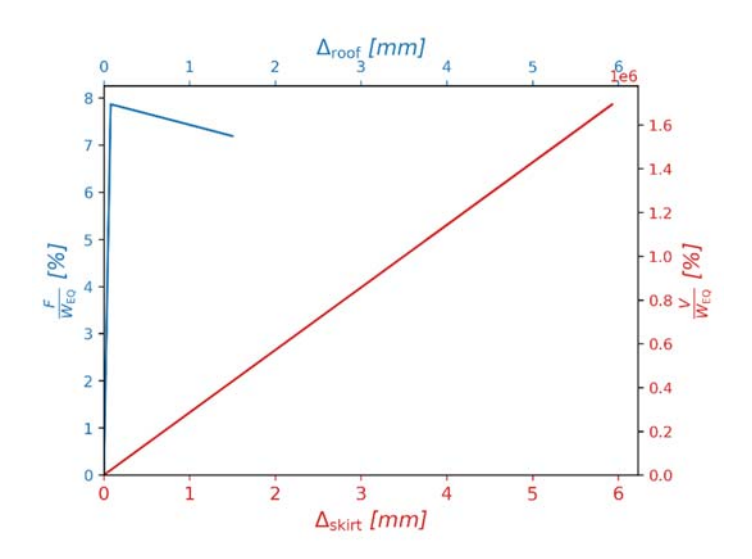


Figure 3-24: Shear Mechanism behaviour during first-mode pushover

The blue-colour graph in Figure 3-24 shows the lateral displacement at the roof level in terms of the applied lateral force (F), shown as a ratio of this force to the  $W_{EQ}$ . As it can be seen, it is consistent with the variation of  $\theta_{roof}$  in Figure 3-23 in terms of the decreasing trend in black-colour graph. After reaching to a threshold of applied lateral force, the roof lateral displacements decrease due to the P- $\Delta$  effect caused by the rotation of the rocker indicating the activation of the rocking mechanism.

### 3.7.2. Engagement of the Shear Mechanism

To verify if the shear mechanism will be engaged as intended, a second pushover analysis was conducted. In this analysis, the resultant of the lateral load (F) was applied as point load at the level of 0.1H. Red-colour graph in Figure 3-25 shows the entire process including the post-yielding behaviour of the shear mechanism via relation of horizontal displacement of the rocker ( $\Delta_b$  or  $\Delta_{skirt}$ ) and the base shear ( $V_b$ ). The gradually increment of

the red-colour graph in post-yielding conditions is consistent with the post-yielding behaviour of Steel01 which was assumed as shear fuse material.

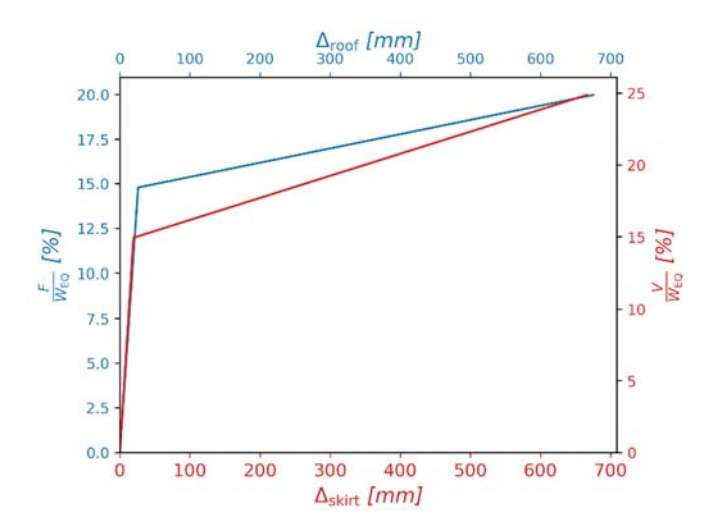


Figure 3-25: Shear mechanism engagement when lateral load is applied at 0.1H

The blue-colour graph in Figure 3-25 shows the variation of the roof lateral displacement with the increase in the applied lateral force ( $F/W_{EQ}$ ). The slope of the graph transitions from a rapid increase in the elastic range of the shear mechanism to a gradual increase after the shear mechanism yielded. The ratio of the applied force (F) to the seismic weight of the structure ( $W_{EQ}$ ) also corresponds to the assigned yielding-strength of the shear mechanism in this model, which was approximately 14.9% of  $W_{EQ}$  according to Figure 3-25. In conclusion, this loading resulted in engaging the shear mechanism effectively and reaching to the yielding point.

#### 3.8. Parametric Nonlinear Response History Analyses

To perform the parametric study, NLRHAs was conducted using enough ground motion records recommended by ASCE 7-22 and NBCC 2020 codes [18], [49], ensuring capture of the system's nonlinear dynamic behaviour accurately. The model is analysed for two different site locations (Los Angeles, California, United States and Vancouver, British Columbia, Canada). For each site, the appropriate suites of ground motions records that

reflect the site's seismicity are selected and scaled according to corresponding code requirements. This process is carried out for each generic building listed in Table 3-2.

## 3.9. Ground Motion Selection and Scaling

## 3.9.1. Los Angeles Site

The buildings are assumed to be located in Los Angeles, California, U.S., which is in a high seismicity zone. The dominant faults in Los Angeles area are reverse and strike-slip faults [56]. The Los Angeles city is located near several faults, Figure 3-26.

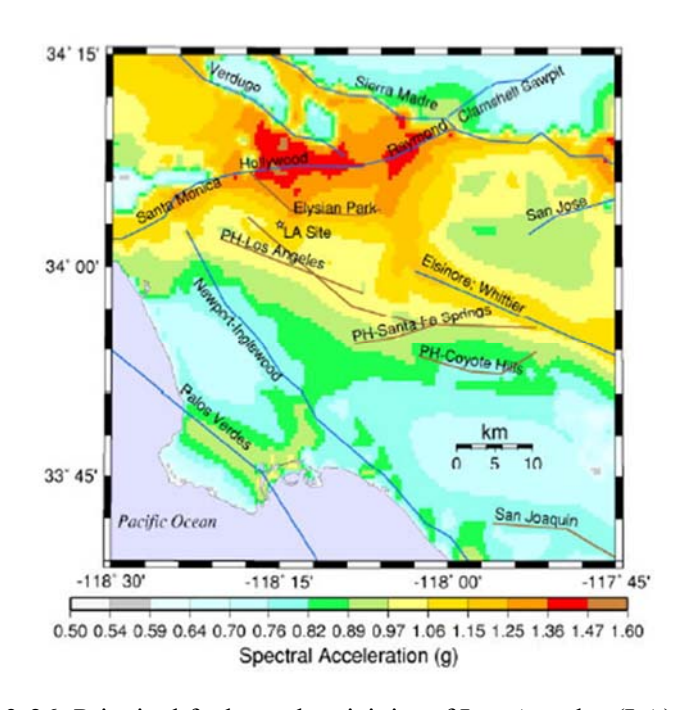


Figure 3-26: Principal faults at the vicinity of Los Angeles (LA) site [67]

Los Angeles site is located at a latitude of 34.054, and longitude of -118.242. The risk category of the building and site class have been chosen as II (the risk category applies to most common buildings) and site class C respectively, according to ASCE/SEI 7-22 [18]. Based on the seismic hazard models [68], the parameters for selecting ground motion records are summarized in Table 3-12.

Table 3-12: Parameters to select ground motion records for analyses

Parameters	Values
Magnitude	6 - 9
R <sub>rup</sub> (km)	0-120
$R_{\rm jb}$ (km)	0-120
V <sub>s30</sub> (m/s)	180-1150
D <sub>5-95</sub> (sec)	15-60
Fault Type	All Types
Damping Ratio	5%
Component	RotD100 (maximum direction)

To scale the ground motions, according to ASCE/SEI 7-22 [18], it is required to determine the lower bound of the scaling period range as minimum of  $T_{90}$  (the highest-numbered mode corresponding to 90% cumulative modal mass participation) or 0.2  $T_a$  (fundamental period). To find  $T_{90}$ , modal analyses had been conducted for corresponding fixed-base version of generic buildings. The upper bound is considered as  $2T_a$  as well. The results of these analyses have been shown in Table 3-13.

Table 3-13: Period range [18], for scaling ground motions for buildings of different heights

Number of stories (n)	$T_{\rm a}({ m s})$	T <sub>90</sub> (s)	Mode (90% mass participation)	0.2 <i>T</i> <sub>a</sub> (s)	Lower bound: min (T <sub>90</sub> , 0.2 T <sub>a</sub> ) (s)	Upper bound - $2T_a$ (s)
15	1	0.018	5	0.2	0.018	2
30	2	0.036	5	0.4	0.036	4
50	3	0.054	5	0.6	0.054	6
70	4	0.118	4	0.8	0.118	8
100	5	0.147	4	1	0.147	10
120	6	0.176	4	1.2	0.176	12

The selected ground motions for each generic building with their scale factors and the weight assigned to scale the ground motions over their respective period ranges [18], are listed in Table 3-14. These records were amplitude-scaled to match the target MCE spectrum for site class C. The scale factors were obtained using PEER NGA-West2 [69]. In this table, near-fault events are specified with an underline.

Table 3-14: Scale factors for buildings of different heights in Los Angeles site location

	Scale factors								
RSN	15-story	30-story	50-story	70-story	100-story	120-story			
	Weigh	nts: [0.2-0.6-0.2	:]	Weights: [0	.3-0.6-0.1]	[0.45-0.45-0.1]			
<u>6</u>	3.4517	3.2494	3.5873	3.9211	4.1742	4.3205			
14	-	-	6.814	-	-	-			
15	5.3564	6.2823	-	7.5945	7.7696	7.806			
20	4.8087	3.1482	3.3337	3.8348	4.1845	4.3095			
36	-	-	5.5684	5.5719	5.4244	5.2702			
57	3.5514	6.3282	-	-	-	-			
<u>143</u>	<u>1.0655</u>	<u>1.1876</u>	1.0801	<u>1.0131</u>	1.0164	1.0452			
169	2.9378	2.8295	2.8781	3.0525	3.0999	3.1398			
266	6.2186	4.4504	3.993	4.0577	4.0707	4.1388			
<u>292</u>	2.7206	2.2389	2.0472	2.0976	2.1929	2.2881			
300	4.9694	3.8901	4.963	6.1992	7.0108	7.2649			
313	3.606	4.0014	5.5223	6.7375	7.8103	8.2627			
341	-	-	-	6.4341	7.0385	7.2925			
342	5.189	4.6581	6.6142	-	-	-			

Figure 3-27 shows the MCE response spectra for the Los Angeles site as well as scaled ground motions for the 15-story building used to match the spectrum. Similar plots of MCE response spectra and scaled ground motions for other generic buildings, using the scale factors in Table 3-13, are provided in Appendix B.

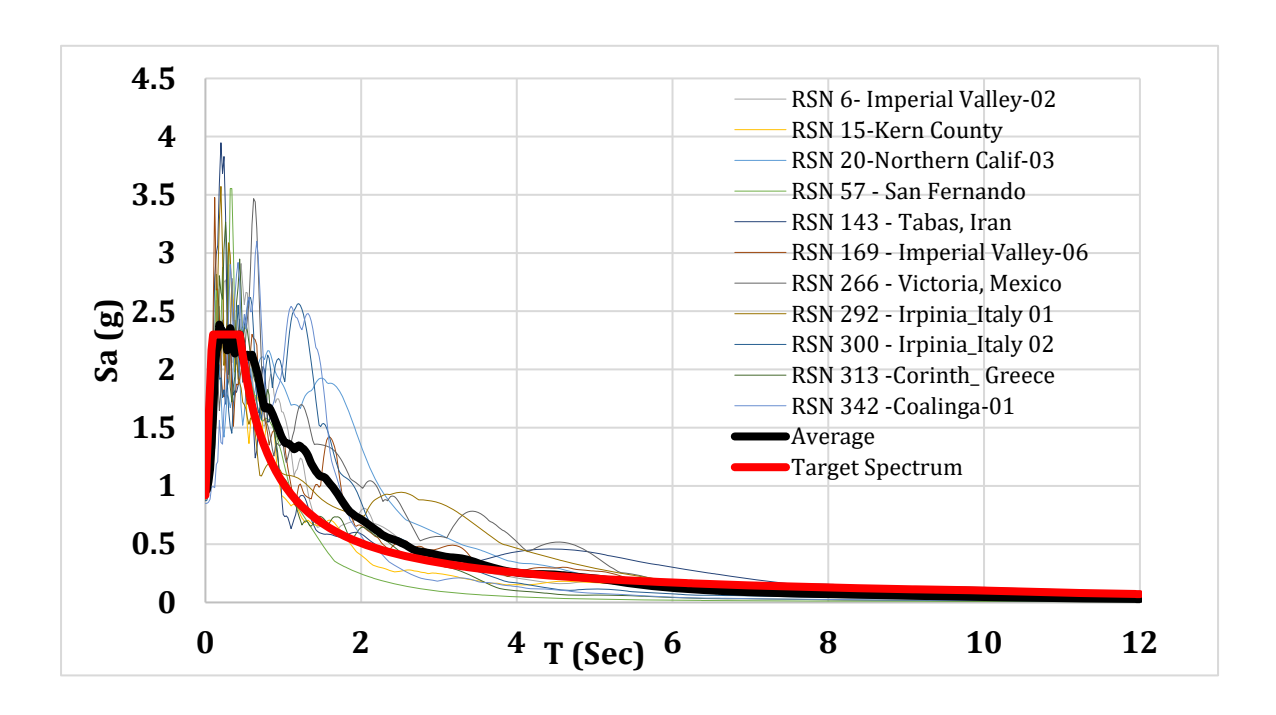


Figure 3-27: MCE response spectra and ground motions scaled for 15-story building,  $T_1$ = 1 sec

#### 3.9.2. Vancouver Site

To extend the findings of this research to a representative Canadian site to assess the applicability of the results under local seismic condition, the buildings are assumed to be located in Vancouver, British Columbia, Canada (latitude:  $49.261^{\circ}$ N, longitude:  $-123.114^{\circ}$ W). Vancouver is categorized as a high seismic hazard area in Canada. The seismic category SC4 was assigned for this site location (City Hall of Vancouver) [28]. The site designation (Xs) was assigned as Site Class D (stiff soil) [70]. Site Class D corresponds to stiff soil conditions with a Vs30 range of 180 - 360 m/s, representing the maximum hazard for this category, Figure 3-28.

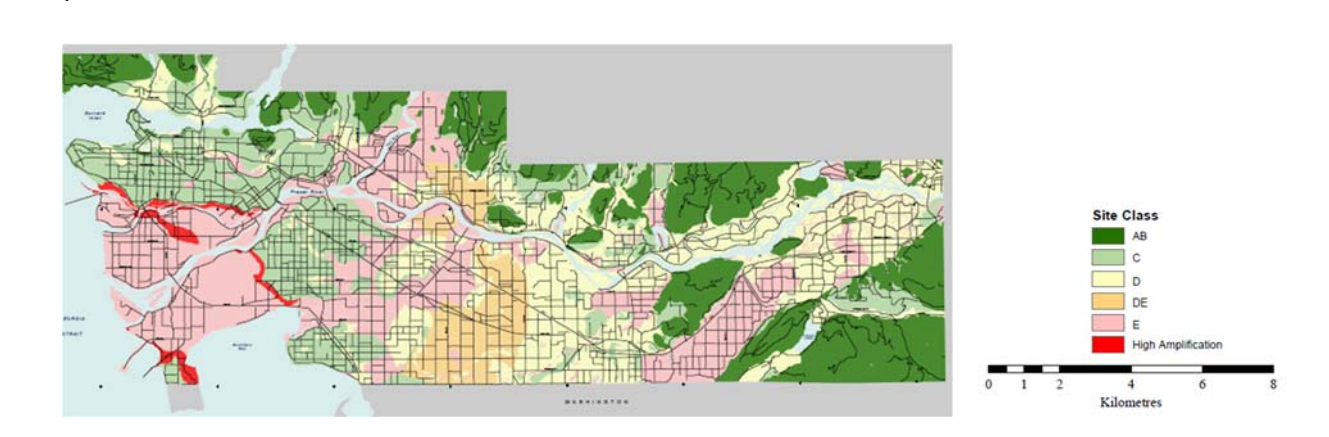


Figure 3-28: Map of distribution of different site classes in Vancouver [70]

According to the disaggregation results for Site Class D in Vancouver provided by Kolaj et al. [71], the dominant source is in-slab earthquake faults for the lower-bound and interface earthquake faults for the upper-bound of Target Response Spectrum ( $T_{RS}$ ). Thus, two different sources (in-slab and interface) contribute to the seismic hazard model [71]. For the lower-bound of Target Response Spectrum ( $T_{RS1}$ ), defined by the period range (0.15-2) seconds, the in-slab contribution dominates except for fundamental periods  $T_1 \le 3$  seconds. In contrast, for the upper-bound spectrum ( $T_{RS2}$ ), spanning (0.176-12) seconds, as well as for  $T_{RS1}$  when  $T_1 > 3$  seconds, the interface contribution becomes dominant.

The assumptions to select ground motion records for MCE level in a class D site for each suite of ground motion (one for in-slab and another for interface earthquake faults) has been summarized in Tables 3-15 to 3-17. The value of 250 m/s for  $V_{\rm s30}$  was selected according to the assumption of seismic hazard model by Kolaj et al. [71].

Table 3-15: Properties of earthquake events for different scenario-specified in Vancouver

Scenario-specified	$T_{\mathrm{RS}}\left(\mathbf{s}\right)$	Magnitude	Distance (km)	$V_{s30}$ (m/s)
In-slab earthquakes	[0, 0.2)	5 - 7	Less than 60	180-360 (250)
Interface earthquake	[0.2, 12]	6.5 - 9	60-130	180-360 (250)

Table 3-16: Properties of earthquake events for In-slab source in Vancouver

In-slab Earthquakes	
Fault Type	Any Type
Magnitude	5-7
R <sub>JB</sub> (km)	0 - 60
R <sub>rup</sub> (km)	0 - 60
$V_{ m s,30}({ m m/s})$	180 - 360
D <sub>5</sub> -95 (sec)	15 - 60
Spectral ordinate	RotD100
Damping ratio (%)	5

Table 3-17: Properties of earthquake events for Interface source in Vancouver

Interface Earthquakes	
Fault Type	Any Type
Magnitude	6.5 - 9
R <sub>JB</sub> (km)	50 - 130
R <sub>rup</sub> (km)	50 -130
$V_{ m s,30}({ m m/s})$	180 - 360
D <sub>5-95</sub> (sec)	15 - 60
Spectral ordinate	RotD100
Damping ratio (%)	5

Figure 3-29 shows the MCE response spectra as well as scaled ground motion for  $T_{\rm RS1}$  and in-slab source when T < 3 sec for a 15-story building. Similar plots are provided for other generic buildings, using the ground motions and corresponding scale factors listed in Table 3-18. The scale factors were obtained using PEER NGA-West2 [69]. In this case, two suites of ground motion records will be used in time history analysis where each suite is scaled

over scenario-specified period range,  $T_{RS}$ . The design seismic demand for structural responses should be taken as the largest of mean values of each suite when each suite contains at least 11 ground motions [28].

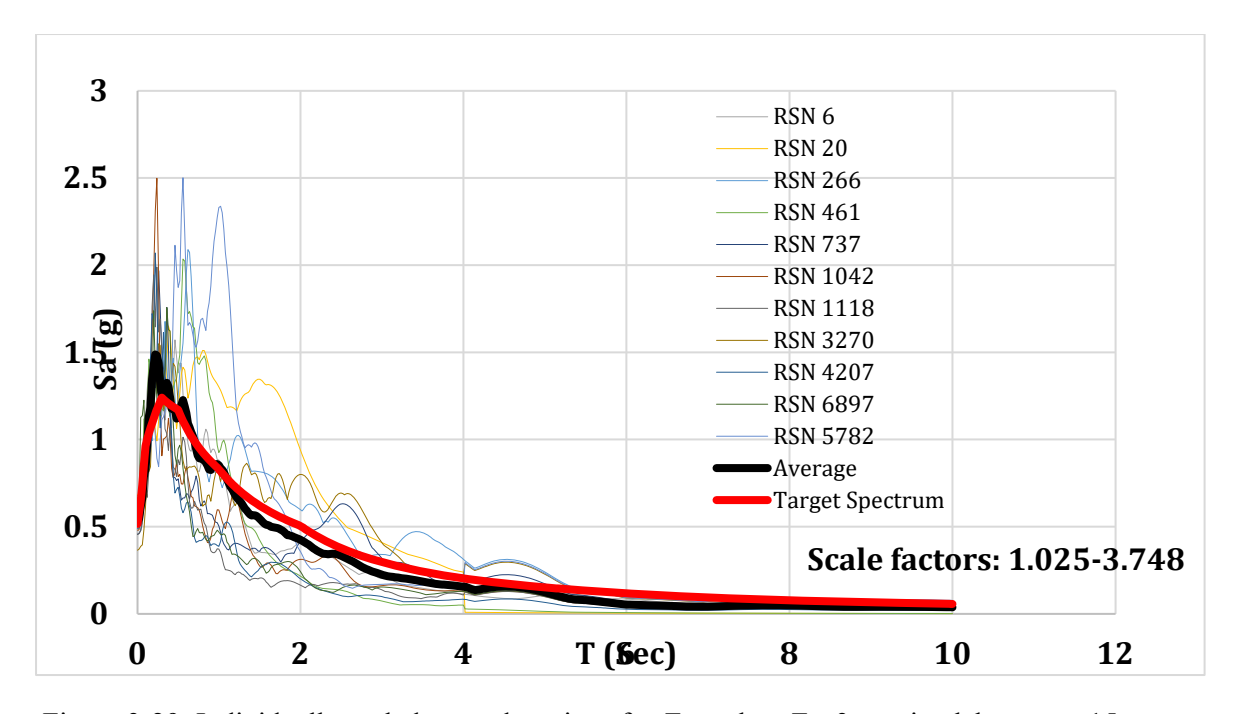


Figure 3-29: Individually scaled ground motions for  $T_{\rm RS1}$  when T < 3 sec, in-slab source, 15-story building according to NBCC [49], Vancouver site

Table 3-18: Ground motion and scale factors for all buildings for  $T_{RS1}$ , in-slab sources, Vancouver site

No.	RSN	Earthquake	Year	Station	$M_{ m W}$	R rup (km)	Scale factor- 15 Story	Time step (sec)
1	6	Imperial Valley-02	1940	El Centro Array #9	6.95	6.09	1.8647	0.01
2	20	Northern Calif-03	1954	Ferndale City Hall	6.5	27.02	3.3601	0.005
3	266	Victoria_ Mexico	1980	Chihuahua	6.33	18.96	3.7480	0.01
4	461	Morgan Hill	1984	Halls Valley	6.19	3.48	2.1727	0.005
5	737	Loma Prieta	1989	Agnews State Hospital	6.93	24.57	2.6964	0.005
6	1042	Northridge-01	1994	N Hollywood - Coldwater Can	6.69	12.51	1.5550	0.01
7	1118	Kobe_ Japan	1995	Tadoka	6.9	31.69	1.5384	0.01
8	3270	Chi-Chi_ Taiwan-06	1999	N Hollywood ColdwateCan	6.3	45.29	3.5544	0.005
9	4207	Niigata_ Japan	2004	NIG017	6.63	12.81	1.0250	0.01
10	5782	Iwate_ Japan	2008	Misato_ Miyagi Kitaura - B	6.9	47.02	3.6231	0.01
11	6897	Darfield_ New Zealand	2010	DSLC	7	8.46	1.5934	0.005

Table 3-19 shows the scale factors used for all generic building in Vancouver site, where each ground motion suite is scaled to match the  $T_{\rm RS2}$  range when interface source dominates. Similar plots of MCE response spectra and scaled ground motions for other generic buildings, using the scale factors in Table 3-18 and 3-19, are provided in Appendix B

Table 3-19: Ground motion and scale factors for all buildings for  $T_{RS2}$ , interface sources, Vancouver site

RSN			Scale fa	actors		
_	15-story	30-story	50-story	70-story	100- story	120 story
_			Weights: [0	.1-0.8-0.1]		
571	2.0866	2.5511	2.8317	3.0029	3.1065	3.2024
862	4.1801	4.3073	-	-	-	-
888	-	-	3.3749	3.4924	3.4924	3.7371
1155	4.5657	4.5049	4.4453	4.2880	4.2010	4.2430
1317	2.7947	2.9555	3.0626	3.1647	3.2156	3.2763
1634	2.7593	6.3282	1.5878	1.6644	1.7251	1.7836
1810	3.7094	1.1876	3.7014	3.5512	3.4419	3.4075
3672	2.4523	2.8295	2.5391	2.6543	2.7125	2.7834
6243	5.7787	-	-	-	-	-
5793	-	5.2811	5.6372	5.8875	6.0635	6.2469
1092	4.6255	5.2266	5.5069	5.8304	6.0907	6.3293
1629	4.4495	3.0028	2.6335	2.4574	2.2879	2.1987
756	5.0521	-	-	-	-	-
744	-	3.1473	3.2537	3.2537	3.2537	3.2537

## 3.10. Parametric Analyses

After determining the scale factors, a fixed-base core stick model is developed for each of the generic building. These six models are used to compute the base overturning moment  $(M_{b,MCE})$  and base shear  $(V_b)$ , derived from the mean values of the NLRHAs results conducted at the MCE level (mean of analyses' results for 11 ground motion records). The obtained  $M_{b,MCE}$  is used to determine the rocking activation moment  $(M_{rock})$ , and the parameters of the rocking mechanism  $(d_{c2c}$ , and D).  $V_b$  is used to define the initial stiffness

of the shear mechanism ( $K_{b1}$ ). The lower bound of the shear mechanism strength ( $V_y$ ) is determined using obtained  $M_{rock}$ .

In the next step, another model is developed for each of the generic building, where the shear mechanism is assumed to remain elastic to compute  $V_{\rm 1M0V}$ , following another series of NLRHAs conducted on the six new models. The resulting  $V_{\rm 1M0V}$  is used to determine the maximum shear mechanism strength. Finally, complete models—including all components illustrated in Figure 3-16—are developed for each generic building (another set of six models). The effects of various parameters on seismic responses are evaluated through multiple series of NLRHAs. As a result of 810 parameter combinations subjected to the ground motions suites, two series of plots are generated, which collectively form seismic performance spectra.

In this system, it should be noted that not all design parameters are inherently independent. Certain parameters are mechanically coupled by definition, such as the rocker depth (D) and the Moment Reduction Factor  $(R_{\rm M})$ , or the Shear Reduction Factor  $(\mu_{\rm V})$  and the required initial stiffness of the shear mechanism  $(K_{\rm bl})$ . These interdependencies are not a result of the chosen modeling strategy, but rather reflect the physical nature of the MechRV3D system. Therefore, the parametric analyses were conducted by fixing one parameter at a time and varying others within practical ranges, in order to capture the influence of each while respecting these inherent couplings. This approach ensures that the results remain physically consistent and that the observed dependencies can be systematically quantified.

#### 3.11. Design Code Requirements for Seismic Responses

To control damage caused by excessive displacements, peak inter-story drift ratios, represented as  $\delta_s$ , are used to assess the seismic performance of high-rise buildings with the MechRV3D system incorporated at the base. In rocking systems, IDRs is the sum of the

drift from the elastic deformation of the superstructure and the drift caused by the rigid-body rotation of the entire structure at its base. By including the contributions from both the superstructure's elastic deformation (flexure and shear) and the rigid-body base rotation, the total inter-story drift ratio (IDR) provides a comprehensive measure of the building's overall seismic deformation [15].

The primary objective of the MechRV3D system is to achieve a low-damage performance state in the superstructure, exceeding the typical Life Safety objective of conventional fixed-base design [15]. To quantify this enhanced performance, the inter-story drift ratios (IDRs) must be compared against stringent acceptance criteria associated with minimal damage.

Accordingly, this study adopts the performance limits from established performance-based seismic design guidelines, such as the PEER TBI Guidelines [31] and ASCE 41-17 [18]. These documents define specific acceptance criteria based on inter-story drift ratio (IDR) thresholds for achieving an Immediate Occupancy (IO) performance level. For a concrete core-wall structure, the IO limit is typically in the range of 0.5% to 1.0%, a value chosen to prevent significant damage to both non-structural components and the primary structure itself. This provides a direct, rational, and performance-based benchmark for evaluating the effectiveness of the MechRV3D system.

Since peak IDR response should be evaluated by performance objectives such as life safety or immediate occupancy, design codes set allowable drift limits, which vary with building type, performance level, and seismic intensity [18], [28]. To achieve an Immediate Occupancy (IO) objective, a designer might target a maximum IDR of 0.5%. The spectra can be used to find the combination of system parameters that meets this stringent target.

For a less critical structure, a Low-Damage objective might target a maximum IDR of 1.0%. Meeting the conventional Life Safety (LS) objective would correspond to an IDR of approximately 1.5% - 2.0%. [18], [29].

At the same time, it is crucial to control the deformations at the base to levels that are practical to achieve. In design codes, base displacement is typically considered for base-isolated structures, and the corresponding limits are adjusted based on various factors such as building height, the type of isolation system (e.g., elastomeric bearings or sliding bearings), and the intended performance objective [18], [49].

In the context of MechRV3D system, base displacement ( $\Delta_b$ ) is a particularly important parameter for the shear mechanism. Excessive deformation at the base can lead to unrealistic strain demands and potential fracture in the shear mechanism. Additionally, large base displacements affect the stability of the mega-columns. When there is significant relative displacement between the top and bottom ends of the mega-columns, their ability to carry axial gravity loads could be compromised.

The performance spectra developed in this study provide the resulting  $\Delta_b$  as well as  $\delta_s$  for a given set of design parameters. This allows a designer to directly assess the trade-offs between these two responses ( $\Delta_b$  and  $\delta_s$ ) and select a system configuration that keeps the base displacement within an acceptable range for their specific components. For example, a practical upper-bound limit for  $\Delta_b$  might be on the order of 800 mm, a value justified by the component capacity and stability analyses detailed in Section 4.6.

#### 3.12. Summary of Methodology

To better predict the behaviour of the MechRV3D system, it is necessary to develop an improved design procedure. The previous procedure was based on a model that did not account for the size limitations of the rocker and the P- $\Delta$  effect of the mega-columns

involved in the rocking mechanism. To address the influence of these factors on the system's structural behaviour, the design parameters were revised in the first step.

After determining the range of parameters, parametric analyses were conducted using NLRHAs on the developed model described in this Chapter (Figure 3-16). The acceptable seismic response for maximum inter-story drift ratio is assumed to be 1.5% to meet the requirement of building codes. The other seismic response, maximum base displacement (\$\Delta\_{b,max}\$) is assumed 800 mm. The seismic response results obtained from the parametric analyses generate new sets of plots—referred to as seismic performance spectra—which are used to develop the design procedure for the MechRV3D system.

In regions where the governing design is controlled by wind, the wind-induced overturning moment at service level ( $M_{\text{wind}}$ ) can exceed the seismic moment at the Service Level Earthquake ( $M_{\text{b,SLE}}$ ). In such cases, the rocking activation moment ( $M_{\text{rock}}$ ) should be set greater than  $M_{\text{wind}}$  to prevent undesired rocking under service-level conditions. Since  $M_{\text{rock}}$  is determined from , $M_{\text{b,MCE}}$  using the Moment Reduction Factor ( $R_{\text{M}}$ ), increasing  $M_{\text{rock}}$  implies that a smaller  $R_{\text{M}}$  must be adopted .Moreover,  $M_{\text{rock}}$  directly affects the minimum yield strength of the shear mechanism ( $V_y$ ) through the term of  $M_{\text{rock}}/h_{\text{eff}}$  in  $V_y$  Equation 3-7. Therefore, a larger  $M_{\text{rock}}$  requires a different  $V_y$ , resulting in different stiffness at the base that changes the trade-off between base displacement and inter-story drift ratio.

The shear mechanism must be checked to ensure it does not engage under service wind loads and remains elastic, with potential consideration for fatigue effects. Additionally, a supplemental damping system (like a TMD) may be required to manage occupant comfort under frequent wind-induced accelerations.

## 4. Results and Discussion

## 4.1. Procedure for Constructing Seismic Performance Spectra

Following the parametric analyses, families of seismic performance spectra were developed. The introduction of a new design parameter— $h_c$  (the height of the megacolumns)—led to additional sets of results. Yet, this research continues to focus on maximum base displacement ( $\Delta_b$ ) and peak inter-story drift ratio ( $\delta_s$ ) as the primary performance metrics. These two response quantities were selected because they represent the fundamental design trade-off inherent in this type of uncoupled system.  $\delta_s$  is the key indicator of damage in the superstructure and  $\Delta_b$  dictates the deformation demand on the base mechanism's components.

While peak floor acceleration is a critical metric for assessing damage to non-structural components and contents, it was not included as a primary response quantity in this parametric study. It is expected that the system's inherent mechanisms of period elongation and force-limiting will effectively control floor accelerations, a conclusion that would be explicitly verified in a detailed, project-specific design.

To effectively visualize the influence of the new geometric parameters, this study presents the results in two complementary sets of seismic performance spectra. The first set of plots uses mega-column height ( $h_c$ ) as the primary horizontal axis for fixed values of the shear reduction factor ( $\mu_V$ ). This format directly illustrates the trade-offs associated with a key geometric design choice. The second set uses the shear reduction factor ( $\mu_V$ ) as the horizontal axis for fixed values of mega-column height ( $h_c$ ). This allows for a clear investigation of the influence of the shear mechanism's strength on system performance.

Together, these two presentations provide a comprehensive view of the design space, enabling engineers to make informed decisions about both the system's physical geometry and its force-limiting characteristics. In each set, separate plots were provided for each distinct value of the moment reduction factor ( $R_{\rm M}$ ). The vertical axes represented seismic responses (with each response potentially shown on either side in a combination plot). The effect of different initial stiffness of the shear mechanism was illustrated using different curves for each specified parameter related to r  $K_{\rm bl}$  within each plot.

To avoid generating an excessive number of seismic performance spectra and to provide a broader acceptable range of  $\mu_V$  that aligns with designers' requirements, the first set of plots was sketched for only three specific values of  $\mu_V$  as constant parameter. These values are selected as the lower bound ( $\mu_V = 0$ ), the upper bound ( $\mu_V = 1$ ), and the midpoint ( $\mu_V = 0.5$ ).

## 4.1.1. Performance-Based Design Framework and the Role of Performance Targets

The seismic performance spectra developed in this study are intended to be used within a Performance-Based Design (PBD) framework. In this approach, the design process does not start with prescriptive rules, but with the selection of explicit performance targets that define acceptable levels of damage and deformation. These targets are typically expressed as limits on key engineering demand parameters. For this study, two primary performance targets are considered:

- A limit on the maximum inter-story drift ratio ( $\delta_{S,lim}$ ): This is a serviceability and damage-control limit state for the superstructure. A designer might select a stringent target (e.g.,  $\delta_{S,lim}$ = 0.7%) for an Immediate Occupancy objective, or a more common target (e.g.,  $\delta_{S,lim}$ = 1.5%) for a Life Safety objective.
- A limit on the maximum base displacement (Δ<sub>b,lim</sub>): This is a practical and stability-based limit state for the base mechanism. A designer would select a target (e.g., Δ<sub>b,lim</sub> = 800 mm) based on the physical deformation capacity of the shear fuse components and the stability of the mega-columns.

The performance spectra presented in the following sections serve as the primary design tool. They allow an engineer to enter with their chosen performance targets ( $\delta$ s,lim and  $\Delta$ b,lim) and identify a feasible set of design parameters ( $h_c$ ,  $\mu_V$ ,  $r_K$ b1, etc.) that will ensure the final structure meets these objectives. This process is illustrated in detail in the design example in Section 4.5.

#### 4.2. Seismic Performance Spectra for Shear Reduction Factor ( $\mu_V$ ) as Constant

This set of plots shows the variation of seismic responses, the maximum of base displacement ( $\Delta_b$ ) and the maximum of inter-story drift ratio ( $\delta_s$ ), against the height of mega-columns ( $h_c$ ). In these spectra, the results are organized according to discrete values selected for the  $r_K_{bl}$ ,  $R_M$  and fundamental period (T), based on the ranges established in Chapter 3. The parametric study was then conducted in three separate sets, where the shear reduction factor ( $\mu v$ ) was held constant within each set at one of three specific values of its range: the lower-bound, the upper-bound and the mid-point.

To plot the spectra, the peak seismic responses under each ground motion record was obtained and the mean value of all peak values for each suite of ground motion records was taken as the final design response, a procedure in accordance with ASCE 7 and NBCC design codes [18], [49]. The plots in this chapter are spectra for the Los Angeles and Vancouver sites.

Nevertheless, considering the required diameter of the mega-column for a 120-story building as 6400 mm, a height smaller than 6 m would result in a very short and stocky column, which is not practical. Furthermore, from the nonlinear analysis, it was found that the analysis would diverge for mega-columns' heights smaller than 4 m due to the lack of stability against lateral displacement demand. For a given lateral base displacement ( $\Delta$ ), a shorter column must undergo a significantly larger rotation angle that could exceed its

defined safe range to keep its load-carrying capacity. As a result, such a short column would lose its stability. The mechanics of this stability limit are discussed in more detail in Subsection 4.6.

#### 4.2.1. Seismic Performance Spectra for $\mu_V = 0$ , Los Angeles

Each plot in this Subsection to Subsection 4.2.6 presents the maximum base displacement  $(\Delta_b)$  on the left vertical axis and the maximum inter-story drift ratio  $(\delta_s)$  on the right vertical axis, plotted against the varying height of the mega-columns on the horizontal axis. Solid lines represent the variation of  $\Delta_b$ , while dashed lines correspond to  $\delta_s$ . The different colours of the graphs indicate different values of  $r_K_{b1}$ , with blue, orange, and green representing values of 4, 6, and 8, respectively.

The results in this Subsection ( $\mu_V = 0$ ), consistently show that increasing the mega-column height ( $h_c$ ) increases base displacement ( $\Delta_b$ ) while decreasing inter-story drift ( $\delta_s$ ), Figure 4-1. From these graphs, when ( $T_1 \le 3$  s), seismic responses are highly sensitive to  $h_c$  below 6 m. The decrease in inter-story drift ratio with increasing mega-column height indicates greater stiffness at the base, which implies a reduction in the negative stiffness ( $K_{P-Delta}$ ) of the mega-columns in Equation 3-9 as  $h_c$  increases.

The bilinear trend observed in the graphs results from defining  $h_c$  at only three discrete points (2.5, 6, and 12). Incorporating additional intermediate values within the range [2.5, 12] would likely yield a smoother and more representative trend. Nonetheless, the current results remain reliable and adequate for drawing meaningful conclusions.

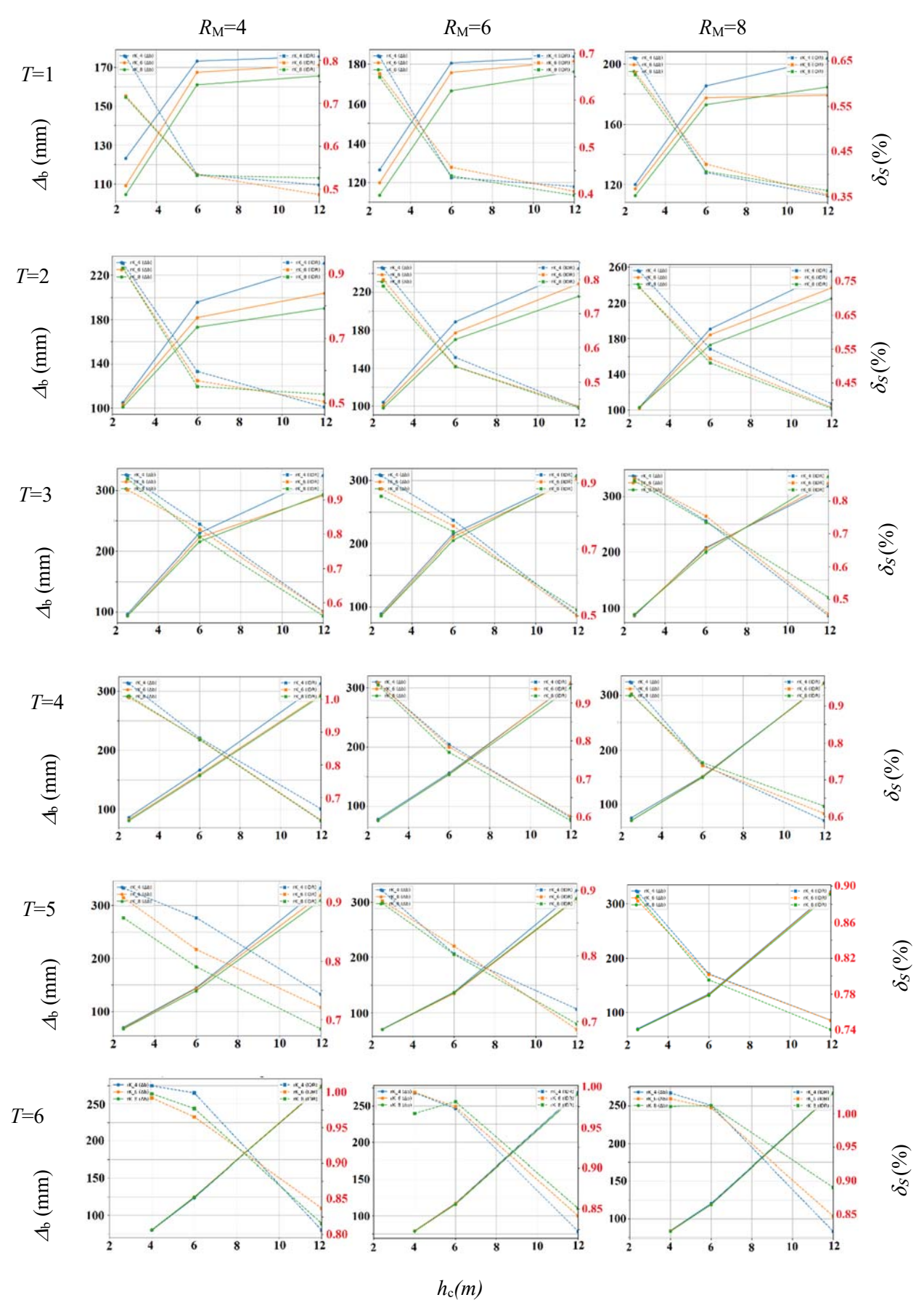


Figure 4-1: Combined plots for inter-story drift ratio and base displacement,  $\mu_V = 0$ , Los Angeles

### 4.2.2. Seismic Performance Spectra for $\mu_V = 0.5$ , Los Angeles

For the case of  $\mu_V = 0.5$ , Figure 4-2, the same general trends are observed: an increase in mega-column height ( $h_c$ ) leads to an increase in base displacement ( $\Delta_b$ ) and a decrease in inter-story drift ratio ( $\delta_s$ ). However, a key difference from the  $\mu_V = 0$  case is the reversed trend in  $\delta_s$  for taller buildings (100- and 120-story), especially for  $r_L K_{b1} = 4$  and  $h_c < 6$  m. This indicates that a stronger shear mechanism ( $\mu_V = 0.5$ ), when combined with reduced initial stiffness (smaller  $r_L K_{b1}$ ) and greater negative stiffness (smaller  $h_c$ ), leads to the dominance of the negative stiffness effect, which adds force in the direction of displacement and thereby amplifies the inter-story drift ratio.

In the  $\mu_V = 0.5$  case, the seismic response exhibits a greater sensitivity to the initial stiffness factor  $(r_{-}K_{b1})$ . Consistently, a higher initial stiffness (a larger  $r_{-}K_{b1}$ ) results in a reduction in both the maximum base displacement ( $\Delta_b$ ) and the inter-story drift ratio ( $\delta_s$ ).

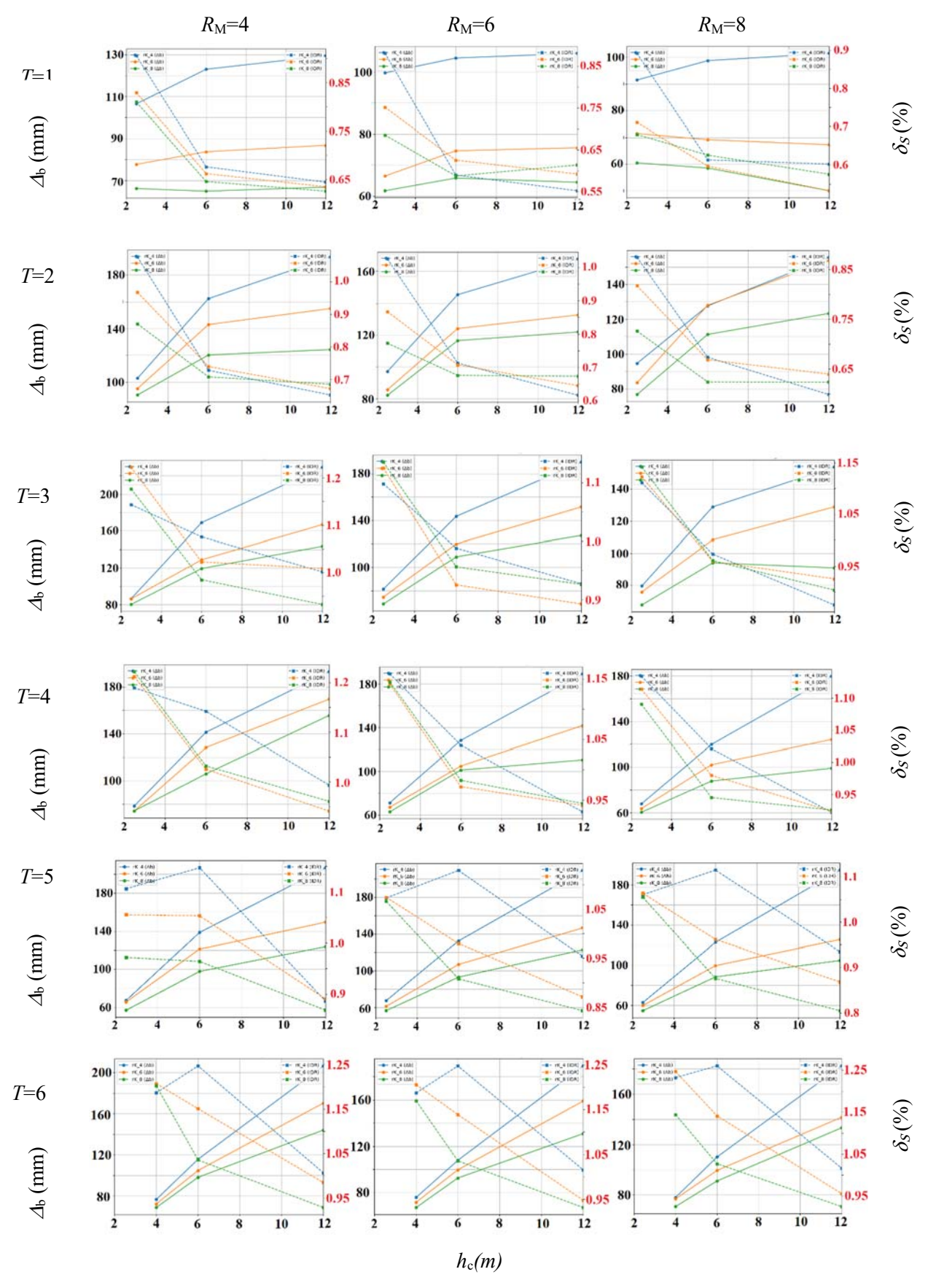


Figure 4-2: Combined plots for inter-story drift ratio and base displacement,  $\mu_V$ =0.5, Los Angeles

# 4.2.3. Seismic Performance Spectra for $\mu_V = 1$ , Los Angeles

For the  $\mu_V = 1$  case, Figure 4-3, the response of the base displacement ( $\Delta_b$ ) remains largely consistent with the previous cases across all building periods. However, in this case, the reversed trend of the inter-story drift ratio ( $\delta_s$ ) begins at  $T_1 \ge 3$  s and is observable not only for  $r_K_{b1} = 4$ , but also for greater initial stiffness of the shear mechanism. This indicates that the effect of increased negative stiffness (smaller  $h_c$ ) becomes more pronounced when a stronger shear mechanism is employed (higher  $\mu_V$ ).

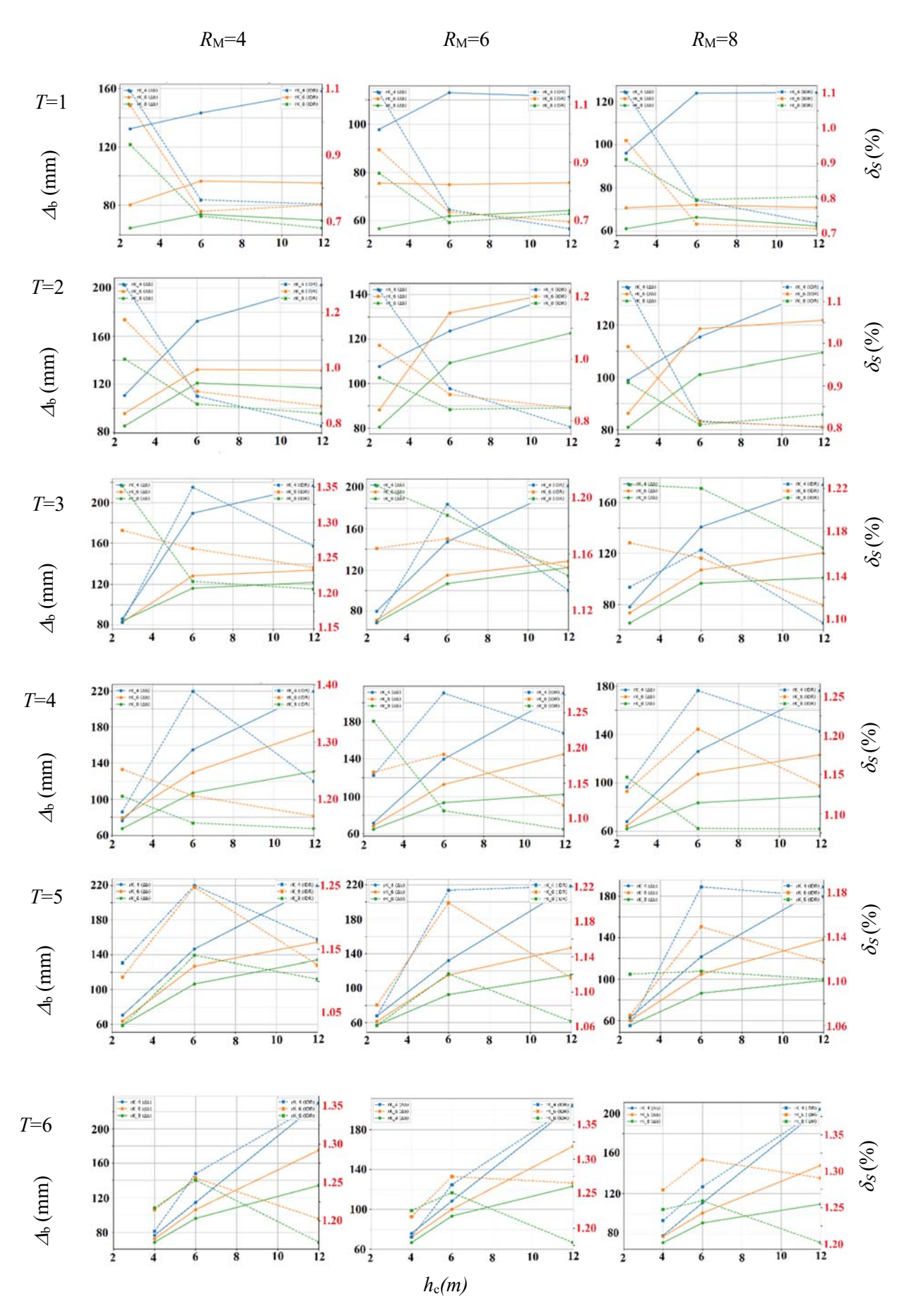


Figure 4-3: Combined plots for inter-story drift ratio and base displacement,  $\mu_V = 1$ , Los Angeles

# **4.2.4.** Seismic Performance Spectra for $\mu_V = 0$ , Vancouver

The seismic performance spectra for the Vancouver site, Figure 4-4, exhibit the same qualitative trends as those for Los Angeles when  $\mu_V = 0$ . However, the magnitudes of the seismic responses  $(\Delta_b \text{ and } \delta_s)$  are consistently lower, primarily due to the less intense MCE target spectrum associated with Vancouver. In these graphs, for  $T_1$ =2 and 3 s, a reversed trend of  $\Delta_b$  is observed when  $h_c > 6$  m, where the base displacement decreases as  $h_c$  increases. This indicates an increase in base stiffness, which may be related to the reduced negative stiffness and the relatively higher initial stiffness  $(r_K_{b1})$  in these particular cases.

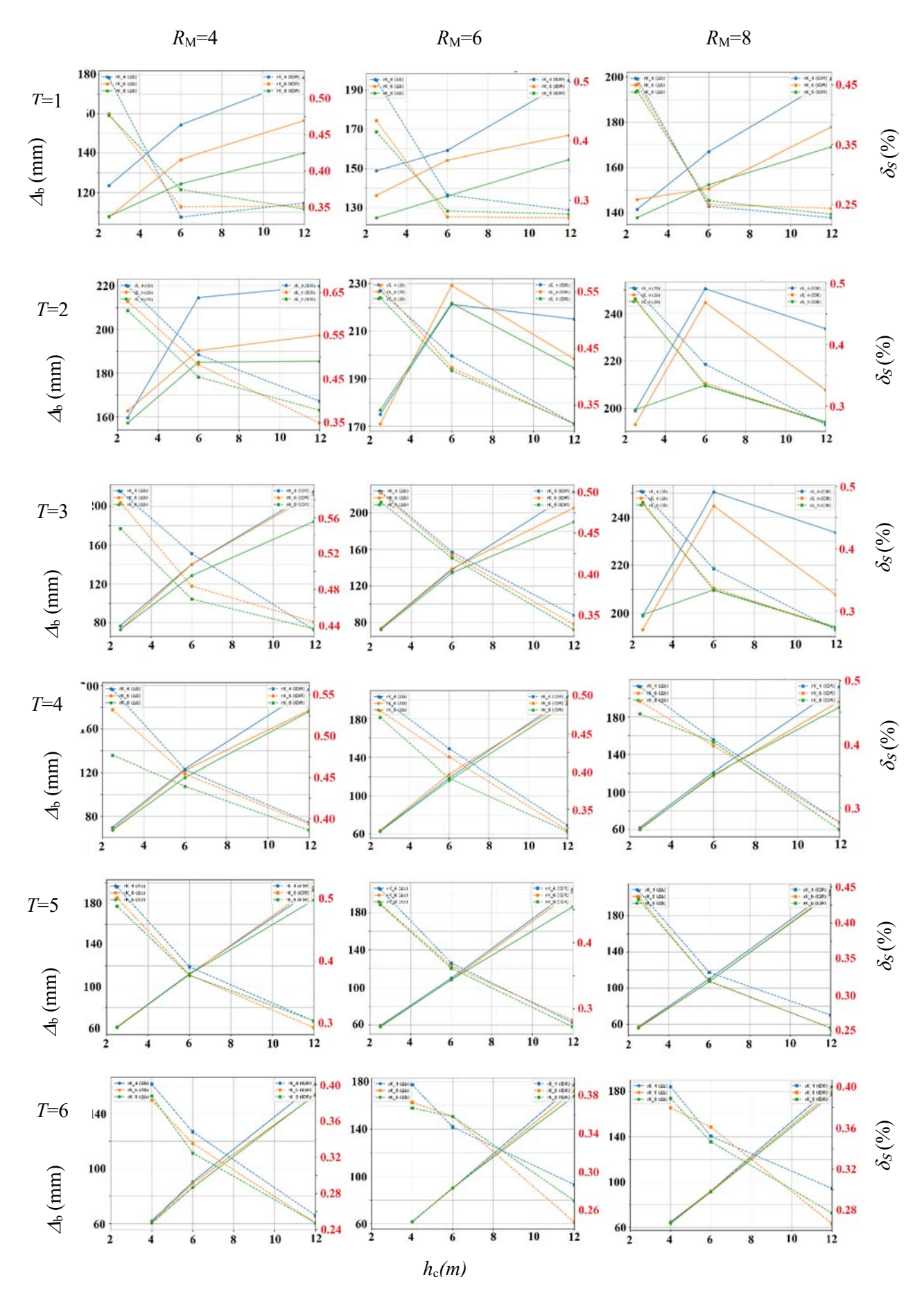


Figure 4-4: Combined plots for inter-story drift ratio and base displacement,  $\mu_V = 0$ , Vancouver

# 4.2.5. Seismic Performance Spectra for $\mu_V = 0.5$ , Vancouver

For the Vancouver site, the seismic performance spectra for  $\mu_V = 0.5$ , Figure 4-5, exhibit the same qualitative trends as those for Los Angeles with lower magnitudes of the seismic responses  $(\Delta_b \text{ and } \delta_s)$ , as it was discussed in the  $\mu_V = 0$  case. The reversed trend of  $\Delta_b$  (decreasing as  $h_c$  increases) is now observed for  $T_1 = 1$  and 2 s. It appears that the increase in  $\mu_V$  has also influenced the results.

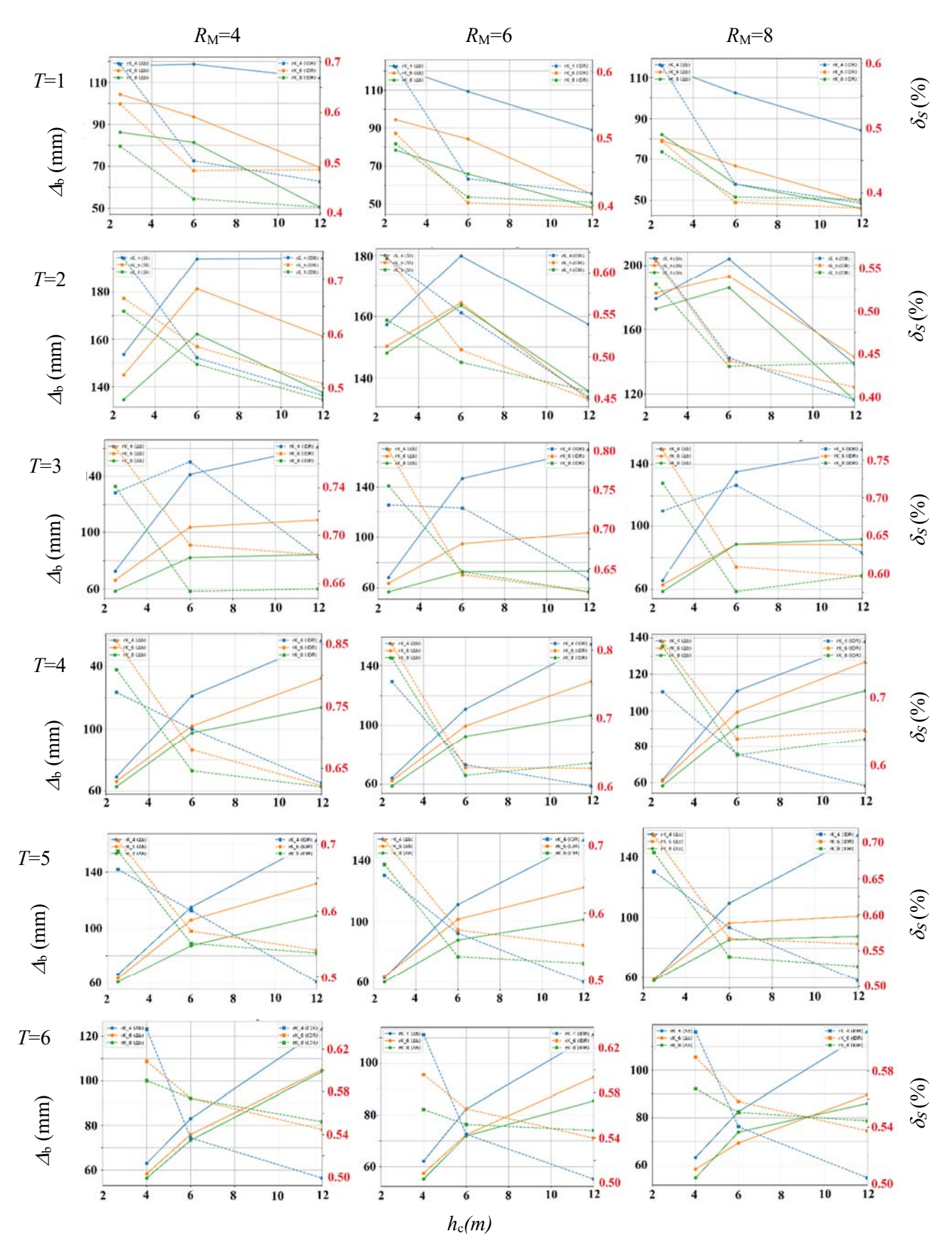


Figure 4-5: Combined plots for inter-story drift ratio and base displacement,  $\mu_V = 0.5$ , Vancouver

# 4.2.6. Seismic Performance Spectra for $\mu_V = 1$ , Vancouver

In the  $\mu_V = 1$  case, Figure 4-6, the reversed trend of  $\delta_s$  observed for Los Angeles (increasing when  $h_c < 6$  m)) now occurs mostly at the lower initial stiffness factors,  $r_K_{b1} = 4$  and 6. Except this, in general the spectra are similar to Los Angeles one with less magnitude in seismic response as discussed before.

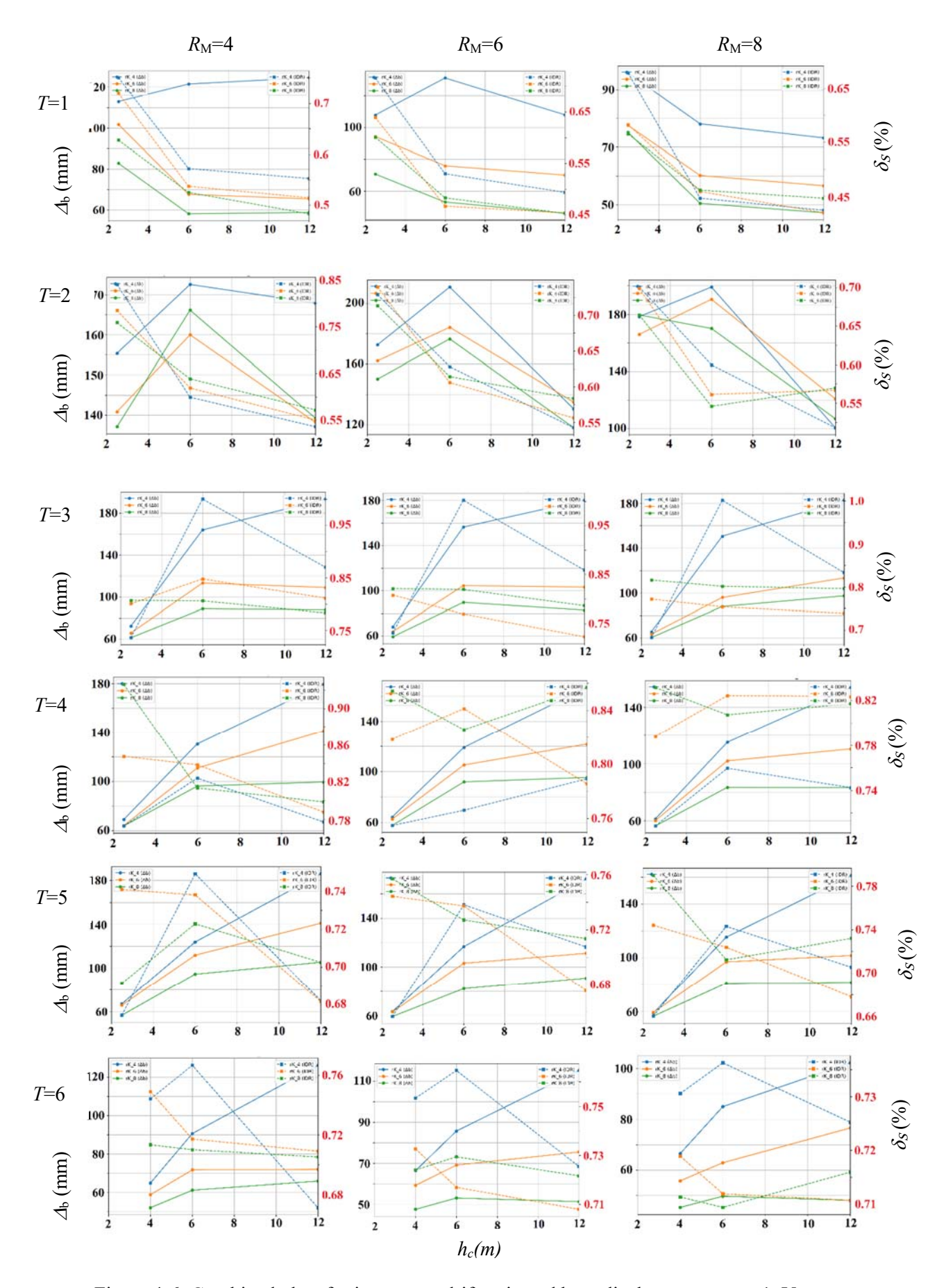


Figure 4-6: Combined plots for inter-story drift ratio and base displacement,  $\mu_V = 1$ , Vancouver

### 4.3. Seismic Performance Spectra for Parameter $h_c$ as Constant

This set of plots include the variation of seismic responses ( $\Delta_b$ ) and ( $\delta_s$ ) against the change of shear reduction factor ( $\mu_V$ ) for specified values of  $r_K_{b1}$ , fundamental period ( $T_1$ ) and  $R_M$  when the height of mega-column is held constant. The height of mega-column is a discrete parameter according to established values in Chapter 3 which includes three different values of 2.5, 6 and 12 m. The general trends for  $\Delta_b$  and  $\delta_s$  are opposite to the previously observed trends when varied with  $h_c$ , indicating that the influence of the negative stiffness of mega-columns on the base stiffness acts in opposition to  $\mu_V$ .

## 4.3.1. Seismic Performance Spectra for $h_c$ =2.5 m ( $h_c$ =4 m for 120-story), Los Angeles

In this subsection through Subsection 4.3.6, each plot follows the same format as the previous series: the vertical axes show  $\Delta_b$  on the left and  $\delta_s$  on the right. However, the horizontal axis now represents varying values of the moment reduction factor ( $\mu v$ ). The solid and dashed lines, as well as the colour coding for different  $r_K_{b1}$  values (blue for 4, orange for 6, and green for 8), remain consistent with the previous plots. The variation observed in each graph reveals how the governing seismic responses ( $\Delta_b$ ,  $\delta_s$ ) are affected by changes in the shear reduction factor ( $\mu v$ ) for each designated value of  $h_c$ , T,  $R_M$  and  $r_{b1}$ .

In Figure 4-7, a general trend is observed when  $\delta_s$  increases and  $\Delta_b$  decrease as  $\mu_V$  increases. However, the seismic response appears to be more sensitive to variations in  $\mu_V$ , particularly when  $\mu_V < 0.5$ . Additionally, increase in the initial stiffness factor  $(r_K_{b1})$  generally leads to a reduction in seismic responses.

For  $T_1 = 6$  s (120-story building), when  $h_c = 2.5$  m, the analysis becomes divergent and the system exhibits instability. It was found that a minimum  $h_c$  value of 4 m is required to maintain system stability for the 120-story building.

An important and counter-intuitive trend is observed for the 120-story building. In the very low-strength range ( $0 \le \mu_V \le 0.2$ ), an increase in the shear mechanism strength leads to a decrease in the inter-story drift ratio ( $\delta_s$ ), contrary to the general trade-off. Additionally, in this case, when the shear fuses become stronger ( $\mu_V > 0.2$ ), especially at lower values of  $r_K_{b1}$ , negative  $\Delta_b$  values are observed, suggesting numerically divergent behaviour in the results.

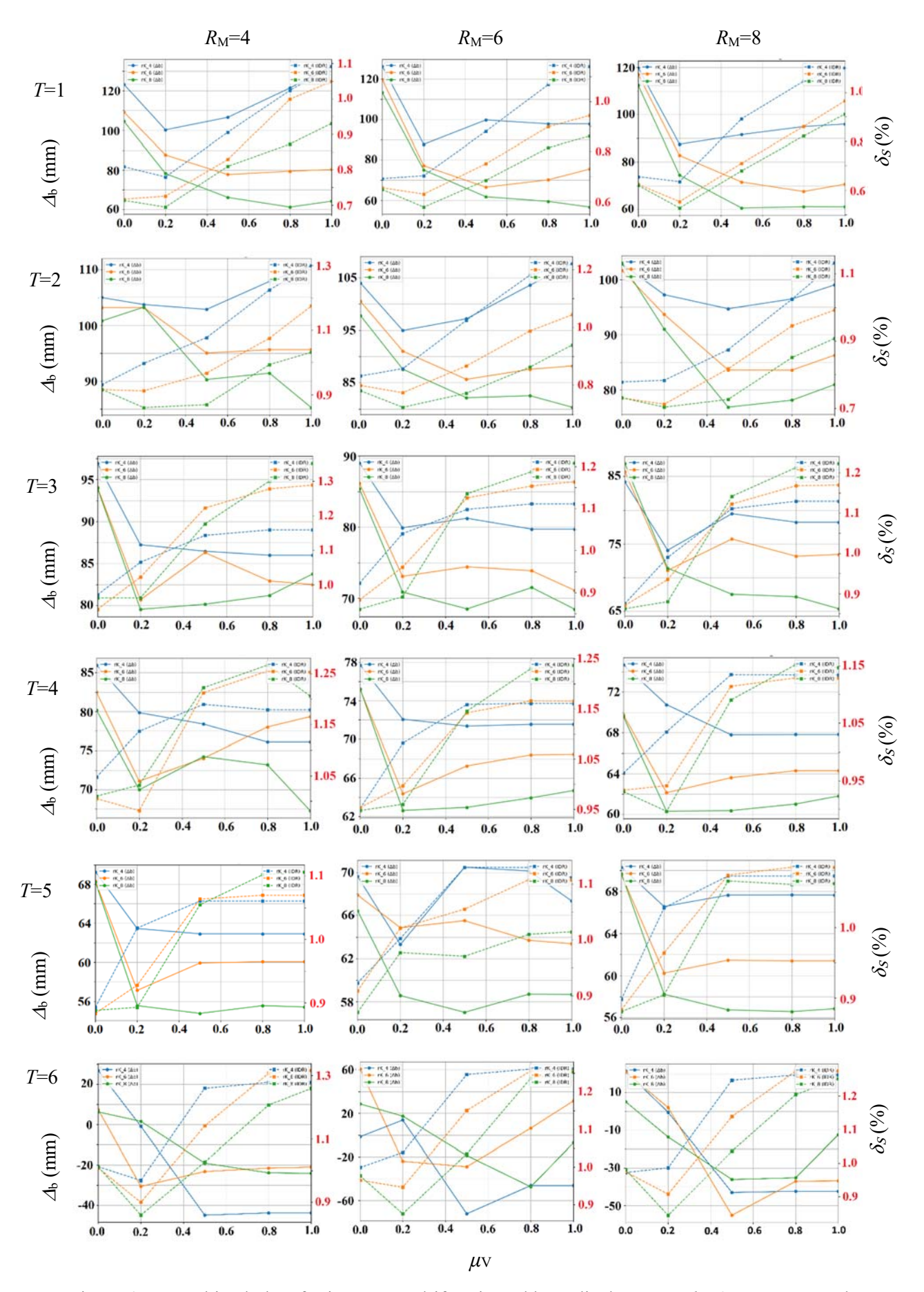


Figure 4-7: Combined plots for inter-story drift ratio and base displacement,  $h_c$ =2.5 m, Los Aneles

# 4.3.2. Seismic Performance Spectra for $h_c = 6$ m, Los Angeles

In this set of results, Figure 4-8, seismic responses exhibit a trend similar to those observed for  $h_c = 2.5$  m, with a general decrease in base displacement ( $\Delta_b$ ) and a general increase in peak inter-story drift ratio ( $\delta_s$ ) as the shear fuse becomes stronger (i.e., as  $\mu v$  increases). Similar deviations from the general trend are also observed for the 120-story building ( $T_1 = 6$  s). Compared to the corresponding results for  $h_c = 2.5$  m at any  $T_1$ , using a taller megacolumn ( $h_c = 6$  m) leads to larger base displacements.

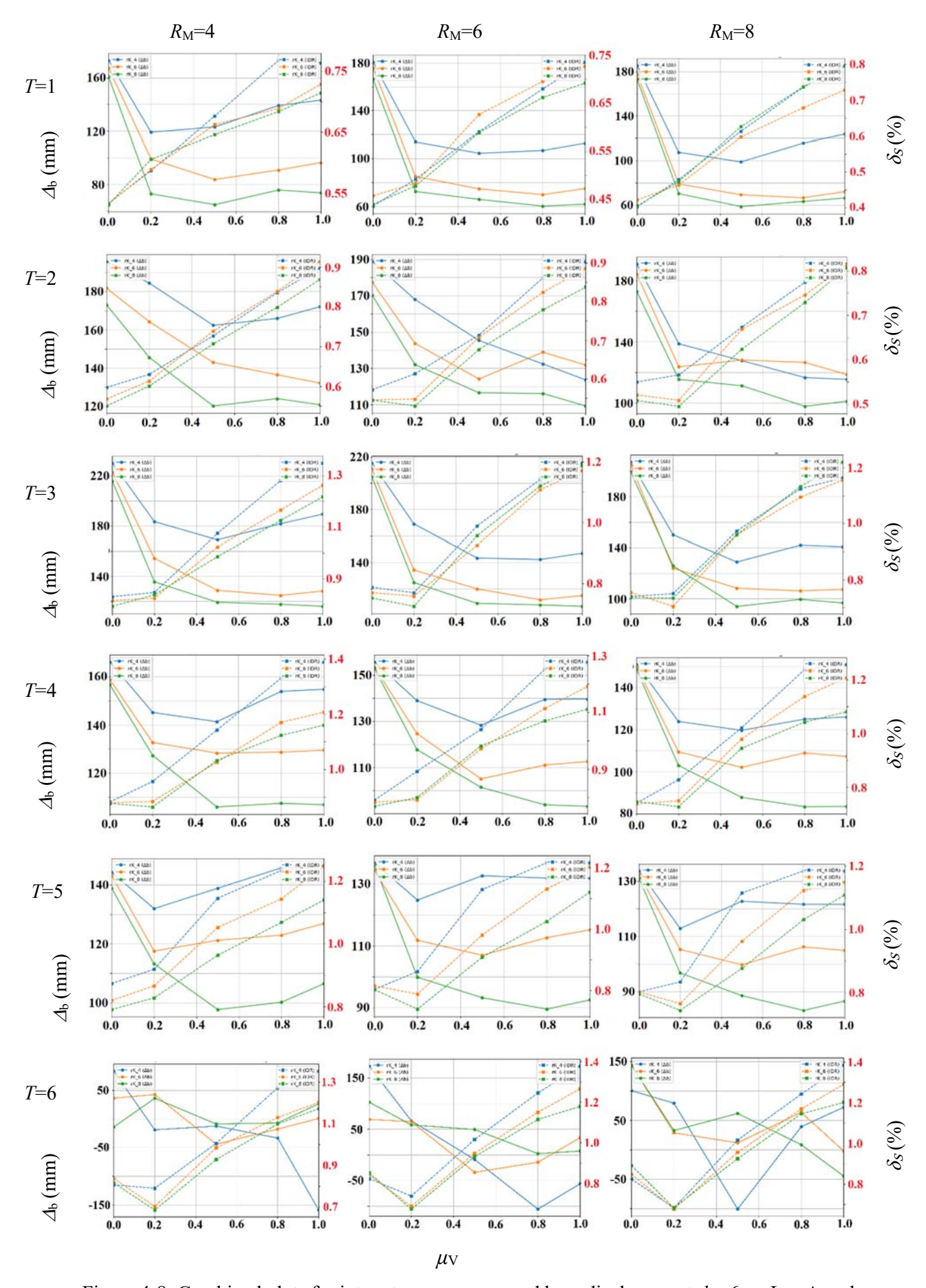


Figure 4-8: Combined plots for inter-story drift ratio and base displacement,  $h_c$ =6 m, Los Angeles

# 4.3.3. Seismic Performance Spectra for $h_c$ =12 m, Los Angeles

In the case of  $h_c = 12$  m, Figure 4-9, the results exhibit the similar general trend to those observed for lower values of  $h_c$ . Once again, using taller mega-columns leads to greater base displacement ( $\Delta_b$ ) values compared to corresponding results at any  $T_1$ . For the 120-story building ( $T_1 = 6$  s), it was found that 12 m mega-columns exhibit instability, and even with higher mega-columns, deviations from the general trend (negative  $\Delta_b$  and an initial decrease in  $\delta_s$ ) are still observed in this case.

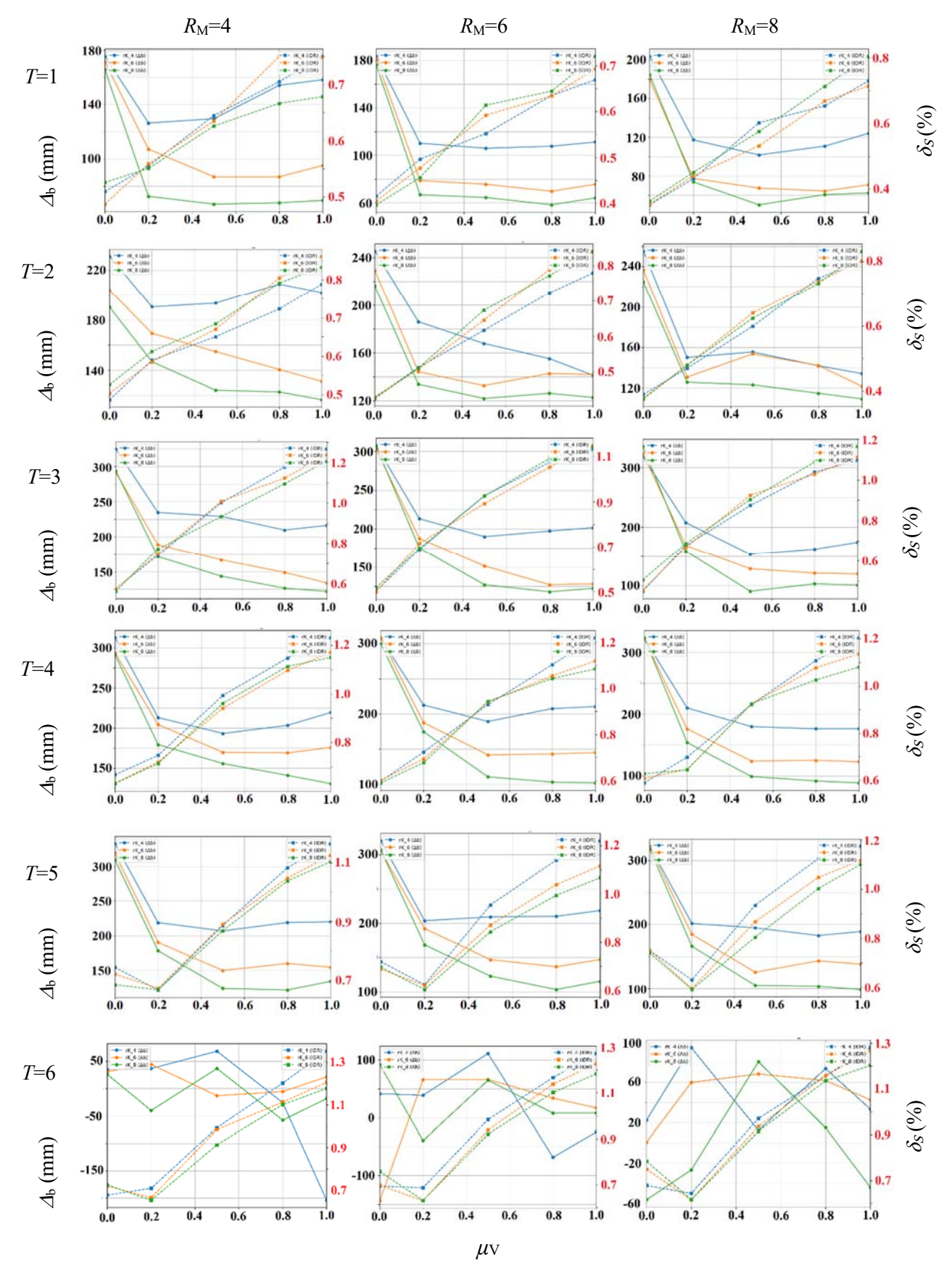


Figure 4-9: Combined plots for inter-story drift ratio and base displacement,  $h_c$ =12 m, Los Angeles

### 4.3.4. Seismic Performance Spectra for hc=2.5 m (hc=4 m for 120-story), Vancouver

For the Vancouver site, seismic responses show similar trends to those observed at the Los Angeles site when  $h_c = 2.5$  m—namely, a general decrease in base displacement ( $\Delta_b$ ) and an increase in peak inter-story drift ratio ( $\delta_s$ ) as  $\mu_V$  increases, Figure 4-10. However, significant local deviations are observed in the base displacement results in some cases. Specifically, at  $\mu_V = 0.2$ , the base displacement ( $\Delta_b$ ) experiences a sharp, abrupt decrease, followed by an unexpected increase as  $\mu_V$  approaches 0.5 for  $T_1 = 3$  and 4 s. Beyond this range, the curve resumes its expected gradual downward trend.

The unexpected decrease in base displacement indicates the dominance of the negative stiffness of the mega-columns, resulting from the specific combination of assigned shear strength and initial stiffness.

For the 120-story building ( $T_1 = 6$  s), the minimum required height for the mega-column remains 4 m, and negative  $\Delta_b$  values indicate system instability—consistent with the findings from the Los Angeles site.

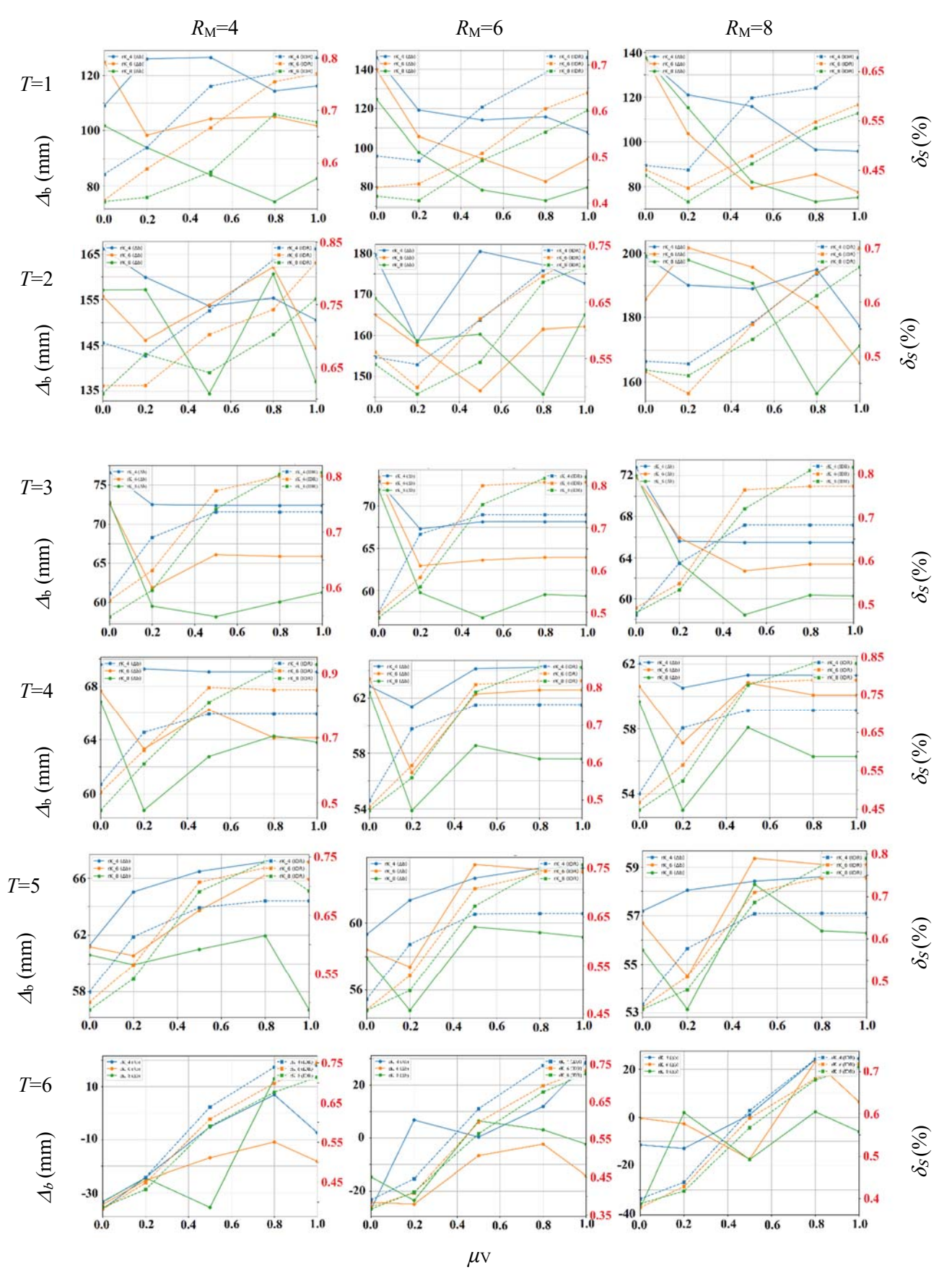


Figure 4-10: Combined plots for inter-story drift ratio and base displacement,  $h_c$ =2.5 m, Vancouver

# 4.3.5. Seismic Performance Spectra for $h_c = 6$ m, Vancouver

For hc = 6 m at the Vancouver sites, Figure 4-11, the results exhibit the expected trend observed in the corresponding Los Angeles cases: as  $\mu_V$  increases,  $\Delta_b$  decreases and  $\delta_S$  increases. Unlike the results for hc = 2.5 m, local deviations are not observed here. Using taller mega-columns results in larger  $\Delta_b$ . For 120-story building ( $T_1 = 6$  s), negative  $\Delta_b$  values are still observed.

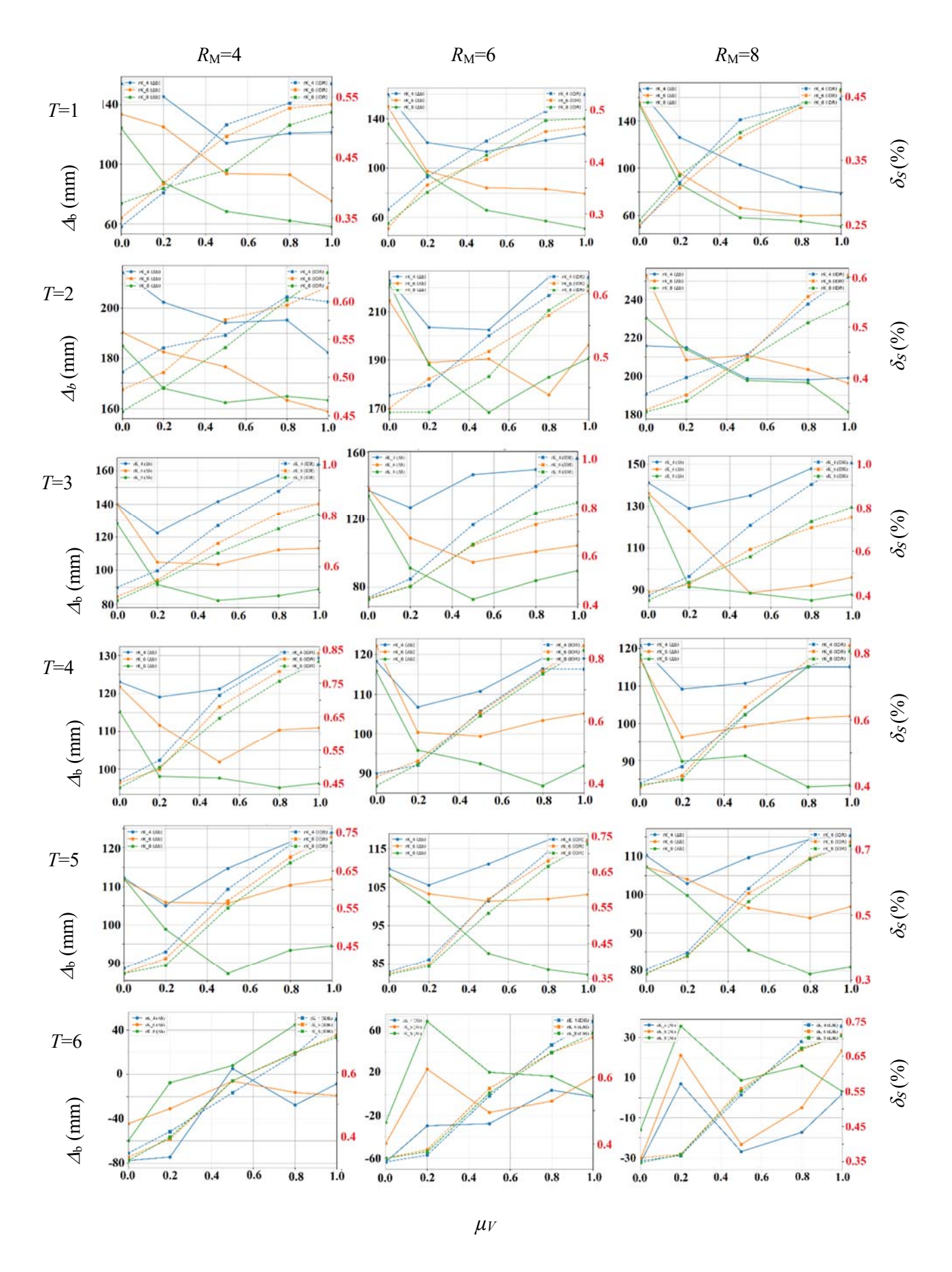


Figure 4-11: Combined plots for inter-story drift ratio and base displacement,  $h_c$ =6 m, Vancouver

# 4.3.6. Seismic Performance Spectra for $h_c$ =12 m ( $h_c$ =15 m for 120-story), Vancouver

The general trend of the results in this case, Figure 4-12, are consistent with the expected trend observed at the corresponding Los Angeles results. Once again, higher mega-columns are required for 120-story building and negative  $\Delta_b$  values are still observed.

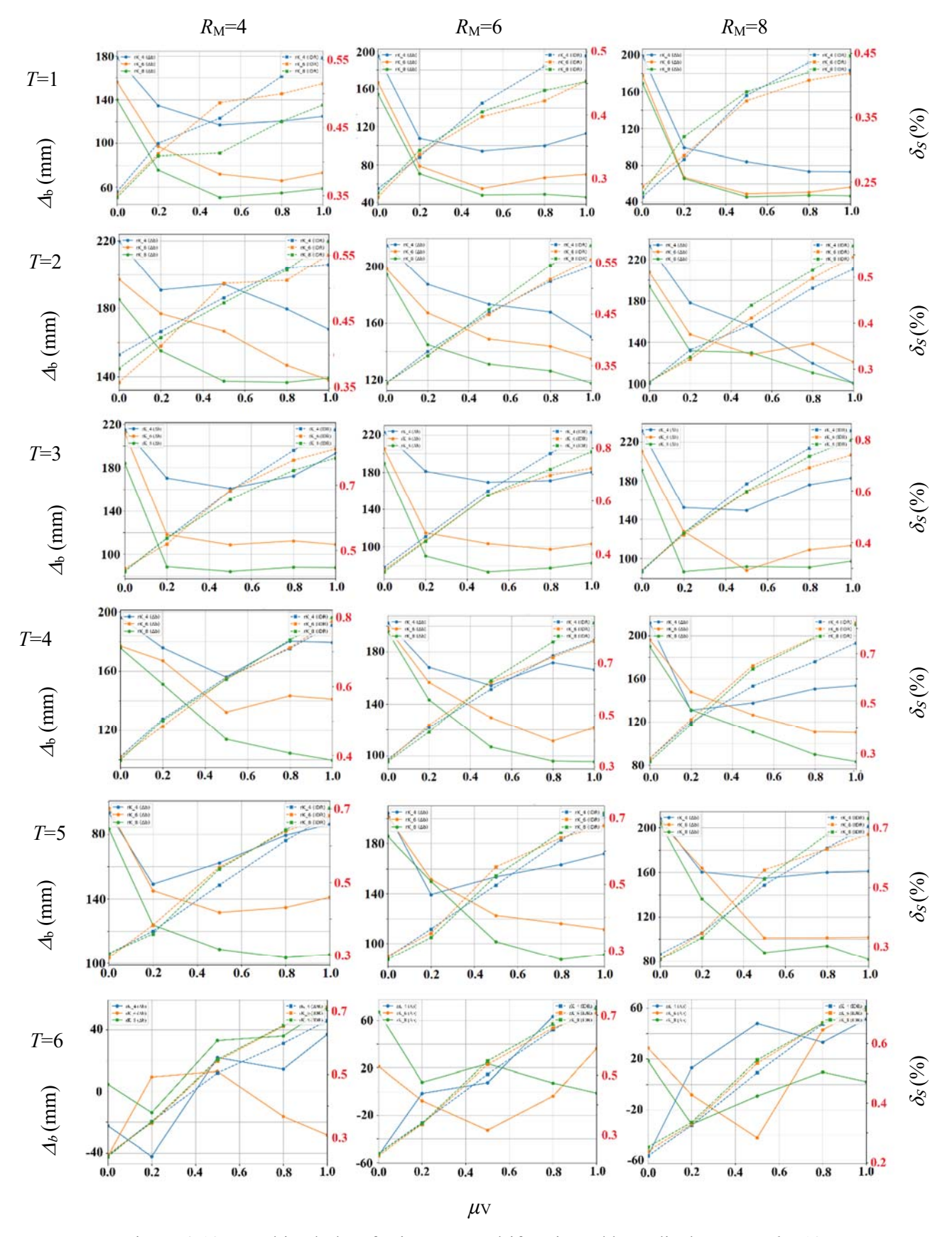


Figure 4-12: Combined plots for inter-story drift ratio and base displacement,  $h_c$ =12 m, Vancouver

#### 4.4. Summary of Results from Seismic Performance Spectra

The seismic performance spectra consistently reveal a fundamental design trade-off inherent in the MechRV3D system. An important observation from the spectra is that the seismic responses ( $\Delta_b$  and  $\delta_s$ ) show relatively little sensitivity to the Moment Reduction Factor ( $R_M$ ). This is a direct consequence of the dependency between parameters in the design procedure used for this study. A change in  $R_M$  directly influences the calculated shear strength ( $V_y$ ) and, consequently, the initial stiffness of the shear mechanism ( $K_{b1}$ ). This inherent coupling between the moment capacity and the shear stiffness largely compensates for the change in  $R_M$ , leading to final seismic demands that remain within a relatively narrow range.

A higher initial stiffness factor  $(r\_K_{b1})$  generally reduces both response parameters. When the mega-column height  $(h_c)$  is varied, an increase in height leads to a desirable reduction in inter-story drift  $(\delta_s)$  but at the cost of increased base displacement  $(\Delta_b)$ . This trend is highly sensitive to  $h_c$  below 6 meters for shorter-period buildings  $(T_1 \le 3 \text{ s})$ , but becomes approximately linear for taller, longer-period structures.

Similarly, when the shear mechanism strength (controlled by  $\mu_V$ ) is varied, a stronger fuse (greater  $\mu_V$ ) effectively reduces  $\Delta_b$  but increases  $\delta_s$ . The system is most sensitive to this parameter in the low-strength range ( $0 \le \mu_V \le 0.2$ ), as indicated by the steep initial slopes of the performance curves. For the Vancouver site, the distinct "dip-and-rise" behaviour in the intermediate shear strength range suggests a complex interaction between the system's shear fuse properties and the negative stiffness of mega-columns.

The analyses of the 120-story building ( $T_1 = 6$  s) revealed several critical stability limits that define the system's feasible application range at this extreme height. For  $h_c = 2.5$  m, the analysis became divergent. It was found that a minimum height of  $h_c = 4$  m is required

to prevent this instability for 120-story building. The instability observed in the shorter mega-columns is caused by the P- $\Delta$  effect. The gravity load ( $W_{SC}$ ) acting on a displaced mega-column creates a destabilizing action that can be represented by a negative stiffness. This negative stiffness is inversely proportional to the column height ( $h_c$ ) [72]. A shorter mega-column generates a larger destabilizing effect. For the 120-story building with its immense gravity load, this effect becomes so large for short columns that it overwhelms the shear mechanism's stiffness, causing the observed instability.

Stability issues were also observed for taller mega-columns in 120-story building under specific conditions. Even with 15 m height of mega-columns, the system continued to exhibit complex behaviours, including the counter-intuitive initial decrease in  $\delta_s$  and divergent increasement of  $\Delta_b$  at high  $\mu v$  values. Given the observed trend of increasing of  $\Delta_b$  with constant  $h_c$  as  $\mu v$  increases ( $\mu v > 0.5$ ), one possible solution is to employ stronger shear fuses in taller buildings to counteract the negative stiffness associated with the mega-columns. However, providing this high strength may be impractical, suggesting that the 120-story building is operating near the practical performance limits of the MechRV3D system.

#### 4.5. Preliminary Design Procedure Using Seismic Performance Spectra

Based on the performance spectra, procedure for preliminary design of MechRV3D system incorporated high-rise buildings is developed as shown in Figure 4-13:

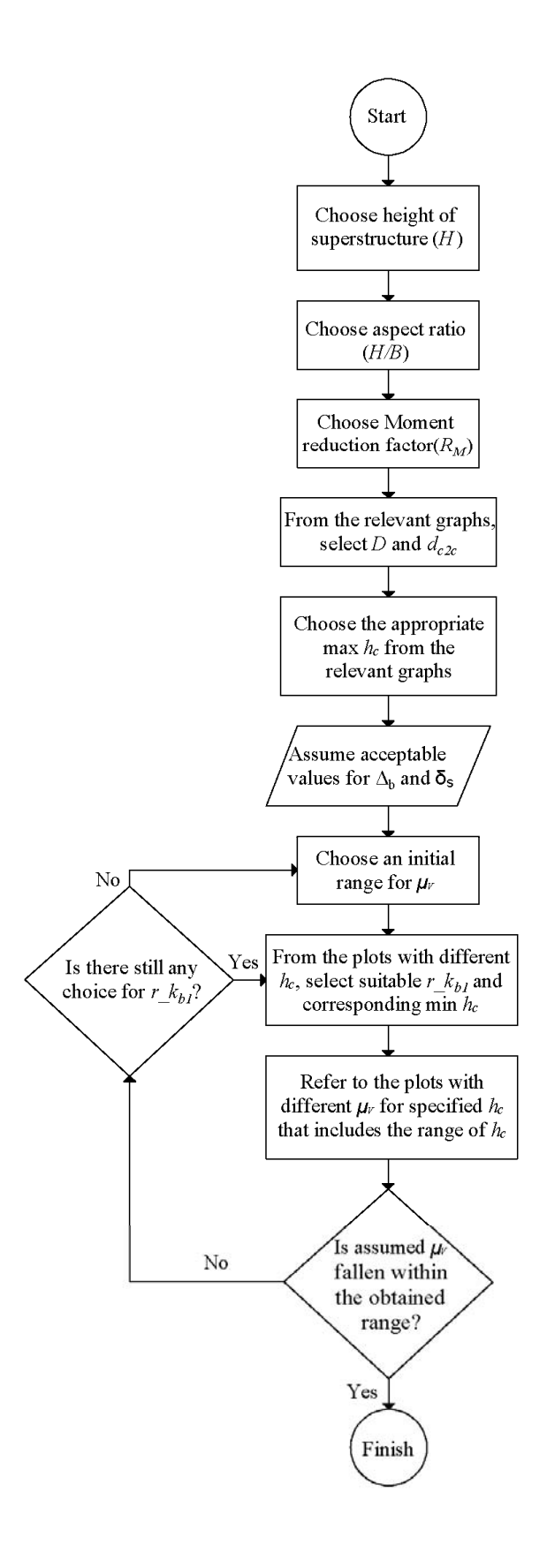


Figure 4-13: Flowchart suggested to preliminary design of MechRV3D system

- 1. Selection of superstructure height: Based on the client's requirements, a value for the height of the superstructure is chosen from the specified range of design parameters,  $\{45, 90, 150, 210, 300, 360\}$  m in this research. These values correspond to superstructure number of stories of  $\{15, 30, 50, 70, 100, 120\}$  and fundamental periods  $T_1 = \{1, 2, 3, 4, 5, 6\}$  as represented in the design spectra ( Other values between 45 and 360 m may also be considered. While the procedure remains unchanged, the corresponding design spectra must be consistently prepared).
- 2. Selection of floor dimensions of the superstructure: As discussed in Chapter 4 for the parametric analysis, each specified height corresponds to an aspect ratio from the range {3, 4, 5, 5, 6, 6}, respectively. For example, for a 15-story building with a height of 45 m, the aspect ratio (*H/B*) is 3, meaning the floor dimension will be 15 m. However, there is no strict limitation requiring the aspect ratio to be 3 for a 15-story building; the suggested values in each case are reasonable references for analysis. It is possible to use any value greater than 3, but the primary consideration is to maintain practicality and avoid overly slender or excessively broad buildings.
- 3. Selection of moment reduction factor (*R*<sub>M</sub>): This selection is guided by the geotechnical report available for the construction site, from which the uniform hazard spectra are derived. Additionally, the strength level targeted in the structural design influences the choice of *R*<sub>M</sub>. If no geotechnical data is available or the desired *R*<sub>M</sub> value falls between established values, one of the ranges [4, 6] or [6, 8] for *R*<sub>M</sub> can be considered. For such scenario, the design spectra corresponding to both the lower and upper bounds of the selected *R*<sub>M</sub> range should be used.

4. Selection of the rocker dimensions: After determining the moment reduction factor (R<sub>M</sub>), the appropriate values for the rocker depth (D) and the centre-to-centre distance between mega-columns (d<sub>c2c</sub>) are selected using the corresponding provided graphs for the relation between d<sub>c2c</sub> and D for each specified R<sub>M</sub> (Appendix A). These graphs are provided for various generic building height and their corresponding base overturning moment at MCE level (M<sub>b</sub>, MCE) for sites in Los Angeles and Vancouver.

The selection of the rocker's dimensions may vary for each project, depending on the available space in the basement. Additionally, for sites other than Los Angeles and Vancouver, if the  $M_{b,\,\text{MCE}}$  obtained from the corresponding fixed-base building significantly differs from the assumption made in this study, a new set of rocker design graphs should be developed by the designer, following the methodology described in Chapter 3.

5. Selection of the maximum allowable height for mega-columns ( $h_c$ ): This value is determined by several criteria, including the height of the superstructure, available space underground, and the space between mega-columns (which may restrict the selection of their diameter). Client specifications may also impose restrictions. In Chapter 3, a range of specified diameters for the mega-columns was defined. The required height of the mega-columns will be governed by the buckling-resistance criterion, which considers these diameter values and the weight of the superstructure, along with the weight of the rocker ( $W_{SC}$ ).

In Chapter 3, several graphs were provided to determine the required height of mega-columns for each specified diameter and corresponding  $W_{SC}$  for different building heights. It is always recommended to choose the most efficient option in

- terms of material usage and available space. The selected value in this step, will determine the upper bound of the possible range for the height of the mega-columns.
- 6. Establish the acceptable range for seismic responses, base displacement (Δ<sub>b</sub>) and inter-story drift ratio (δ<sub>s</sub>): To align with the system's low-damage design objective, the target inter-story drift ratio for this study is adopted from stringent performance-based criteria rather than the life-safety limits of conventional building codes. For base displacement, however, there is no advised range in the design code. Larger values of base displacement increase the likelihood of needing damping devices to control their effect on the structure and mechanism. Therefore, despite the lack of guidance in the design code for base displacement, the designer should carefully restrict it to prevent any unwanted damage.

It should be mentioned that  $\Delta_{b,max}$ , which is used to determine  $K_{b1}$ , is a different parameter from  $\Delta_b$  and is kept fixed at 800 mm as a practical limit for the maximum base displacement. In this context,  $\Delta_b$  is a desired value selected by the designer to meet the specific requirements of each particular project.

7. To use the first set of seismic performance spectra (Section 4.2): A target range for the shear reduction factor ( $\mu v$ ) should be selected in this step. Two primary design strategies are considered: 1- low shear strength ( $0 \le \mu v \le 0.5$ ) which prioritizes maximizing the energy dissipation from the shear mechanism and accepts larger base displacements, 2- high shear strength ( $0.5 < \mu v \le 1.0$ ) which prioritizes stiffness to control and limit the maximum base displacement. The choice between these two strategies depends on the project's specific performance objectives and constraints.

The designer now must refer to the two sets of graphs in Section 4.2 that correspond to the lower and upper bounds of the selected range for  $\mu\nu$ . These set of graphs

representing the relationship between the height of mega-columns and the initial stiffness factor of the shear mechanism while  $\mu_V$  is considered as constant in one of the boundary points (0, 0.5, 1). The validity of the target seismic response  $(\delta_s)$  and  $\Delta_b$  is identified in the shaded area in the plot, which lies between the base displacement graphs and their corresponding inter-story drift ratio graphs. For each specified initial stiffness of the shear mechanism  $(r_{-}K_{b1})$ , the minimum (or maximum, depending on the selected  $\mu_V$  range) acceptable value for  $h_c$  is determined—this is the point at which the hatched area begins to appear. This value defines the lower bound of the acceptable height range for the mega-columns. In this step, the designer can also determine the initial stiffness factor of the shear mechanism  $(r_{-}K_{b1})$  that best corresponds to the preferred height of the mega-columns. The results obtained from the plots for either the lower or upper bound of the  $\mu_V$  should be compatible, or at least overlap, for at least one value of  $r_{-}K_{b1}$ . If

As an example, consider selecting MechRV3D system's design values for a 70-story building located in Los Angeles with a moment reduction factor  $R_{\rm M}=8$ . In the first step, the shear reduction factor  $\mu_{\rm V}$  is assumed to range between 0 and 0.5. Accordingly, plots for  $\mu_{\rm V}=0$  and  $\mu_{\rm V}=0.5$  are used. The design criteria assumed as maximum inter-story drift ratio of 1.1% and a maximum base displacement of 200 mm (which can be larger in practical design).

no overlap occurs, the  $\mu v$  range should be revised, and the other range should be

considered.

Figure 4-14 shows the hatched area where both the seismic response, inter-story drift ratio ( $\delta_s$ ), shown as dashed lines, and base displacement ( $\Delta_b$ ), shown as solid lines, fall within the acceptable range for  $\mu_V = 0$ . In this plot, the base displacement criterion of 200 mm is the governing factor. As shown, for mega-column heights

between 2.5 m and approximately 7.8 m, all values of  $r_{Kb1}$  can be used for defining the initial stiffness of the shear mechanism.

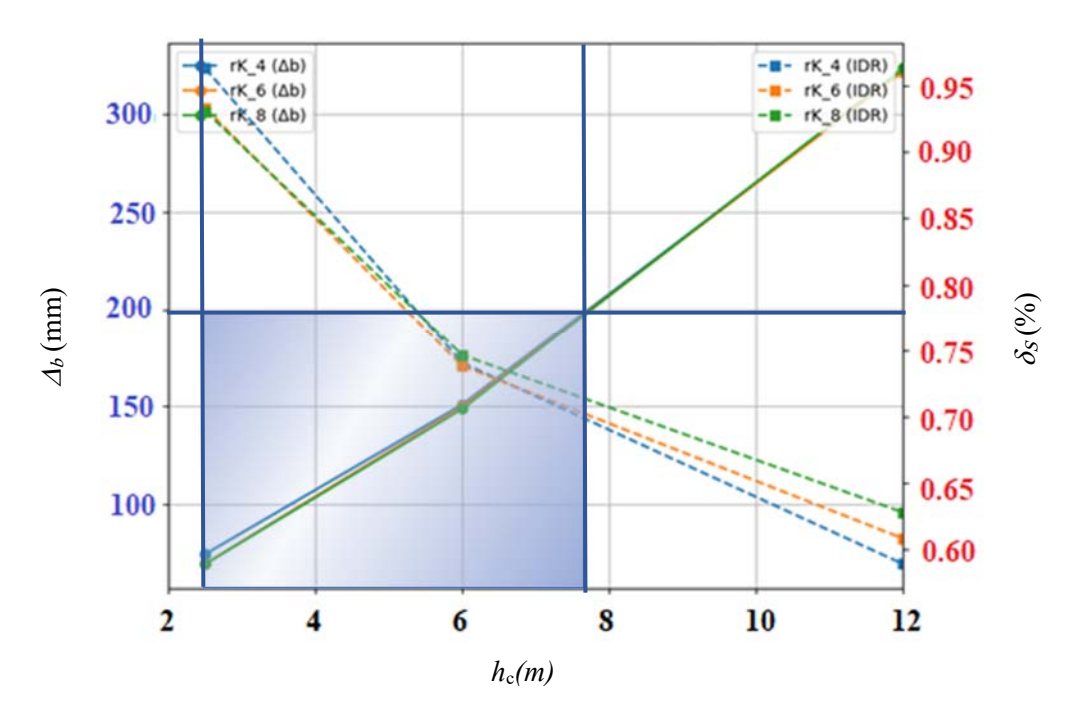


Figure 4-14: Finding the acceptable area for 70-story building when  $R_{\rm M} = 8$ ,  $\mu_{\rm V} = 0$ 

Consistently, Figure 4-15 shows the hatched area where both the seismic response  $(\delta_s)$  and  $(\Delta_b)$  fall within the acceptable range for  $\mu_V = 0.5$ . In this plot, the inter-story drift ratio criterion of 1.1% governs the design. As shown, for  $r_K_{b1} = 8$ , megacolumn heights between minimum value, 2.5 m and 12 m are acceptable. However, for  $r_K_{b1} = 6$  and  $r_K_{b1} = 4$ , the height should not be less than approximately 3 m and 3.8 m, respectively.

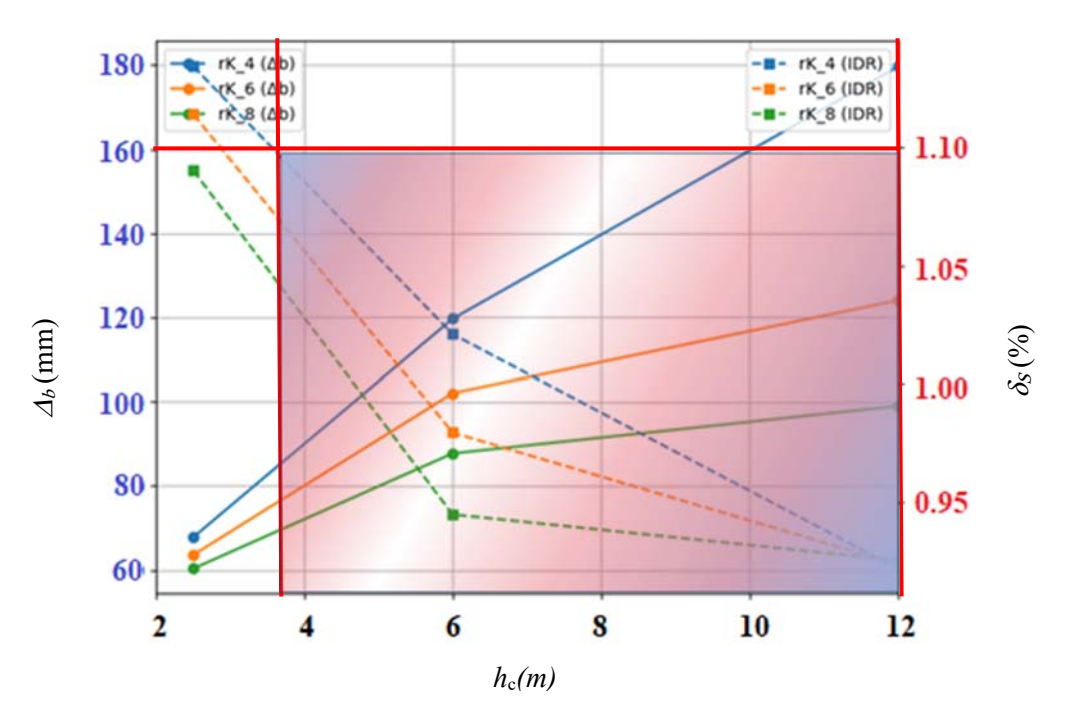


Figure 4-15: Finding the acceptable area for 70-story building when  $R_{\rm M} = 8$ ,  $\mu_{\rm V} = 0.5$ 

From both plots, one possible design choice is  $r_K_{b1} = 4$  with the mega-column height between 4 and 8 m. For a more realistic selection, a height of 8 m can be assumed as the specified value for the mega-columns. The value of  $r_K_{b1}$  is assumed as the smallest as possible to achieve more efficient design.

8. Using the second set of seismic performance spectra (Section 4.3) to verify the selected design strategy for  $\mu_V$ : After determining the appropriate range for the mega-column height in step 7, the designer should refer to the seismic performance spectra corresponding to that height, as presented in Section 4.3. These spectra are provided for three different values of  $h_c$ . Based on the selected range of the mega-column height in step 7, the two set of spectra within which the chosen range either falls between or substantially overlaps should be used for verification.

Next, the designer should examine the area between the base-displacement and inter-story drift ratio graphs for the selected initial stiffness factor of the shear mechanism, ensuring that the allowable seismic response ranges ( $\Delta_b$  and  $\delta_s$ ) are

considered. The corresponding range for the shear reduction factor,  $\mu\nu$ , should then be checked for both plots. The overlap of these ranges should be compared with the assumed  $\mu\nu$  range. The acceptable range for the final design is determined by the overlap between the ranges in the two plots.

To continue with the same example in Step 7, based on the determined megacolumn height of 8 m, the plots for  $h_c = 6$  m and  $h_c = 12$  m are examined to verify whether the assumed range for  $\mu_V = [0, 0.5]$  satisfies the design requirements. In Figure 4-16, the seismic responses are presented for a mega-column height of  $h_c =$ 6 m. In this case, the inter-story drift ratio of 1.1% governs the design restriction. According to the plot, the entire range of  $\mu_V$  is acceptable for all values of  $r_{-}K_{\rm bl}$  in terms of base displacement. However, to meet the inter-story drift limitations, the acceptable ranges of  $\mu_V$  are as follows:

$$[0, 0.6]$$
 for  $r$   $K_{b1} = 4$ ,

$$[0, 0.7]$$
 for  $r$   $K_{b1} = 6$ , and

$$[0, 1]$$
 for  $r K_{b1} = 8$ 

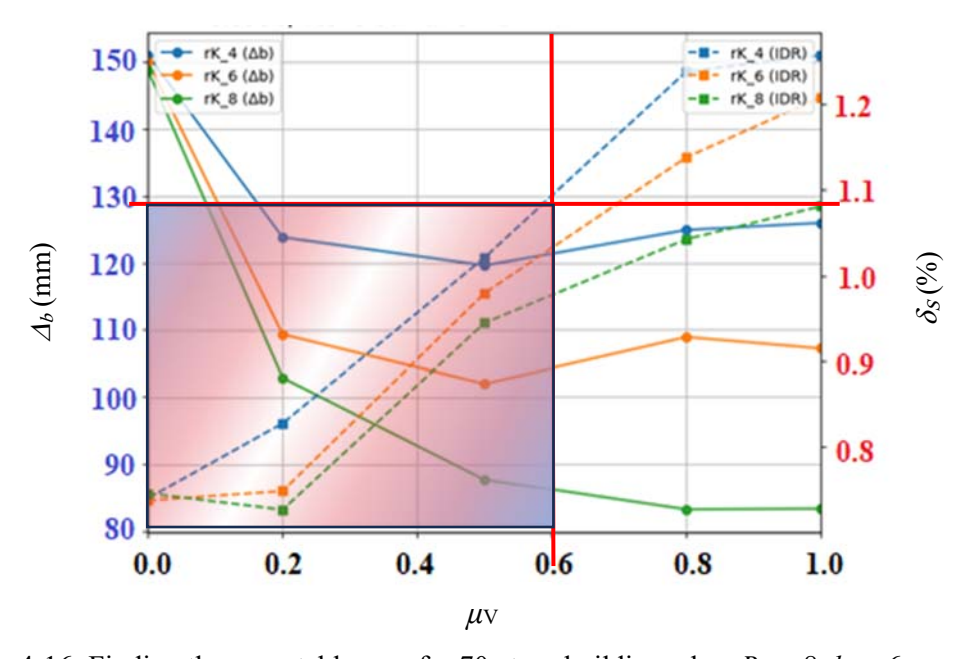


Figure 4-16: Finding the acceptable area for 70-story building when  $R_{\rm M}=8$ ,  $h_{\rm c}=6$  m

In Figure 4-17, for  $h_c = 12$  m, the hatched area indicates the acceptable range of seismic responses across different values of  $r_K_{b1}$ , confined approximately within  $\mu_V \in [0.3, 0.8]$ . This range is nearly consistent for all values of  $r_K_{b1}$ . This result validates both the initial assumption and the selected mega-column height. In this plot, the base displacement limit of 200 mm governs the minimum of the range (0.3), while the inter-story drift ratio of 1.1% dictates the maximum (0.8).

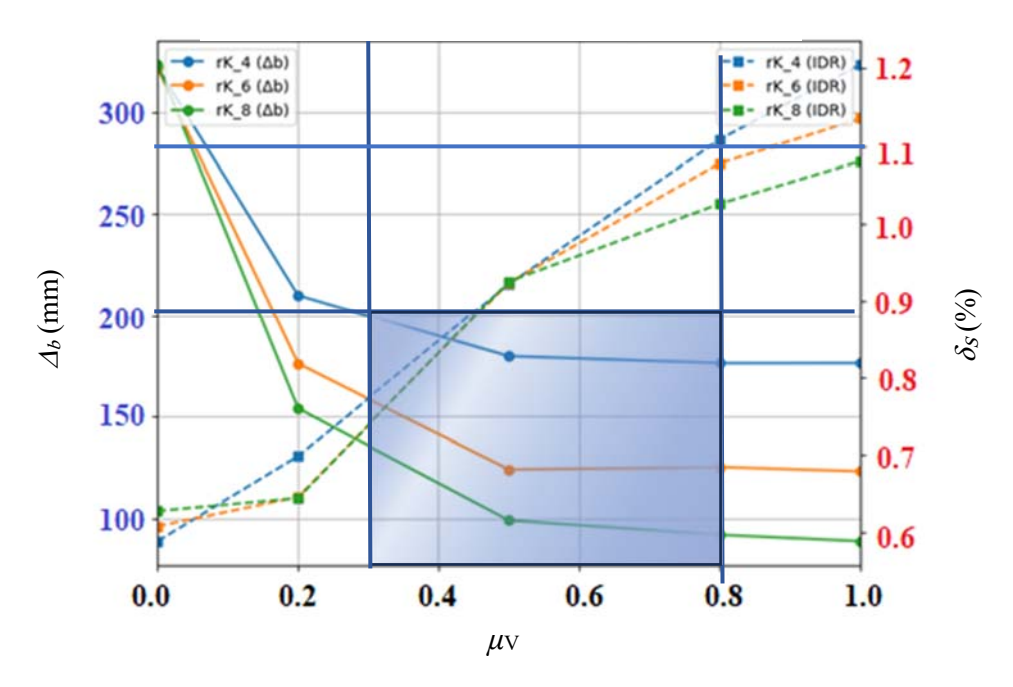


Figure 4-17: Finding the acceptable area for 70-story building when  $R_{\rm M}=8$ ,  $h_c=12$  m

By comparing the obtained ranges of  $\mu\nu$  from Figures 4-16 and 4-17 for  $r_K_{b1} = 4$  (as selected in Step 7), the acceptable range is identified as the overlap between the two: [0.3, 0.8] from Figure 4-17 and [0, 0.6] from Figure 4-16. This results in a final acceptable range of  $\mu\nu \in [0.3, 0.6]$ . Since this range mostly falls within the initially assumed range of [0, 0.5], all previous assumptions are validated, and the design procedure can proceed with:  $\mu\nu \in [0.3, 0.5]$ ,  $h_c = 8$  m and  $r_K_{b1} = 4$ .

9. Approaches in case of inconsistent results: If there is no overlap between the ranges shown in the two plots in step 8, or if their shared range does not align with the initially assumed design strategy of  $\mu_V$ , the designer should first return to Step 6

and select a different value for the initial stiffness of the shear mechanism,  $r_{K_{b1}}$ . If no other acceptable values of  $r_{K_{b1}}$  lead to consistency in Step 8, the designer should then return to Step 7 and consider an alternative range for the moment reduction factor,  $\mu_{V}$ .

The finalized values for  $r_{Kb1}$  should be used to determine  $K_{b1}$  based on the assumptions presented in Chapter 3. For sites other than Los Angeles and Vancouver, this calculated  $K_{b1}$  should be compared with the actual value derived from the site's  $V_{b, SLE}$  to validate the assumption of the initial base displacement being 1/20 of  $\Delta_{b,max}$ . If a significant discrepancy is observed, the design procedure should be repeated using revised assumptions in Steps 7 and 8.

10. Designing the Remaining Properties of the Shear Mechanism: After achieving consistent results in the previous steps, the applicable ranges for several design parameters—such as the height of mega-columns and the shear reduction factor—have been established. Additionally, values for the initial stiffness factor of the shear mechanism, the diameter of the mega-columns, and the dimensions of the rocker have been determined.

As a final step in the design process, the physical properties of the shear mechanism elements—specifically their cross-sectional area and their length (or height)—should be determined according the obtained shear strength and initial stiffness values, and target lateral displacement. The exact design depends on the type of shear fuse employed (e.g., in a BRBF, the basic initial stiffness ( $K_{\rm bl}$ ) is related to the brace axial stiffness (EA/L) through geometry-dependent relations, where E is the material's Young's Modulus, A is the cross-sectional area, and E is the length of the yielding elements).

#### 4.6. Maximum Base Displacement ( $\Delta_{b,max}$ ) and the Stability of Mega-Columns

The important consideration in this part is the maximum allowable lateral displacement at the top of mega-columns as they would sway due to the lateral displacement imposed by the rocker. These columns are considered pined at both ends in terms of structural behaviour, but they behave differently from the pinned-ends columns in a braced frame. They are carrying a large axial gravity load ( $W_{SC}$ ) while being subjected to a significant lateral displacement ( $\Delta_b$ ) at their top. Moreover, the connection of the mega-columns to the foundation may develop considerable reaction forces due to the imposed lateral displacements, which must be accounted for in the design and detailing of the base connection.

The stability of the mega-columns is a critical consideration, as their capacity can be compromised when they are subjected to large lateral displacements. In their inclined position, the gravity load ( $W_{SC}$ ) generates a significant secondary moment ( $M = W_{SC} \times \Delta_b$ ), commonly known as the P- $\Delta$  effect. If this secondary moment becomes too large, the mega-columns may lose their stability.

To prevent this P- $\Delta$  instability, the rotation of the mega-columns ( $\theta_m$ ) must be limited. A reasonable upper limit for this rotation can be established to ensure the stability is maintained. For this study, a maximum rotation of  $\theta_m = 0.26$  radians (approximately 15 degrees) is considered a practical upper bound beyond which P- $\Delta$  effects could become excessive. This rotation limit can be used to determine the maximum allowable base displacement ( $\Delta_{b,max}$ ) for the minimum mega-column height ( $h_c$ ) selected as 3 m. The height of 3 m is slightly above the minimum value of 2.5 m that was selected to provide a reasonable trade-off between inter-story drift ratio and base displacement. Using this height, the maximum allowable base displacement is calculated as:

$$\Delta_{b,max} = \tan(0.26 \, rad) \times 3000 mm = 800 \, mm$$

Therefore, a limit of 800 mm is adopted for ∆b,max. This value, derived from stability considerations of the shortest practical mega-column, provides a conservative and consistent displacement limit for all analyses in this study. This value (800 mm) is also justified as a feasible system limit based on both component capacity and analytical precedent. It corresponds to an achievable strain demand in large-scale BRBFs [73] and is consistent with the large displacement demands observed in analytical studies of other advanced dual-mechanism systems for tall buildings [43]. Furthermore, this limit aligns with the displacement range found to be effective in the foundational numerical validation of the MechRV3D system [15].

## 4.7. Effective Period Elongation of the MechRV3D System

It is important to note that the generic buildings in this study were categorized by the period of the superstructure alone, assuming it is rigidly fixed at the base that can be called nominal fixed-base period ( $T_a$ ). However, the introduction of the flexible base mechanisms results in an effective system period ( $T_{\rm sys}$ ) that is longer than the nominal period. This phenomenon, known as period elongation, is a key feature of any base-decoupling system and its magnitude was found to be a function of the base mechanism's properties.

From the analysis results, the effective period showed high sensitivity to the geometric and stiffness parameters but was completely independent of the shear strength factor ( $\mu$ v). The observed trends are summarized as follows:

1- An increase in the mega-column height ( $h_c$ ) consistently results in a longer effective period. The net total stiffness of the base decrease as  $h_c$  increases. This is because the columns become much more flexible. A decrease in stiffness leads to an increase in the system's period.

- 2- An increase in the initial stiffness factor  $(r_K_{b1})$  results in a shorter effective period. This is a direct consequence of increasing the stiffness of the shear mechanism, which stiffens the entire system.
- 3- An increase in the Moment Reduction Factor ( $R_{\rm M}$ ) results in a longer effective period, as a higher  $R_{\rm M}$  corresponds to a to a greater required rocker mass.

Of these parameters, the mega-column height ( $h_c$ ) was found to have the most dominant influence on period elongation. Consequently, the most critical scenario (the longest effective period) for all generic buildings occurred with the combination of  $R_M = 8$ ,  $r_K_{b1} = 4$ , and  $h_c = 12$  m. The effective periods for all generic buildings under this worst-case scenario obtained from NLRHAs are summarized in Table 4-1:

Table 4-1: Differences between nominal period ( $T_a$ ) and system period ( $T_{sys}$ ) for all generic buildings

Building	Nominal period, fixed-base $(T_a)$	System period in the most critical case (T <sub>sys</sub> )	T <sub>90</sub> for nominal period (T <sub>5</sub> )	$T_{90}$ for system period $(T_{5,sys})$
15-story	1	1.449	0.018	0.033
30-story	2	2.612	0.036	0.064
50-story	3	3.848	0.054	0.093
70-story	4	5.333	0.118	0.122
100-story	5	8.079	0.147	0.155
120-story	6	11.655	0.178	0.183

This period elongation has a direct implication for the ground motion scaling procedure, as the scaling range is defined relative to the fundamental period (0.2  $T_1$  to 2.0  $T_1$ ). For the taller buildings (70-story and higher), where the period elongation is most pronounced, this could potentially shift the required scaling range.

However, for these tall structures, the lower bound of the scaling range is governed by  $T_{90}$ , the period corresponding to 90% mass participation ( $T_5$  in this research). As shown in Table 3-13,  $T_{90}$  is very short and is primarily a function of the superstructure's higher-mode properties, which are not significantly affected by the flexibility of the base. Therefore, the elongation of the first-mode period ( $T_1$ ) does not alter the critical lower bound of the scaling range ( $T_{90}$ ), which is anchored in the peak plateau region of the MCE spectrum.

Consequently, it is concluded that while the period elongation is a significant physical phenomenon, its impact on the validity of the ground motion scaling used in this study is likely minimal. Nevertheless, a targeted sensitivity study using ground motions scaled to the elongated periods would be a valuable area for future research to definitively confirm this conclusion.

Presenting the performance spectra categorized by the nominal fixed-base period  $(T_1)$  is a deliberate and logical choice. The nominal period is a fundamental, unchanging property of the superstructure, and since the MechRV3D system is designed to keep this superstructure essentially elastic,  $T_1$  remains a constant and well-defined reference throughout the seismic response. This makes it a clear and practical starting point for a designer evaluating various base mechanism choices for a known superstructure.

This approach is further validated by the source of the period estimation formula itself. The KBC 2009 formula is calibrated against linear-elastic effective periods measured from real buildings under low-amplitude ambient vibrations. Therefore, the use of a linear-elastic stick model defined by this nominal period is a consistent and rigorous basis for this parametric study, as both the analytical model and its real-world benchmark represent the structure in its undamaged, pre-yielding state.

# 5. Conclusions and Recommendations

#### 5.1. Conclusions

The objective of the current study was to provide a preliminary design procedure for the MechRV3D system that facilitates the use of this new system to improve seismic resilience of high-rise buildings. This was achieved by addressing a key limitation of the initial research: the neglected influence of the rocking mechanism's physical geometry on the overall seismic response. The research objectives set in Chapter 1 have been successfully met, with the main contributions and conclusions summarized below.

- Conclusions on Modelling and Design Parameters (Chapter 3): This research directly addresses the limitations of the previous simplified model by incorporating the physical geometry of the rocking mechanism (*D* and *h*<sub>c</sub>) into the numerical model. New design parameters were established to better capture the behaviour of the MechRV3D system, including the dimensions of the rocker and the height of the mega-columns. A rational procedure was proposed to determine the appropriate range for both the mega-columns height and the rocker dimensions, accounting for the relationship between the rocker dimension, the moment reduction factor (*R*<sub>M</sub>), and the rocker depth (*D*).
- Conclusions on System Behaviour and Performance (results in Chapter 4):

  Explicitly modelling the rocking mechanism's geometry revealed several key aspects of the system's performance and stability. It was found that the megacolumn height governs P-Δ stability, which, combined with practical component sizing constraints, establishes a feasible application limit for the system to buildings of up to approximately 300 m. Consequently, the negative stiffness of megacolumns necessitates the selection of a larger initial stiffness for the shear

mechanism. This, in turn, affects another key seismic response: the inter-story drift ratio ( $\delta_s$ ), demonstrating an indirect relationship between the mega-column height and the required strength of the shear mechanism. The effect of mega-column height was found to be more significant when the height is less than 6 m. According to the revised design procedure presented in this study, a critical design decision is therefore achieving a reasonable balance between a height that is short enough to be practical and tall enough to maintain stability in the inclined position.

• Conclusions on the Preliminary Design Procedure and Application Limits (Chapter 4): The main contribution of this research is the development of a comprehensive preliminary design procedure, built upon a novel set of seismic performance spectra derived from this refined model. These spectra, developed for two different seismic locations, provide engineers with a direct method to account for key geometric parameters, which was not previously possible. The analyses revealed practical limits to the system's application. For instance, the 120- story model became divergent when the mega-columns were shorter than 4 m, while taller columns required impractically large diameters (e.g., 6400 mm for a 30 m height of mega-columns). The results suggest that for 120-story buildings, mega-columns taller than 15 m perform more effectively.

In conclusion, the parametric analyses indicate that the MechRV3D system performs most effectively for buildings up to 300 m in height (approximately 100 stories). Beyond this, the system may not be a suitable choice as it would require excessively large components for the rocking mechanism. This conclusion is particularly valid for RC core wall buildings located on sites where the moment reduction factor ( $R_{\rm M}$ ) is less than 8.

#### 5.2. Recommendation for Future Research

This study aimed to address one of the issues highlighted in the future research section of the initial study that was the investigation of the P- $\Delta$  effect induced by the mega-columns. Other suggested problems remain open for future research and are summarized as follows:

- Extension to 3D Modelling: The parametric analysis model can be extended to a
  three-dimensional configuration to better capture the constraints of the rocking and
  shear mechanisms including torsional response and bi-directional seismic
  excitation.
- Vertical Seismic Load Effects: The effect of vertical seismic loads on the seismic response spectra of the MechRV3D system requires further investigation, as these loads can directly influence both the rocking resistance and the P-Δ stability of the base mechanism.
- Interaction with Leaning Columns: The influence of rocking action and base displacement on the leaning column components, particularly in addressing the challenge of ensuring compatible movement of leaning columns at ground level with the MechRV3D mechanisms. A key challenge is developing practical connection details at the ground level that can accommodate the large, combined horizontal translation and rocking-induced uplift of the base, without damaging the gravity columns or unintentionally restraining the protective system.
- Refinement of the Damping Model: This study employed a classical Rayleigh
  damping model for the superstructure. Future research could investigate the
  influence of more advanced damping models that are less sensitive to stiffness
  degradation during nonlinear response. Additionally, a detailed investigation into
  the energy dissipation and potential for artificial numerical damping at the rocking

- impact interfaces would provide a more complete understanding of the system's energy balance.
- Broader Applications and Site Variability: Application of the MechRV3D system
  to superstructures with lateral load-resisting systems other than RC core wall
  buildings, other shear fuses, and the development of corresponding seismic
  performance spectra for other site locations.
- Optimization of Superstructure-to-Base Stiffness ( $K_{base}$ ) Ratio: This study treated the superstructure stiffness as a predefined input for each generic building. A crucial area for future research is to investigate the optimal stiffness ratio between the superstructure and the base mechanisms ( $K_{base}$ ). Such a study would help to define the most economical designs by exploring the trade-offs between investing in a stiffer superstructure versus a stiffer base mechanism to achieve the desired performance objectives for both inter-story drift ratio and base displacement.
- Conducting parametric analyses using machine learning: A surrogate model can be trained that learns the relationship between input parameters and output response to reduce the computational cost through running NLRHAs but not for a full space of parameters

#### References

- [1] "World Urbanization Prospect 2018, Highlights," United Nation, Department of Economic and Social Affairs, New York, 2019.
- [2] T. Ahmada, A. Aibinua and M. J. Thaheem, "The effects of high-rise residential construction on sustainability of housing systems," Procedia Engineering, vol. 180, pp. 1695-1704, 2017.
- [3] "Year in Review: Tall Trends of 2023," Council on Tall Buildings and Urban Habitat, Chicago, Illinois, 2024.

- [4] C. Christopoulos and C. Zhong, "Towards understanding, estimating and mitigating higher-mode effects for more resilient tall buildings," Resilient Cities and Structures, 1(1), pp. 53-64, 2022.
- [5] A. K. Chopra, Dynamics of Structures: Theory and Applications to Earthquake Engineering. 2nd edition, Upper Saddle River, NJ: Prentice Hall, 2000.
- [6] A. Rutenberg, "Seismic shear forces on RC walls: review and bibliography," Bulletin of Earthquake Engineering, vol. 11, p. 1727–1751, 2013.
- [7] H. Fatemi, P. Paultre and C.-P. Lamarche, "Experimental Evaluation of Inelastic Higher-Mode Effects on the Seismic Behavior of RC Structural Walls," Journal of Structural Engineering, vol. 146, no. 4, 2020.
- [8] S. P. K. E. Weng Y. Kam, "Seismic performance of reinforced concrete buildings in the 22 February Christchurch (Lyttelton) earthquake," Bulletin of the New Zealand Society for Earthquake Engineering, vol. 44, no. 4, pp. 239-278, 2011.
- [9] Y. B. C. C. R. O. H. R. K. H. K. J. O. M. N. J. P. S. Jack P. Moehle, "Guidelines for Performance- Based Seismic Design of Tall Buildings, PEER Report 2010-05," Pacific Earthquake Engineering Research Center, University of California, Berkeley, 2010.
- [10] M. W. Ibrahim Almofti, "THE REDi™ Rating System: A Framework to Implement Resilience-based Earthquake Design for New Buildings," in 10th US. National Conference on Earthquake Engineering, Frontiers of Earthquake Engineering, Anchorage, Alaska, 2014.
- [11] L. Wiebe, C. Christopoulos and S. Pampanin, "Seismic Response of Self-centering Base-rocking Steel Structures," in Ninth Canadian Conference on Earthquake Engineering, Ottawa, Ontario, Canada, 2007.
- [12] X. Wang and Z. Qu, "Advantages of base isolation in reducing the reliability sensitivity to structural uncertainties of buildings," Engineering Structures, vol. 323, 2025.
- [13] Y. Kurama, S. Pessiki, R. Sause and L.-W. Lu, "Seismic Behavior and Design of Unbonded Post-Tensioned Precast Concrete Walls," PCI Journal, vol. 44, no. 3, pp. 72-89, 1999.
- [14] F. Naeim and J. M. Kelly, Design of Seismic Isolated Structures: From Theory to Practice, John Wiley & Sons, 1999.
- [15] F. Tong, PhD dissertation, Department of Civil and Mineral Engineering, University of Toronto, 2020.
- [16] L. S. Beedle, Advances in Tall Buildings, Florence, Kentucky, U.S.A.: Van Nostrand Reinhold, 1986.

- [17] "CTBUH Height Criteria for Measuring and Difining Tall Buildings," Council on Tall Buildings and Urban Habitat, Chicago, Illinois, U.S.A., 2018.
- [18] A. S. o. C. E. (ASCE), Minimum design loads and associated criteria for buildings and other structures (ASCE/SEI 7-22, Chap. 16: Nonlinear response history analysis), American Society of Civil Engineers, 2022.
- [19] L. Wiebe, C. Christopoulos, R. Tremblay and M. Leclerc, "Mechanisms to limit higher mode effects in a controlled rocking steel frame. 1: Concept, modelling, and low-amplitude shake table testing," Earthquake Engineering and Structural Dynamics, vol. 42, no. 7, pp. 1053-1068, 2013.
- [20] R. Golsorkhi, L. Joseph, R. Klemencic, D. Shook and J. Viise, "Performance-based Seismic Design for Tall Buildings: An Output of CTBUH Performance-based Seismic Design Working Group," Council of Tall Buildings and Urban Habitat, Chicago, Illinois, U.S.A., 2017.
- [21] H. Veladi, B. F. Azar and S. R. Gendeshmin, "Quantifying higher mode effects in rocking systems considering shear-flexural behavior," Structures, 27, pp. 542-558, 2020.
- [22] R. C. C. L. M. M. R. W. G. Blakeley, "Seismic shear loading at flexural capacity in cantilever wall structures," Bulletin of the New Zealand Society for Earthquake Engineering, vol. 8, no. 4, pp. 278-290, 1975.
- [23] T. J. S. G. M. C. Domenico Pennucci, "Inelastic higher-mode response in reinforced concrete wall structures," Earthquake Spectra, vol. 31, no. 3, pp. 1493-1514, 2014.
- [24] P. P. Yannick Boivin, "Seismic force demand on ductile reinforced concrete shear walls subjected to western North American ground motions: Part 2 new capacity design methods," Canadian Journal of Civil Engineering, vol. 32, no. 7, pp. 723-737, 2012.
- [25] M. J. N. Priestley, "Does capacity design do the job? An examination of higher mode effects in cantilever walls," Bulletin of the New Zealand Society for Earthquake Engineering, vol. 36, no. 4, p. 276–292, 2003.
- [26] I. Ghorbanirenani, R. Tremblay, P. Léger and M. Leclerc, "Shake table testing of slender RC shear walls subjected to eastern North America seismic ground motions," Journal of Structural Engineering, vol. 138, no. 12, pp. 1515-1529, 2012.
- [27] S. E. A. o. C. (SEAOC), Recommended Lateral Force Requirements and Commentary (7th ed.), Sacramento, CA: Structural Engineers Association of California, 1999.
- [28] National Building Code of Canada (NBCC) 2020, Ottawa, Ontario: National Research Council Canada, 2022.

- [29] J. Baker, J. Bray, C. Crouse, G. Deierlein, R. O. Hamburger, J. Hooper, M. Lew, J. Maffei, S. Mahin, J. O. Malley, J. P. Moehle, F. Naeim, J. P. Stewart and J. Wallace, "Tall Building Initiative, Guidelines for Performance-based Seismic Design of Tall Buildings," Pacific Earthquake Engineering Research Center, Headquarters at the University of California, Berkeley, Berkeley, California, 2017.
- [30] "FEMA P-58-1, Seismic Performance Assessment of Buildings, Volume 1 Methodology.," Applied Technology Council, 2012.
- [31] J. M. J. B. J. B. C. C. G. D. J. H. M. L. J. M. S. M. J. M. F. N. J. S. J. W. Ron Hamburger, "Guidelines for Performance-Based Seismic Design of Tall Buildings, Report 2017/06," Pacific Earthquake Engineering Research Center, Berkeley, 2017.
- [32] M. F. Vassiliou, K. R. Mackie and B. Stojadinović, "A finite element model for seismic response analysis of deformable rocking frames," Earthquake Engineering and Structural Dynamics, vol. 46, pp. 447-466, 2017.
- [33] N. Makris and M. F. Vassiliou, "Sizing the slenderness of free-standing rocking columns to withstand earthquake shaking," Applied Mechanics, 82, pp. 1497-1511, 2012.
- [34] M. F. Vassiliou, S. Burger, M. Egger, J. A. Bachmann, M. Broccardo and B. Stojadinovic, "The three-dimensional behavior of inverted pendulum cylindrical structures during earthquakes," Earthquake Engineering & Structural Dynamics, 46(14), pp. 2261-2280, 2017.
- [35] G. W. Housner, "The behaviour of inverted pendulum structures during earthquakes," Bulletin of the Seismological Society of America, vol. 53, no. 2, p. 403–417, 1963.
- [36] G. M. Nielsen, I. Almufti, S. A. Mahin and M. R. Willford, "Performance of Rocking Core Walls in Tall Buildings Under Severe Seismic Motions," in Proceedings of the 9th U.S. National and 10th Canadian Conference on Earthquake Engineering, Toronto, Ontario, Canada, 2010.
- [37] M. J. N. Priestley, S. (. Sritharan, J. R. Conley and S. Pampanin, "Preliminary Results and Conclusions From the PRESSS Five-Story Precast Concrete Test Building," PCI Journal, vol. 44, no. 6, pp. 42-67, 1999.
- [38] W. H. R. G. H. M. R. I. Skinner, An Introduction to Seismic Isolation, John Wiley & Sons., 1993.
- [39] N. Stratton, N. V. Engelen and R. Ruparathna, "Seismic Isolation of Low-Rise Residential Structures," in Proceedings of the Canadian Society of Civil Engineering Annual Conference 2022, 2022.
- [40] S. Y. H. H. M. H. M. N. Tracy Becker, "Application of Isolation to High-Rise Buildings: A Japanese Design Case Study through a US Design Code Lens," Earthquake Spectra, vol. 31, no. 3, pp. 1451-1470, 2015.

- [41] Y. T. A. N. E. Takaoka, "Shaking table test and analysis method on ultimate behavior of slender base-isolated structure supported by laminated rubber bearings," Earthquake Engineering & Structural Dynamics, vol. 40, no. 5, pp. 551-570, 2011.
- [42] V. Calugaru, Earthquake Resilient Tall Reinforced Concrete Buildings at Near-Fault Sites Using Base Isolation and Rocking Core Walls, PhD dissertation, Berkeley: University of California, 2013.
- [43] V. Calugaru and M. Panagiotou, "Seismic response of 20-story base-isolated and fixed-base reinforced concrete structural wall buildings at a near-fault site," Earthquake Engineering and Structural Dynamics, vol. 43, no. 6, pp. 927-948, 2013.
- [44] K. Ogura, I. Kawabata, T. Komuro, K. Soya and T. Terashima, "Seismic response characteristics of high-rise buildings with base isolation system," AIJ Journal of Technology and Design, 3(5), pp. 47-51, 1997.
- [45] Y. Shinozaki, O. Hosozawa and T. Komuro, "Structural Design of Base-isolation System for Tall Building in Japan," in CTBUH 2004 Seoul Conference, Seoul, 2004.
- [46] L. Wiebe and C. Christopoulos, "Performance-Based Seismic Design of Controlled Rocking Steel Braced Frames. II: Design of Capacity-Protected Elements," Structural Engineering, vol. 141, no. 9, 2015.
- [47] L. A. T. B. S. D. C. (LATBSDC), An Alternative Procedure for Seismic Analysis and Design of Tall Buildings Located in the Los Angeles Region, 2023 edition with 2024 Supplements, Los Angeles, CA: Los Angeles Tall Buildings Structural Design Council, 2024.
- [48] M. H. S. G. L. F. Frank McKenna, "Nonlinear Finite-Element Analysis Software Architecture Using Object Composition," Journal of Computing in Civil Engineering, vol. 24, no. 1, pp. 95-107, 2010.
- [49] National Building Code of Canada (NBCC) 2020: Structural commentaries, Ottawa, Ontario: National Research Council Canada., 2025.
- [50] J. Moehle, Y. Bozorgnia, N. Jayaram, P. Jones, M. Rahnama, N. Shome, Z. Tuna, J. Wallace, T. Yang and F. Zareian, "Case Studies of the Seismic Performance of Tall Buildings Designed by Alternative Means: Task 12 Report for the Tall Buildings Initiative," Pacific Earthquake Engineering Research Center, Berkeley, CA, U.S.A., 2011.
- [51] T. Ha, S.-H. S. and H. Kim, "Damping and Natural Period Evaluation of Tall RC," Applied Sciences, 10,1568, 2020.
- [52] A. Singh and S. Mandal, "Effect of Plan and Height Aspect Ratios on Along-wind and Across-wind," Jordan Journal of Civil Engineering, pp. 335-354, 2022.

- [53] M. Jinjie, S. Qingxuan and H. Zhijian, "Optimal Design of Tall Residential Building with RC Shear Wall and with Rectangular Layout," International Journal of High-rise Buildings, 3(4), pp. 285-296, 2014.
- [54] H. E. Ilgin, "Interrelations of slenderness ratio and main design criteria in supertall buildings," International Journal of Building Pathology and Adaptation, 41, pp. 139-161, 2022.
- [55] A. Dixit, "Single-beam analysis of damaged beams: Comparison using Euler–Bernoulli and Timoshenko beam theory," Journal of Sound and Vibration, vol. 333, no. 18, pp. 4341-4353, 2014.
- [56] "ASCE Hazard Tool," 2025. [Online].
- [57] "2020 National Building Code of Canada Seismic Hazard Tool," Government of Canada, 6 4 2021. [Online]. Available: https://www.seismescanada.rncan.gc.ca/.
- [58] GeoPentech, "Geotechnical investigation: Proposed development at 1201 South Grand Avenue, Los Angeles, California," Geotechnical Investigation Report, Santa Ana, CA, 2020.
- [59] American Concrete Institute, American Concrete Institute, 2025.
- [60] C. S. A. CSA A23.3-24, CSA A23.3-24: Design of concrete structures, Mississauga, ON: CSA Group, 2024.
- [61] CEN, Brussels: European Committee for Standardization, 2004.
- [62] E. C. f. Standardization, Eurocode 3: Design of steel structures Part 1-1: General rules and rules for buildings (EN 1993-1-1), Brussels, Belgium: CEN, 2005.
- [63] P. G. D. P. M. D. T. T. D. M. P. C. Jun Xia, "Case Study: Shanghai Tower," CTBUH Journal, no. 2, pp. 12-19, 2016.
- [64] G. Giakoumelis and D. Lam, "Axial capacity of circular concrete-filled tube columns," Journal of Constructional Steel Research, 60(7), pp. 1049-1068, 2004.
- [65] A. Dutta and R. O. Hamburger, "A case study of a 40-storey buckling-restrained braced frame building located in Los Angeles," The Structural Design of Tall and Special Buildings, 19(1–2), pp. 77-93, 2009.
- [66] S. M. C. C. R. Sabelli, "Seismic demands on steel braced frame buildings with buckling-restrained braces," Engineering Structures, vol. 25, no. 5, pp. 655-666, 2003.
- [67] S. Harmsen, "Site-specific seismic-hazard maps and deaggregation in the western United States using the NGA models for ground-motion prediction," Geological Survey, Reston, VA, U.S.A., 2011.
- [68] "USGS," 2014. [Online].

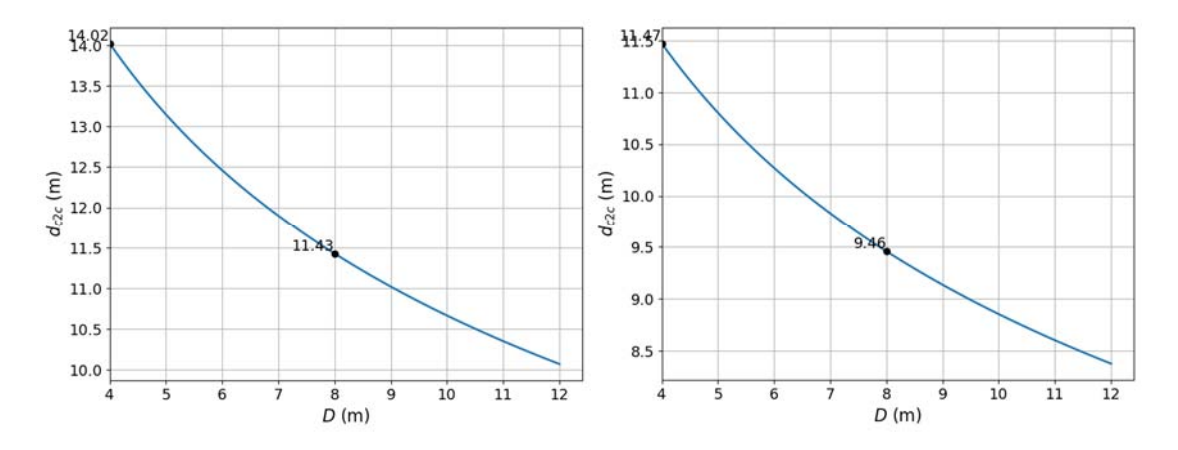
- [69] "PEER Ground Motion Database," Pacific Earthquake Engineering Research Center, [Online]. Available: https://ngawest2.berkeley.edu/.
- [70] P. A. Monahan, Soil Hazard Map of the Lower Mainland of British Columbia for Assessing the Earthquake Hazard Due to Lateral Ground Shaking, Calgary, Alberta: Monahan Petroleum Counsulting, 2005.
- [71] M. Kolaj, S. Halchuk and J. Adams, "Deaggregation of NBCC 2020 seismic hazard for selected Canadian cities," in In Proceedings of the Canadian Conference Pacific Conference on Earthquake Engineering, Vancouver, BC., 2023.
- [72] R. G. R. Z. W. McGuire, Matrix Structural Analysis (2nd ed.), John Wiley & Sons, 2000.
- [73] S. M. C. C. R. Sabelli, "Seismic demands on steel braced frame buildings with buckling-restrained braces," Engineering Structures, vol. 25, no. 5, pp. 655-666, 2003.
- [74] J. A. Bachmann, M. F. Vassiliou and B. Stojadinovic, "Rolling and rocking of rigid uplifting structures," Earthquake Engineering & Structural Dynamics, 48 (14), pp. 1556-1574, 2019.
- [75] K. E. Bantilas, I. E. Kavvadias and L. K. Vasiliadis, "Seismic response of elastic multidegree of freedom oscillators placed on the top of rocking storey," Earthquake Engineering & Structural Dynamics, 50 (5), pp. 1315-1333, 2021.
- [76] A. M. D'Altri, G. Vlachakis, S. d. Miranda and P. B. Lourenço, "Rocking block simulation based on numerical dissipation," Nonlinear Dynamics, 112(20), pp. 17843-17862, 2024.
- [77] N. Makris and M. F. Vassiliou, "Planar rocking response and stability analysis of an array of free-standing columns capped with a freely supported rigid beam," Earthquake Engineering & Structural Dynamics, 42(3), pp. 431-449, 2013.
- [78] NZS 3101: part 1, concrete structure standard; part 2:.Commentary on the design of concrete structures, Wellington (1982): New Zealand Standards, 1995,2006.
- [79] T. a. M. A. (. Ministry of Land, Korean Building Code Structural (KBC 2009), Seoul: Republic of Korea, 2009.

# **Appendix A: Rocker Dimension Correlations**

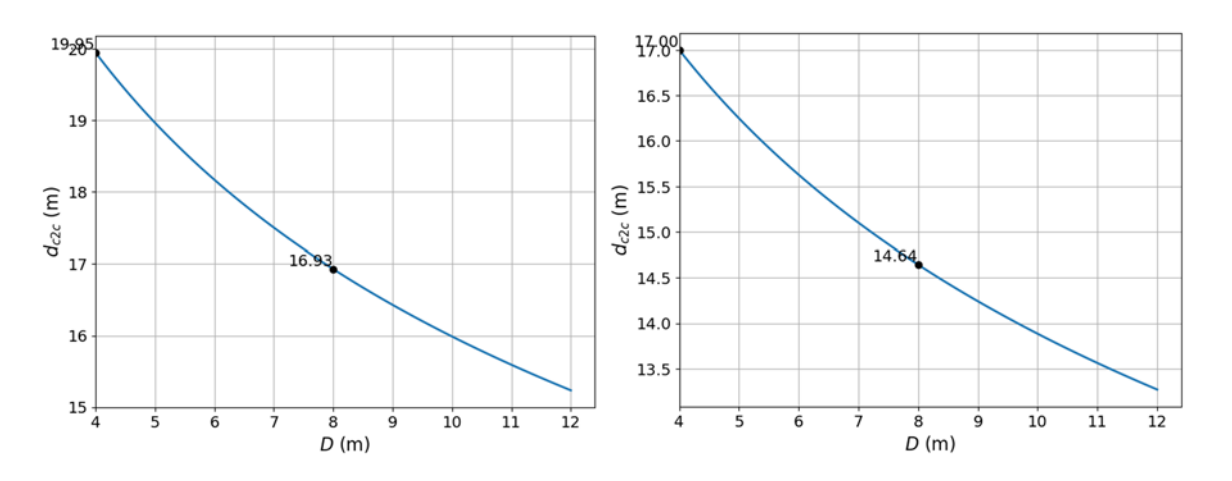
Los Angeles

Vancouver

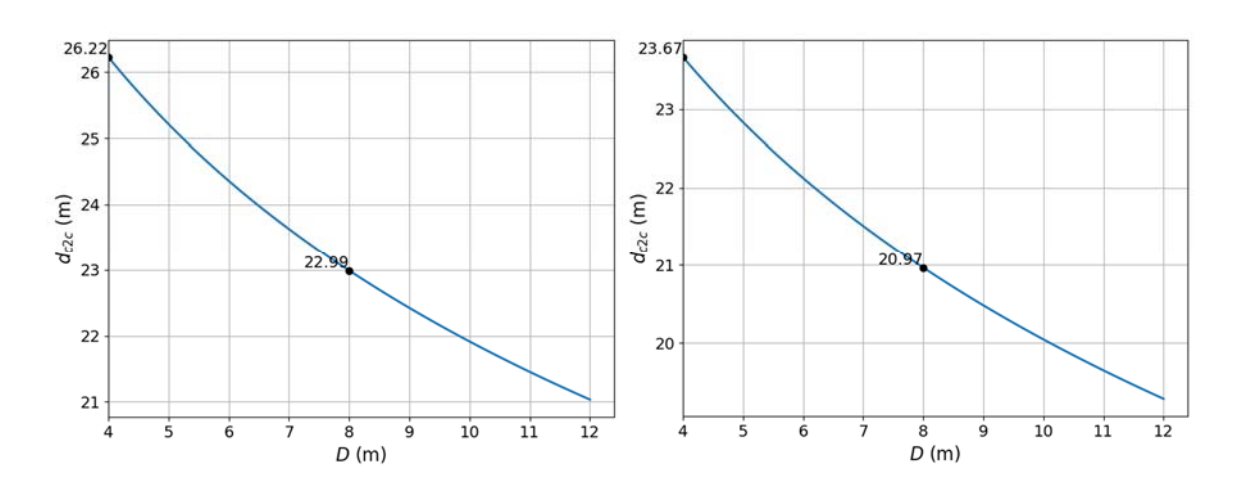
15-story Buildings,  $R_{\rm M} = 4$ 



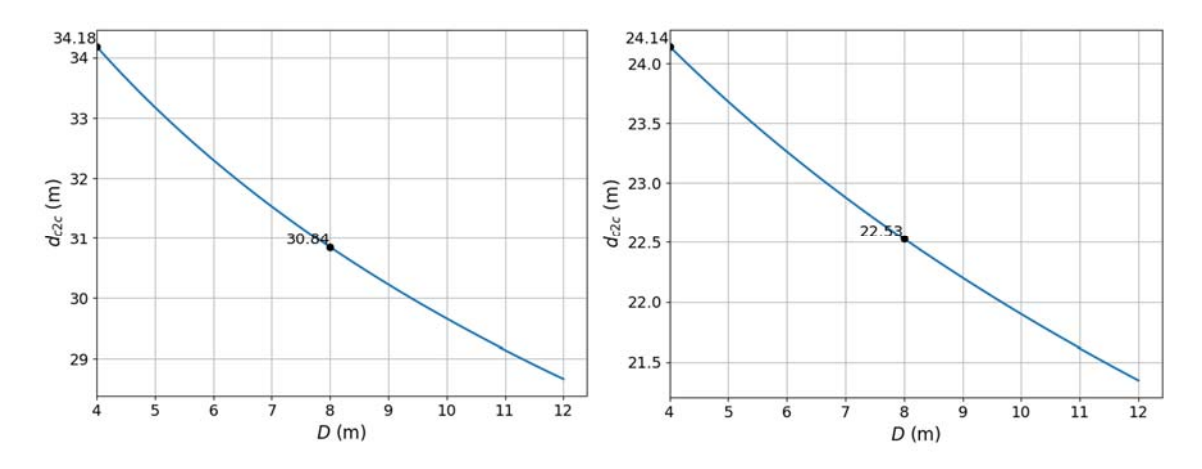
30-story Buildings,  $R_{\rm M} = 4$ 



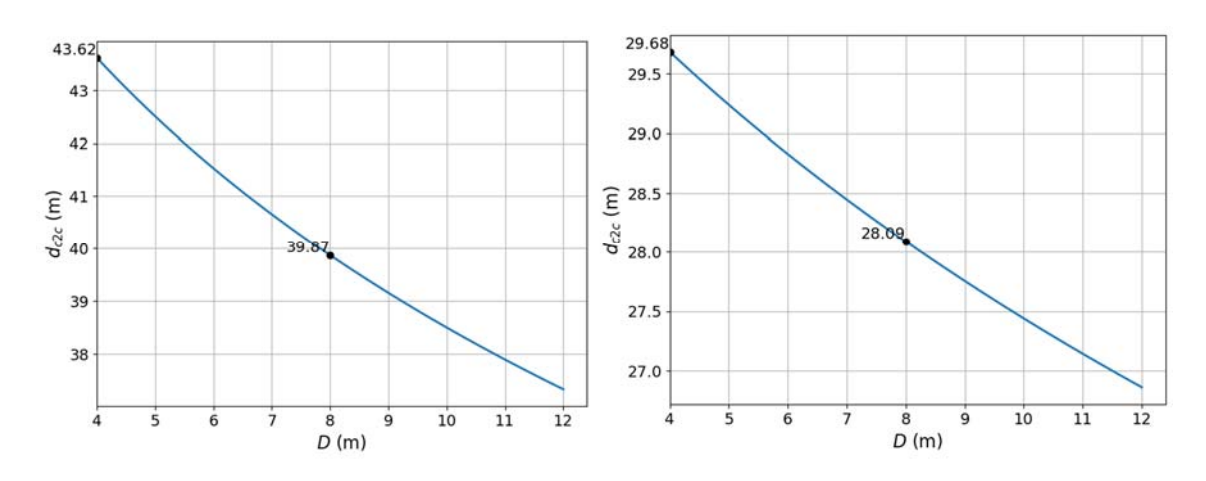
50-story Buildings,  $R_{\rm M} = 4$ 



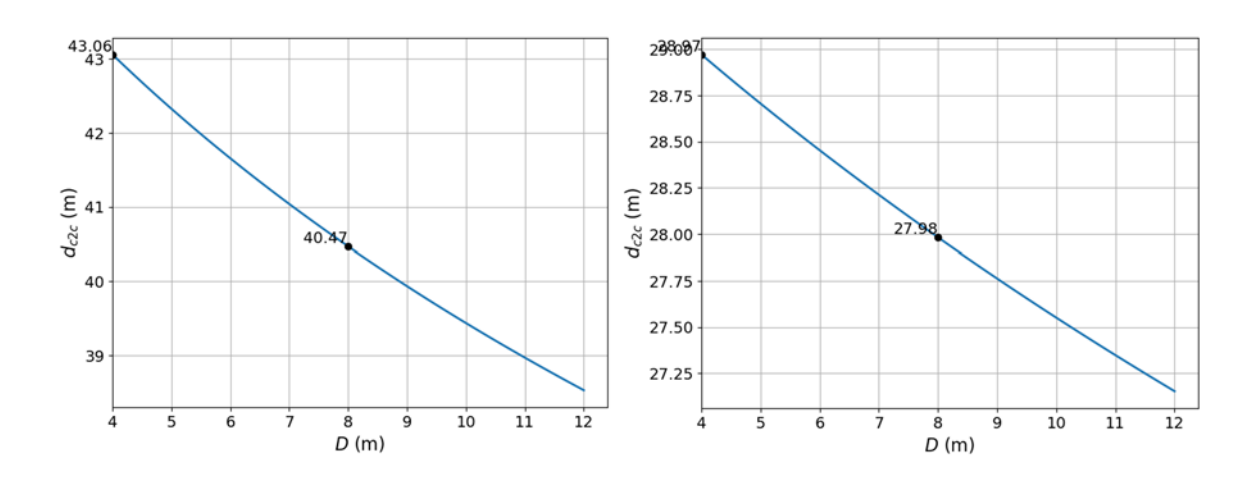
70-story Buildings,  $R_{\rm M} = 4$ 



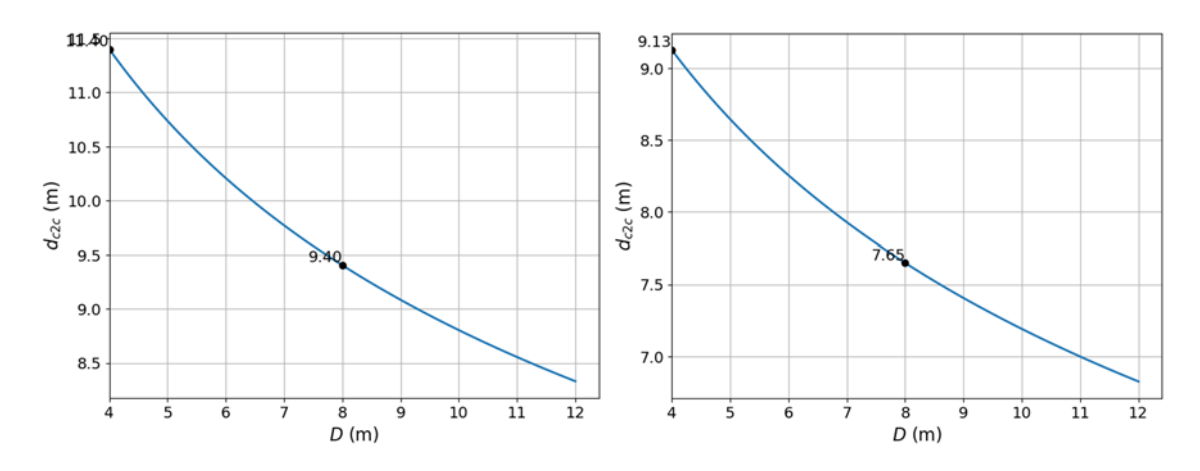
100-story Buildings,  $R_{\rm M} = 4$ 



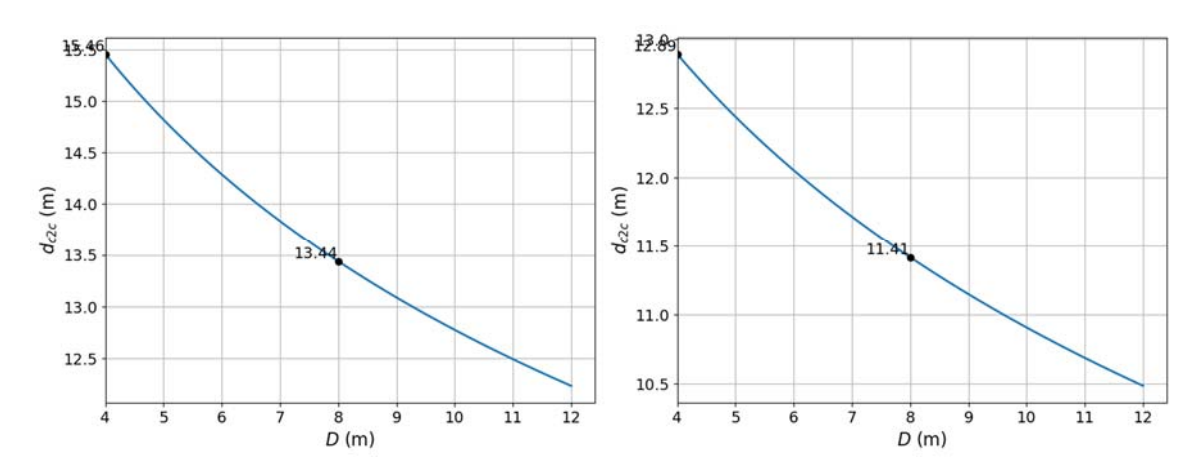
120-story Buildings,  $R_{\rm M} = 4$ 



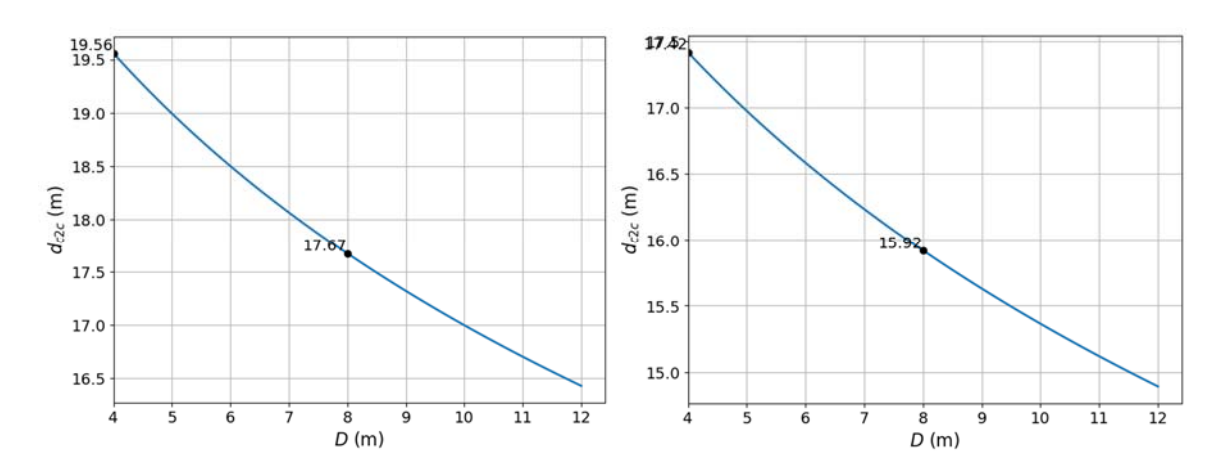
15-story Buildings,  $R_{\rm M} = 6$ 



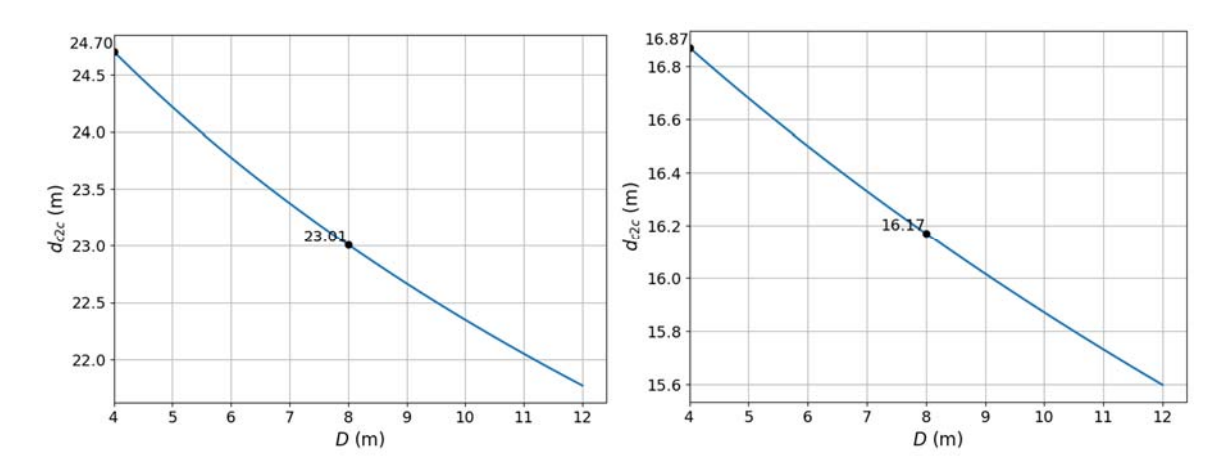
30-story Buildings,  $R_{\rm M} = 6$ 



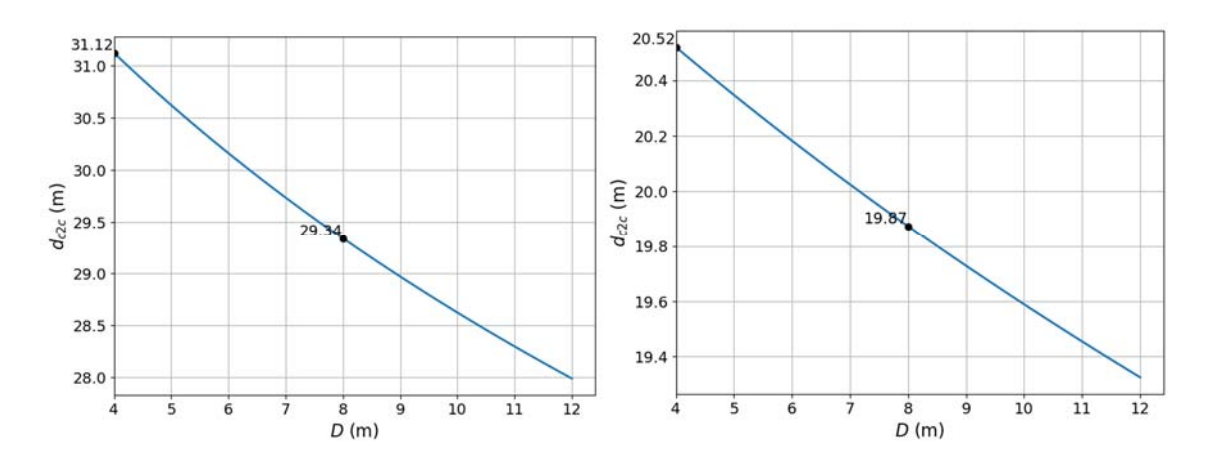
50-story Buildings,  $R_{\rm M} = 6$ 



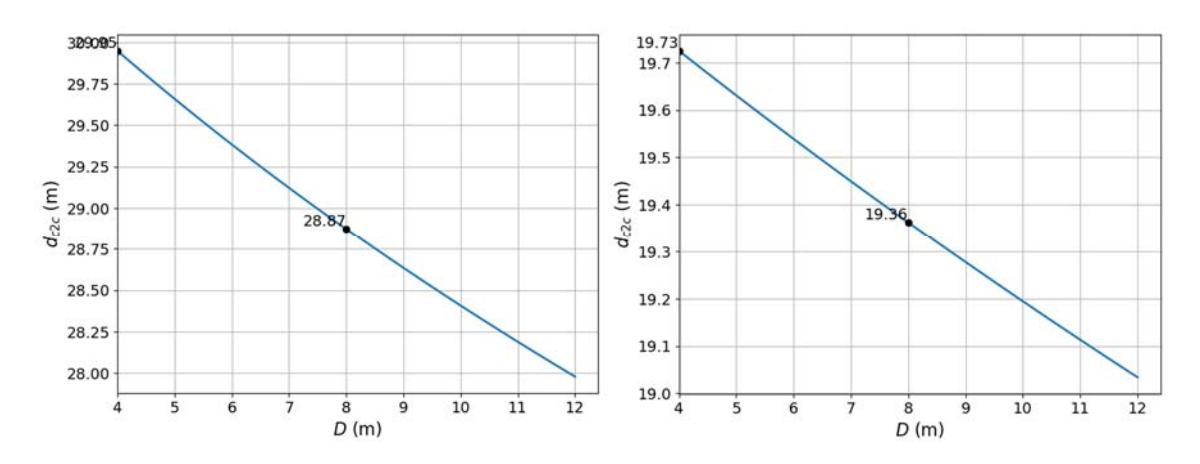
70-story Buildings,  $R_{\rm M} = 6$ 



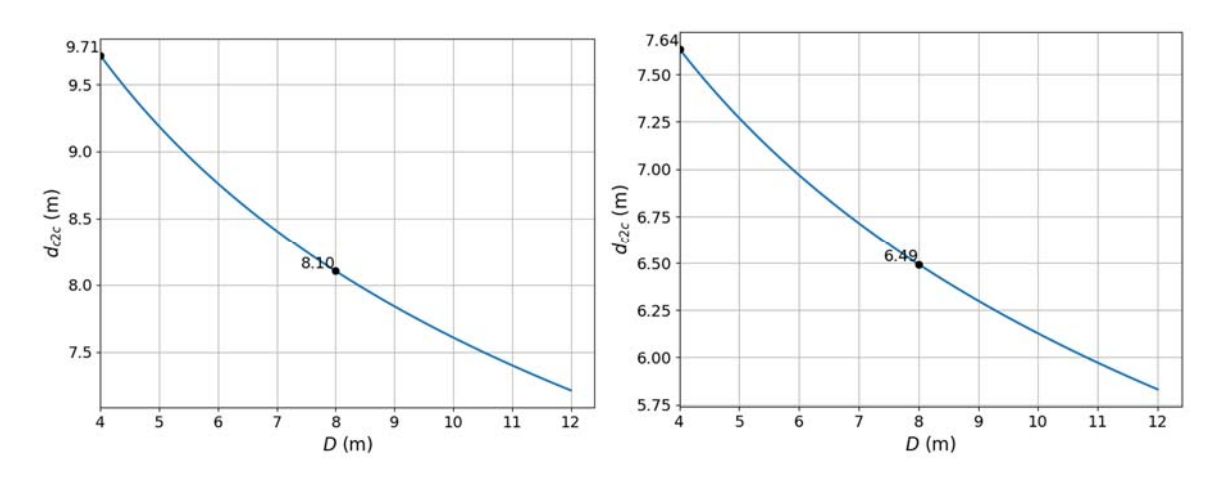
100-story Buildings,  $R_{\rm M} = 6$ 



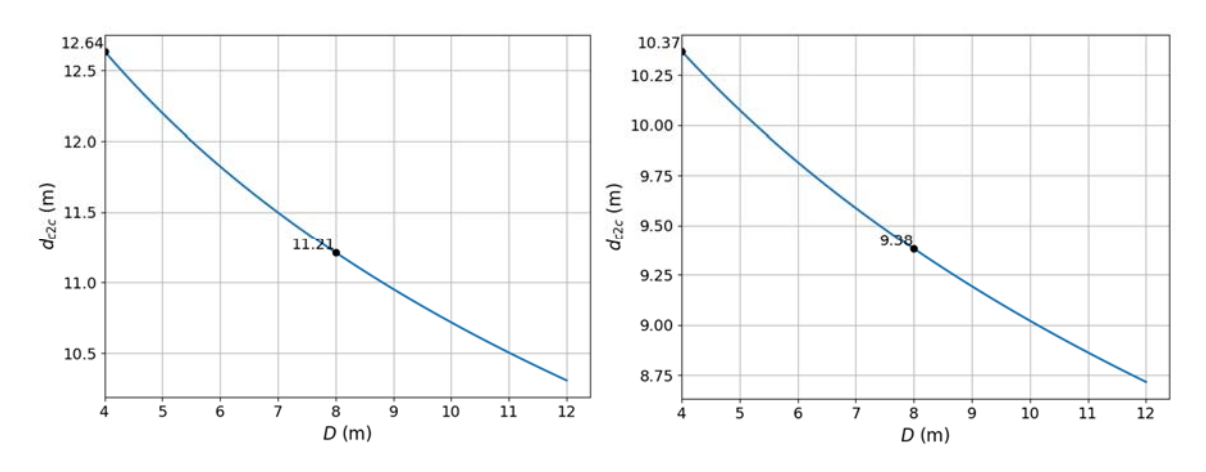
120-story Buildings,  $R_{\rm M} = 6$ 



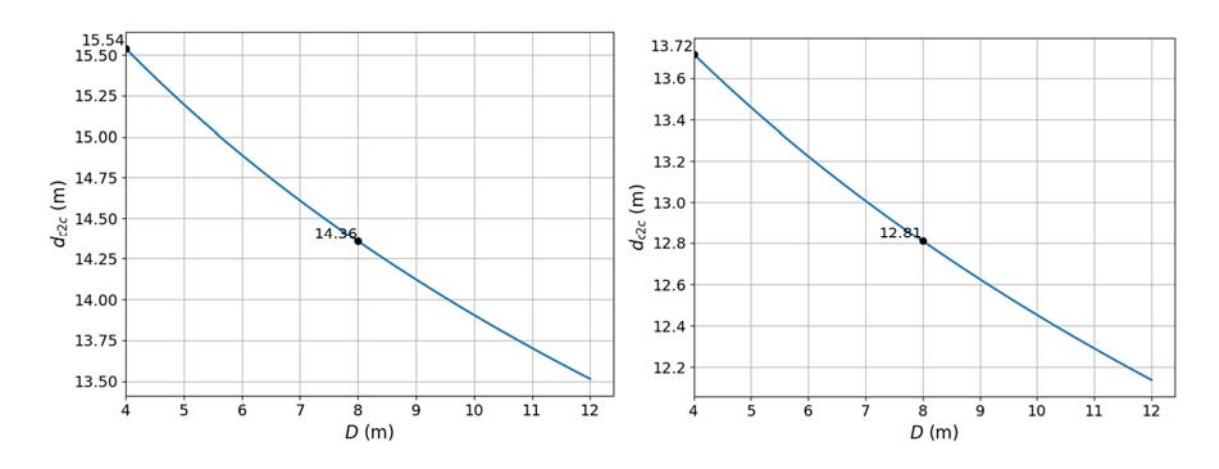
15-story Buildings,  $R_{\rm M} = 8$ 



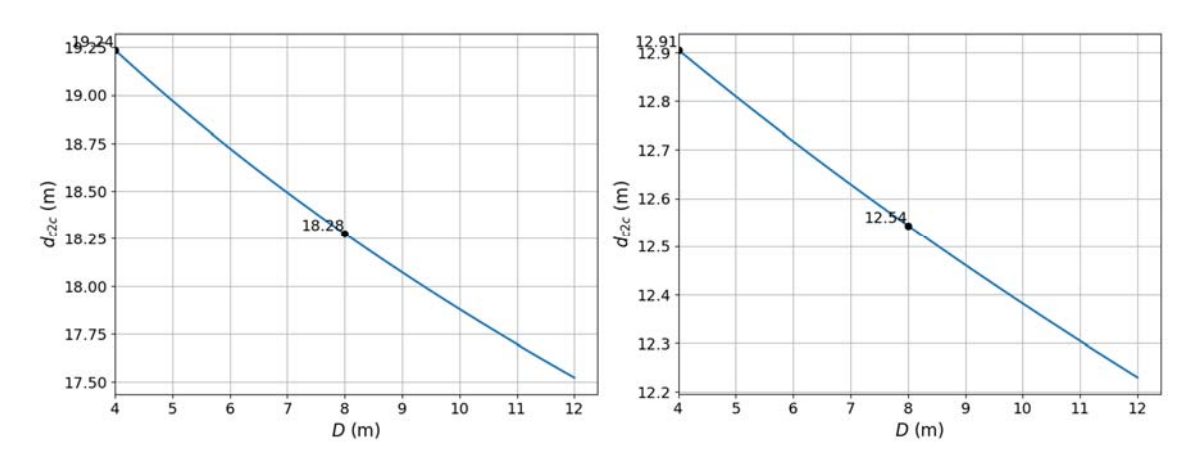
30-story Buildings,  $R_{\rm M} = 8$ 



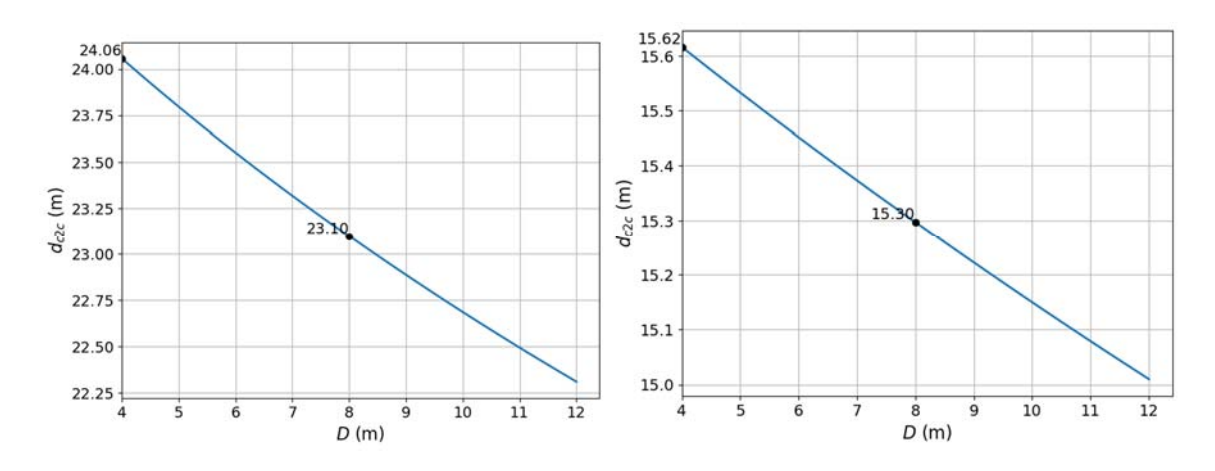
50-story Buildings,  $R_{\rm M} = 8$ 



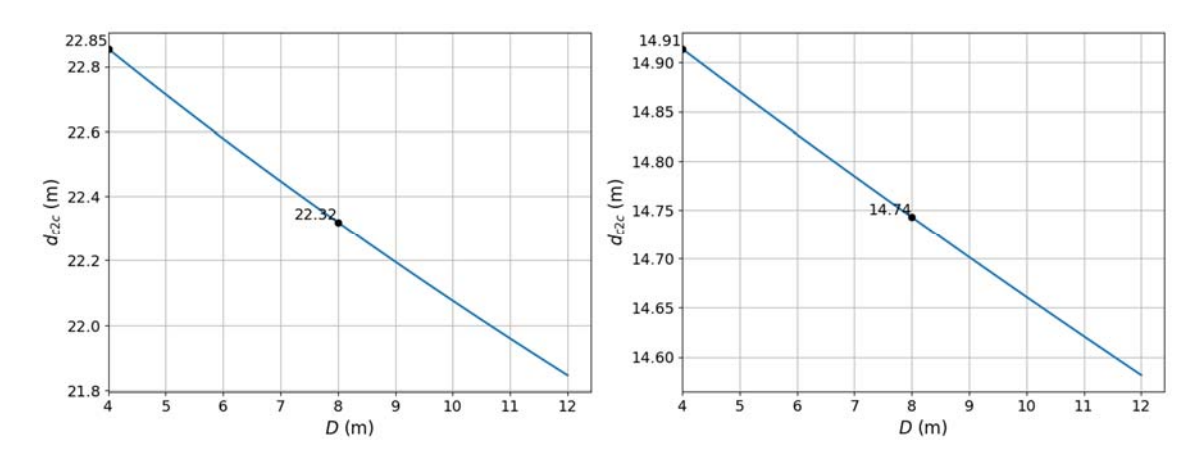
70-story Buildings,  $R_{\rm M} = 8$ 



100-story Buildings,  $R_{\rm M} = 8$ 



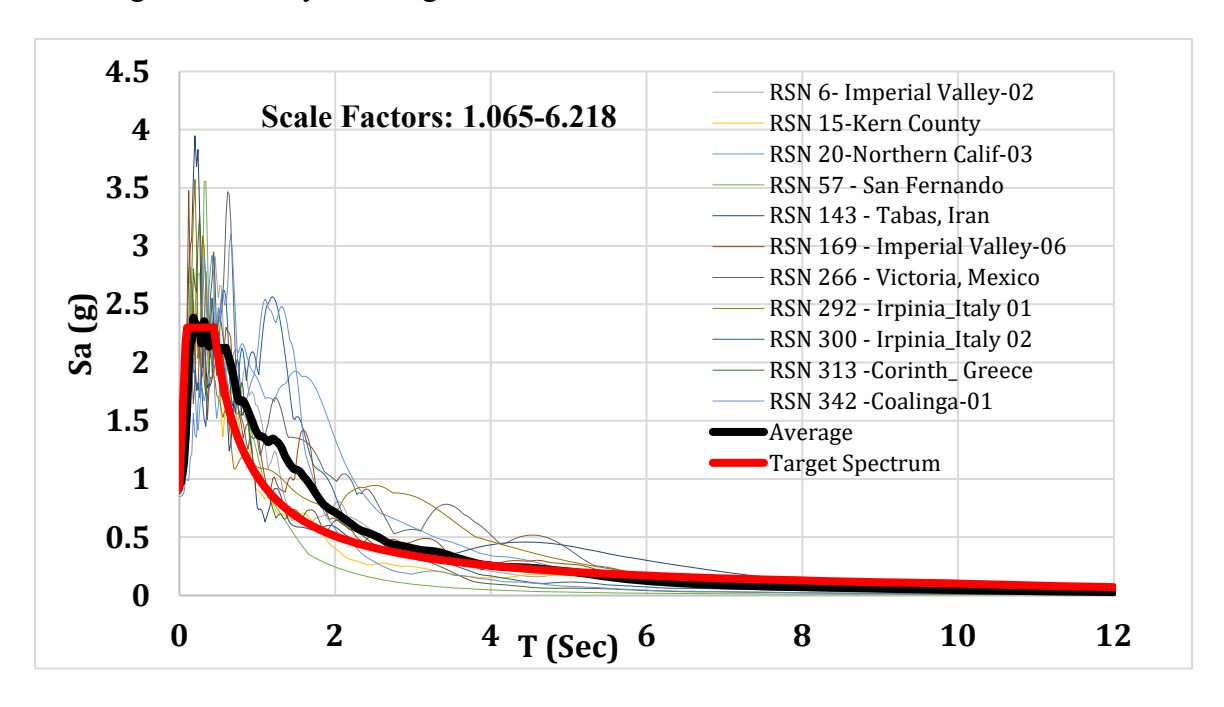
120-story Buildings,  $R_{\rm M} = 8$ 



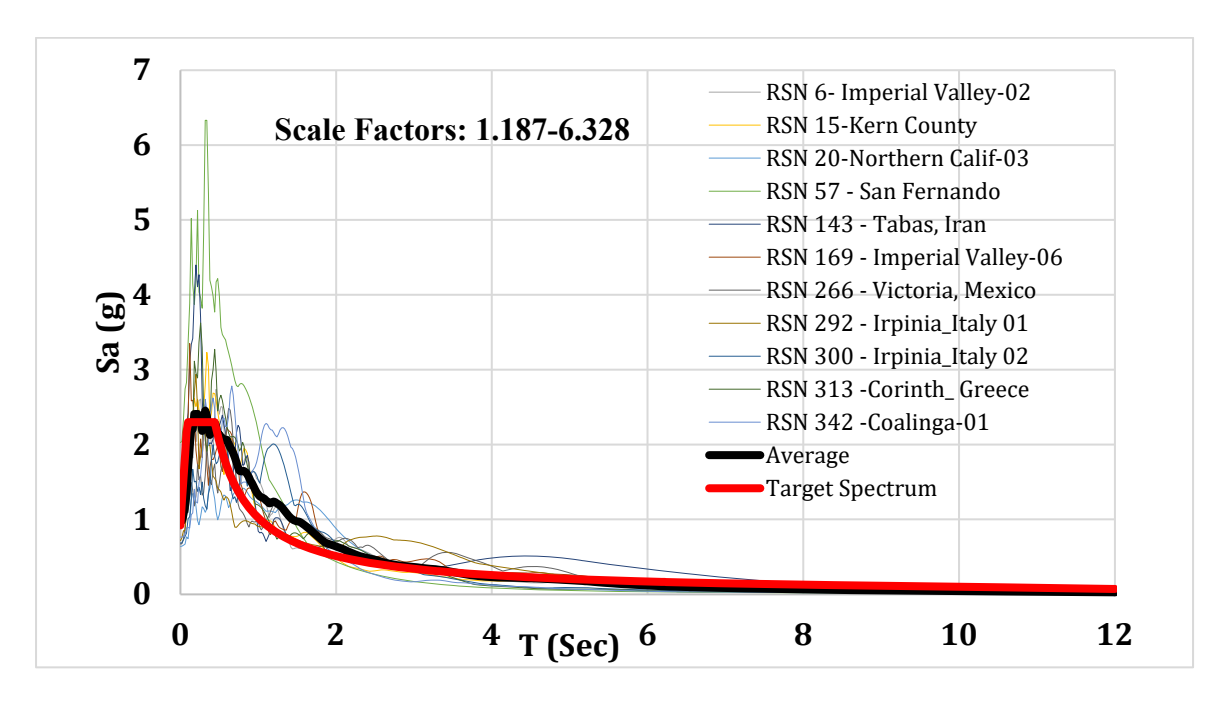
# Appendix B: Selected and Scaled Ground Motions for All Generic Buildings at MCE Level

# **Los Angeles Site:**

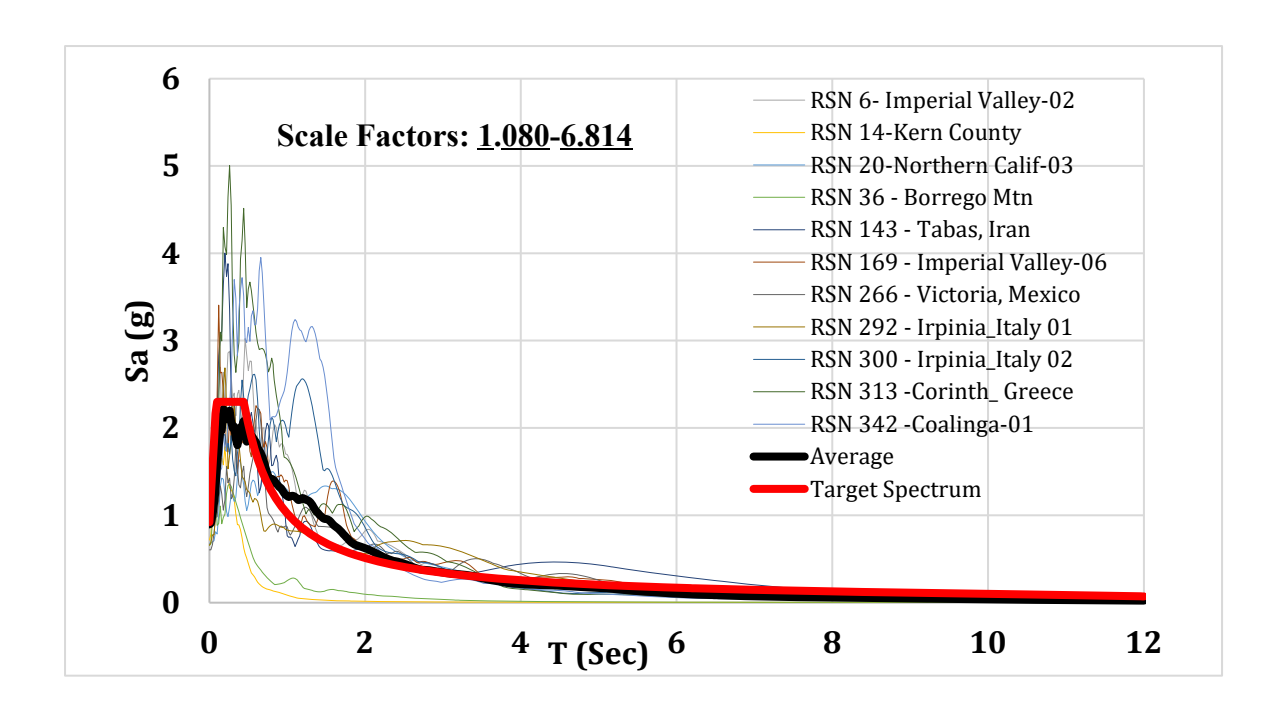
Los Angeles, 15-story Building:



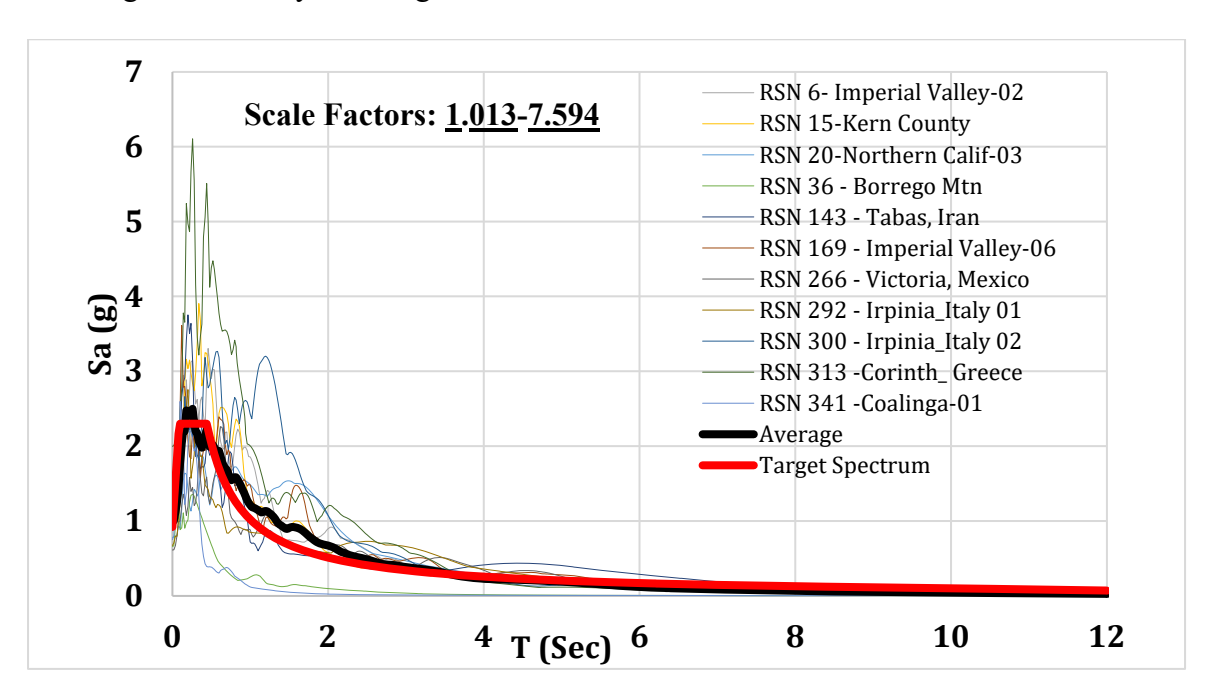
Los Angeles, 30-story Building:



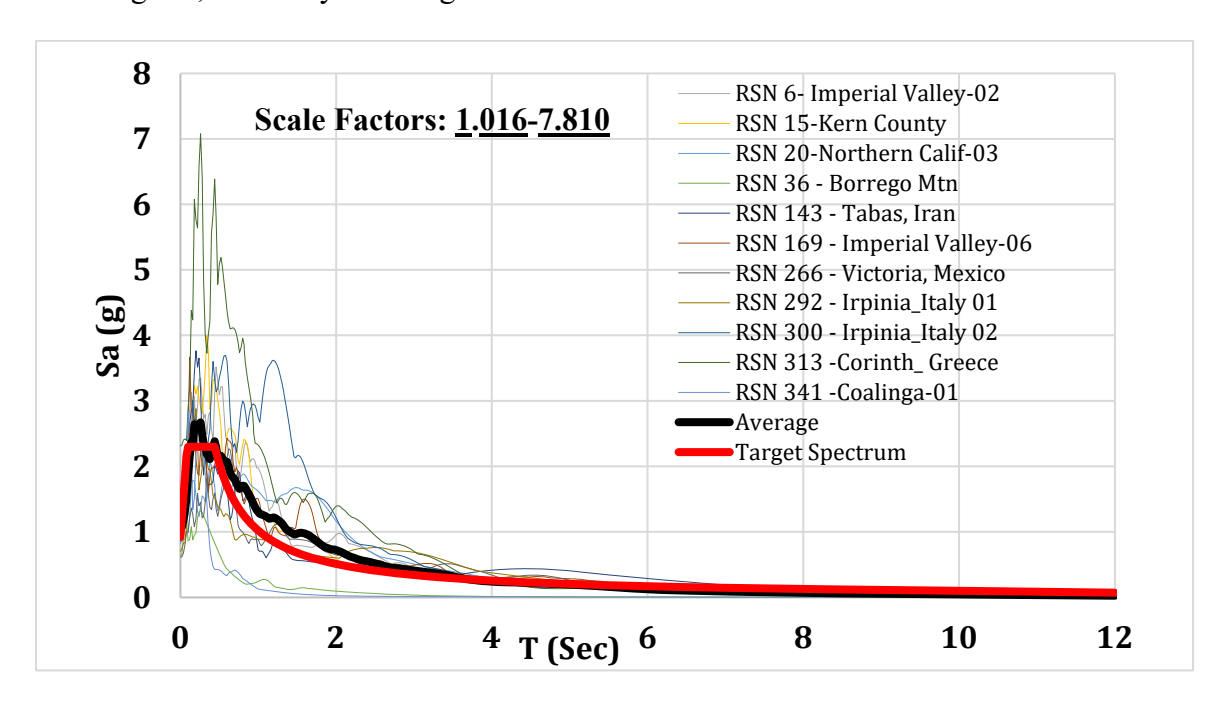
# Los Angeles, 50-story Building:



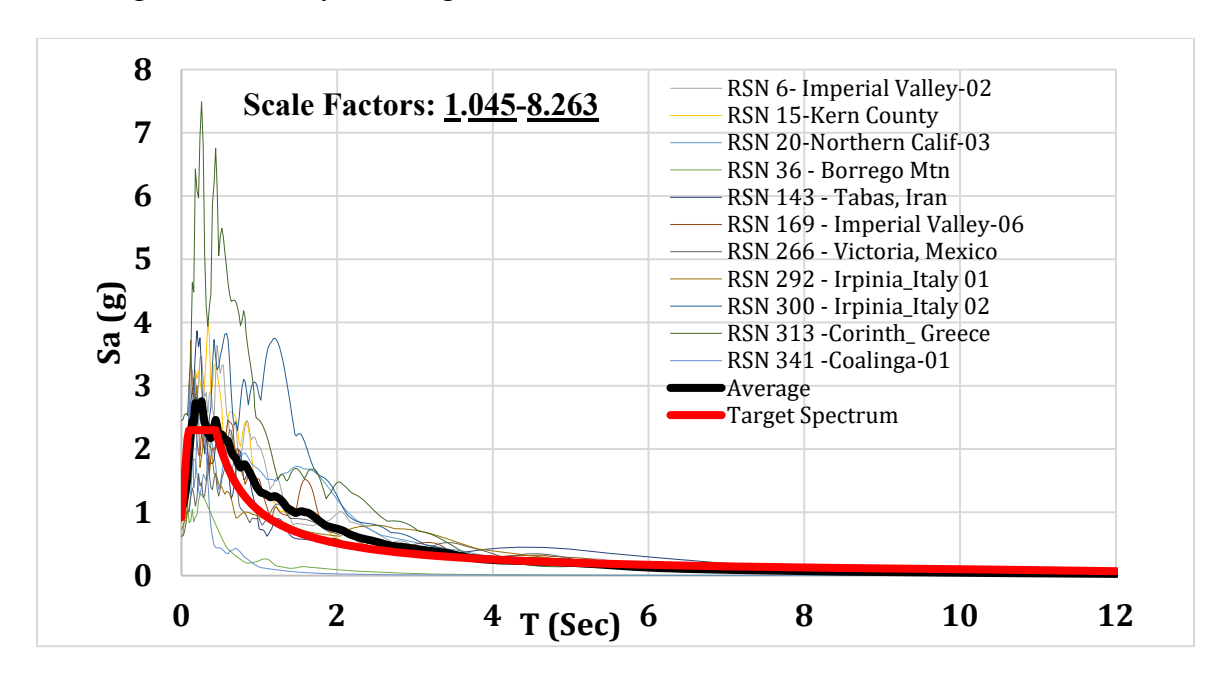
# Los Angeles, 70-story Building:



# Los Angeles, 100-story Building:

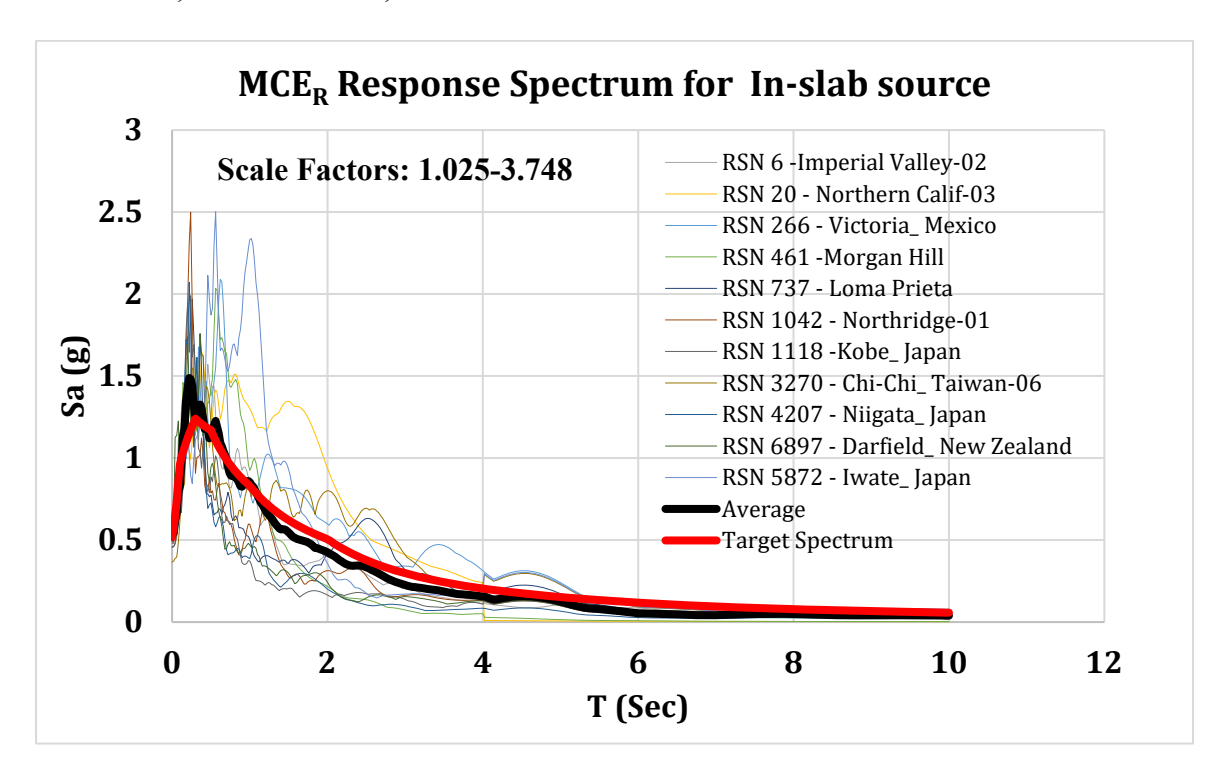


# Los Angeles, 120-story Building:

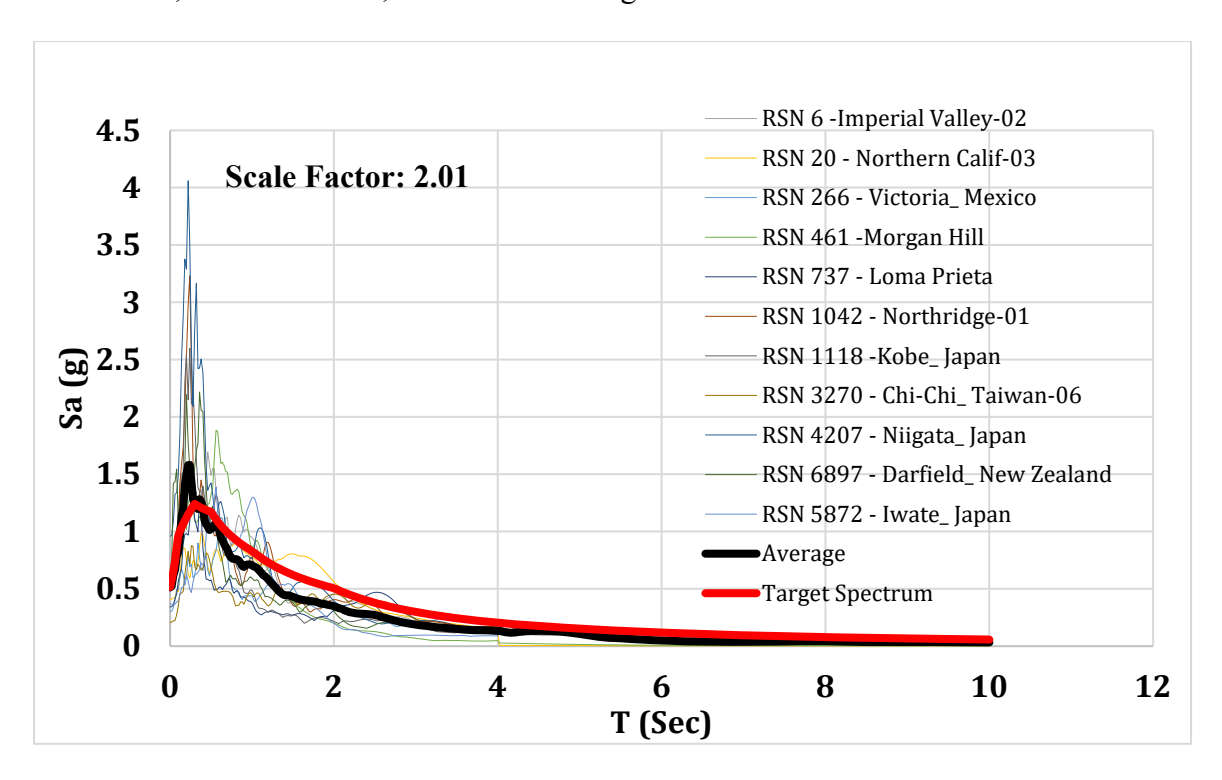


#### Vancouver Site:

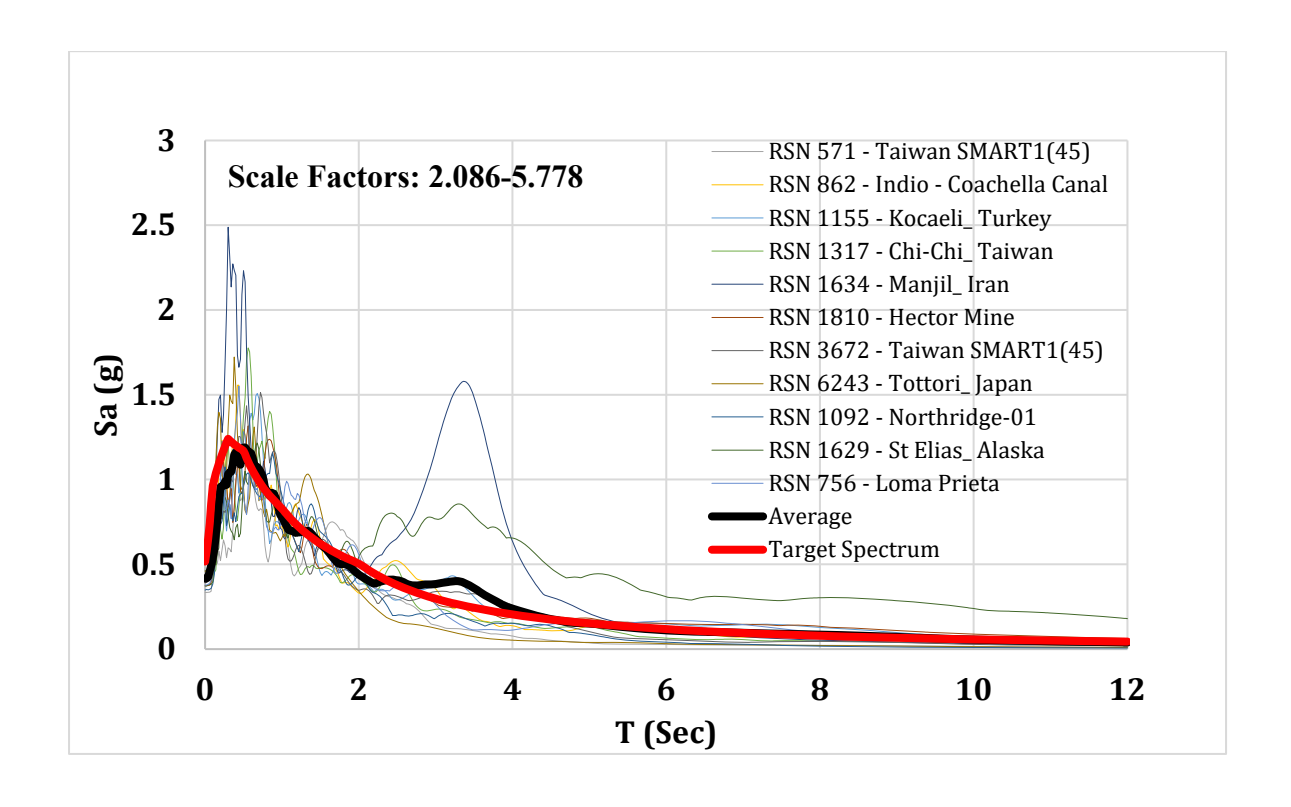
Vancouver, In-Slab Source, Scaled with Different Factors:



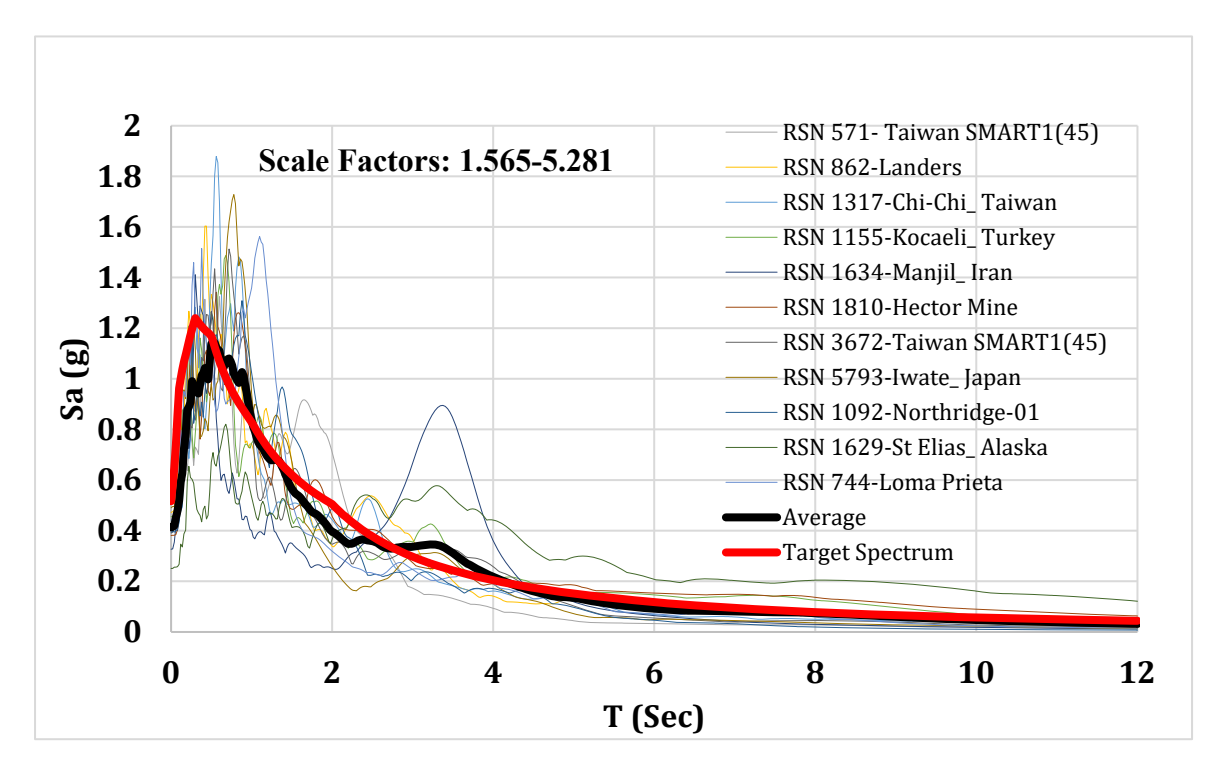
Vancouver, In-Slab Source, Scaled with a Single Factor:



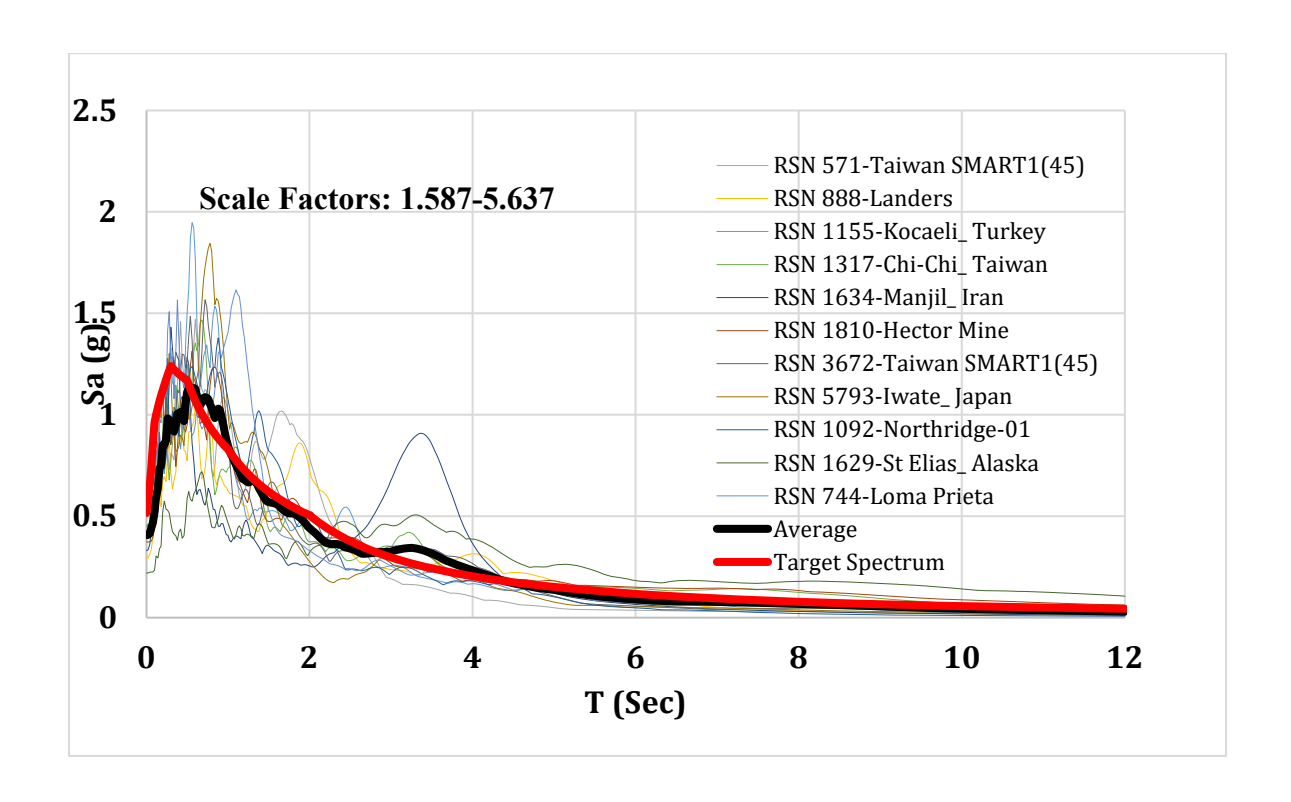
Vancouver, Interface Source, 15-story Building:



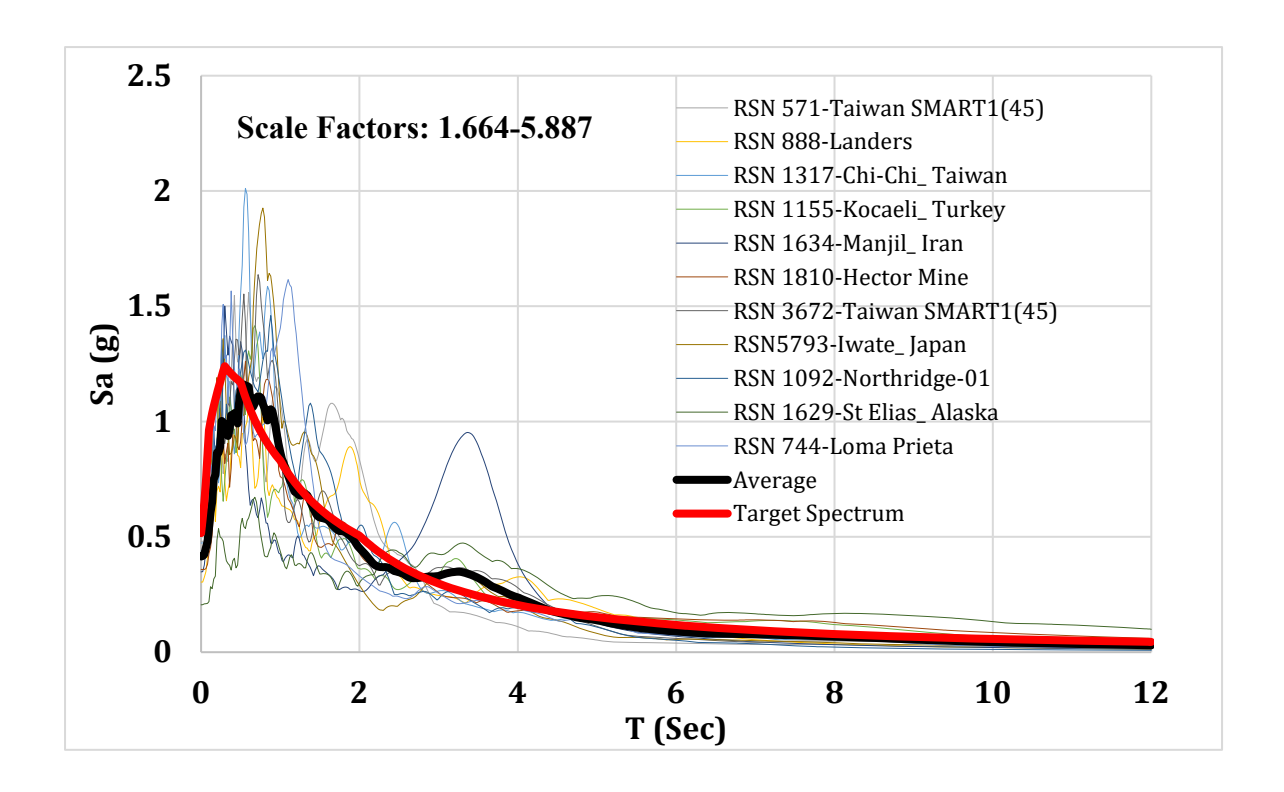
Vancouver, Interface Source, 30-story Building:



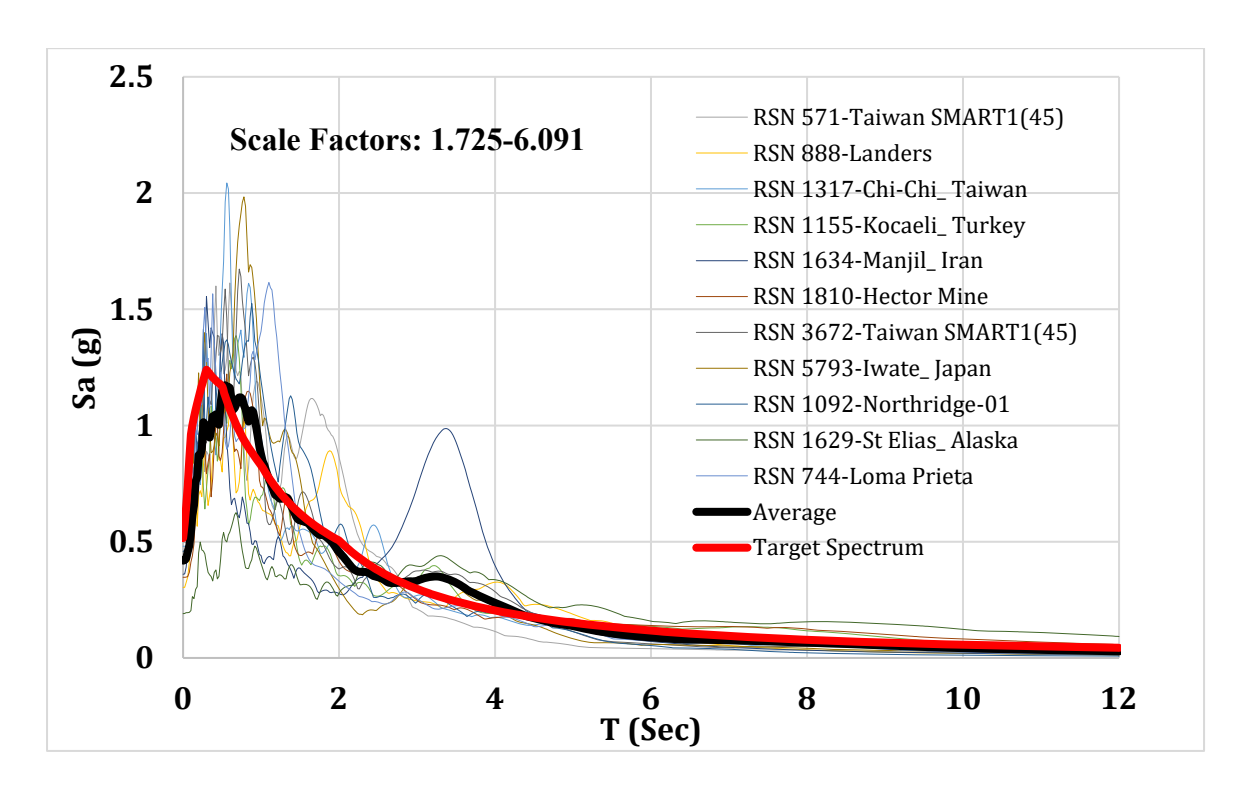
Vancouver, Interface Source, 50-story Building:



Vancouver, Interface Source, 70-story Building:



Vancouver, Interface Source, 100-story Building:



Vancouver, Interface Source, 120-story Building:

